BIOMECHANICAL MODELING
OF CANINE RETRACTION

Matthew Evans Larson, DDS

A thesis submitted to the faculty of the University of North Carolina at Chapel Hill in partial fulfillment of the requirements for the degree of Master of Science in the School of Dentistry (Orthodontics).

**Chapel Hill
2012**

Approved by:

Ching-Chang Ko

Tung Nguyen

Garland Hershey

Kazuo Hayashi

Emile Rossouw

ABSTRACT

MATTHEW EVANS LARSON: Biomechanical Modeling of Canine Retraction
(Under the direction of Dr. Ching-Chang Ko)

Objective: To create a comprehensive finite element model capable of analyzing the biomechanics of canine retraction. **Methods**: A half maxilla virtual model with an extracted first premolar was created from human computed tomography data. Accurate brackets and an 0.018" archwire were placed to model canine retraction under 0.5N and 1.0N of retraction force. A two-tooth substructural model was isolated to examine the importance of surrounding geometry. Additionally, mesh size and periodontal ligament (PDL) elastic modulus were varied to examine the effect on predictions. Comparisons were made to previously published clinical data. **Results**: The substructural model decreased computational load, but altered maximum stress up to 16.4%. Coarse mesh sizing affected displacement results up to 22% and maximum stress up to 47%. No PDL stiffness was able to accurately represent the clinical data. **Conclusions**: Modeling canine retraction was partially achieved, highlighting the importance of mesh sizing and the need to incorporate remodeling.

ACKNOWLEDGEMENTS

TABLE OF CONTENTS

LIST OF TABLES

LIST OF FIGURES

LIST OF ABBREVIATIONS

2D – Two-dimensional

3D – Three-dimensional

CAD – Computer Aided Design

CAM – Computer Aided Manufacturing

ε – Strain, change in length over initial length (technically engineering strain)

E – Elastic Modulus, Youngs Modulus

FE – Finite Element

FEA – Finite Element Analysis

FEM – Finite Element Modeling

FJORD – Full Jaw Orthodontic Dentition, UNC Copyright, Ko Lab 2011

GPa – Gigapascal = 10^9 Pascals

M/F – Moment-to-Force ratio

MPa – Megapascal = 10^6 Pascals

NURB – Non-uniform Rational B-Spline. Mathematical equation used to help model complex surfaces.

OTM – Orthodontic Tooth Movement

Pa – Pascal, N/m^2, SI unit for pressure and stress

PDL – Periodontal Ligament

μCT – Micro-computed tomography

$\mu\varepsilon$ – microstrain, $10^{-6}\ \varepsilon$

v = Poisson's Ratio

I INTRODUCTION

I.i. Overview

Efficient orthodontic treatment relies on properly understanding how the dentition responds to applied force, yet a comprehensive explanation of tooth movement has been an elusive goal. Humanity first demonstrated an awareness that prolonged force can cause tooth movement as early as 1000 BC, when primitive orthodontic appliances were described by the Greeks and Etruscans (Corruccini & Pacciani, 1989). Written accounts can be found dating from 1728, when Pierre Fauchard introduced the "Bandeau" appliance in his book "The Surgeon Dentist" (Fauchard, 1728). While development of these appliances demonstrated an early understanding that the duration of force application was important in tooth movement, modern orthodontics did not truly begin until Edward Angle introduced appliances precise enough to closely control forces applied to the dentition (Proffit et al., 2007).   Angle's progression from appliances such as the E-arch to the edgewise bracket provided the first mechanism of applying complex force systems to the dentition, allowing more controlled tooth movement.

Since the introduction of the edgewise bracket, our understanding of the biomechanics of tooth movement has grown remarkably. Advancements in the areas of bone biology, periodontal ligament (PDL) properties, and the influence of orthodontic force magnitude and duration have dramatically influenced the orthodontic profession. Providing efficient orthodontic care with minimal side effects requires not only an appreciation of these

biological advancements, but also an understanding of the mechanics required to provide ideal applied loads. The sections below review developments in orthodontic biomechanics and computational techniques that may dramatically improve our understanding of how teeth respond under applied load.

I.ii. Developments in the biology of orthodontic tooth movement

Orthodontic force applied to the dentition exerts load to both the PDL and surrounding alveolar bone. Traditionally, the loading of the PDL has been considered more important and is frequently described by the pressure-tension theory, due to a "pressure side" (bone resorption) and a "tension side" (bone formation) seen histologically (Oppenheim, 1911; Sandstedt, 1904; Schwarz, 1932). In this theory, pressure changes within the periodontal ligament (PDL) cause alterations in blood flow, leading to the production of chemical messengers that activate cell metabolism. The end result in this pathway is the differentiation of osteoblasts and osteoclasts. However, excessive forces will cut off blood flow to the PDL, causing hyalinization (Schwarz, 1932). This necrotic tissue must be removed, leading to undermining resorption and temporarily decreased tooth movement. Additionally, excessive forces may lead to an increase in root resorption (Hohmann et al., 2007; Hohmann et al., 2009; Reitan, 1967).

While the pressure-tension theory describes the response of the PDL to applied force, Julius Wolff recognized as early as 1892 that applied force on bone can alter its final architecture (Wolff, 1892). Many other studies have since documented that bone density and architecture can be affected by applied forces (Burr et al., 1989; Charras et al., 2001; Frost, 2004; Ilizarov, 1989a; Ilizarov, 1989b; Melsen, 1999). Perhaps the most dramatic example

of this is distraction osteogenesis, as first described by Ilizarov (Ilizarov, 1989a; Ilizarov, 1989b). Granted, in distraction osteogenesis, a macroscopic defect is created, and then the resulting callus is stressed, so a different biological process is occurring compared to traditional remodeling. However, Wolff's Law states that applied load will cause bone to remodel regardless of a macroscopic fracture or cell activation in an adjacent PDL. Strain levels in bone can cause a loss of bone density, maintenance of bone density, an increase in bone density, or fatigue fracture of bone (Table 1) (Frost, 2004).

Table 1: Summary of the adaptive response of bone based on applied load (Wolff's Law) (Frost, 2004).

Bone response	Strain level within bone
Loss of bone density	<50-100 $\mu\epsilon$
Maintenance of bone density	50-100 $\mu\epsilon$ to 1000-1500 $\mu\epsilon$
Increase in bone density	1000-1500 $\mu\epsilon$ to ~3000 $\mu\epsilon$
Fatigue fracture of bone	>3000 $\mu\epsilon$

Current orthodontic research found that strains in alveolar bone, not just the PDL, are important in orthodontic remodeling (Baumrind, 1969; Melsen, 1999; Williams & Murphy, 2008). As early as 1969, Baumrind noted when testing three independent samples of 33 rats that the pressure-tension theory did not fully explain his findings. Changes in the rate of cell replication in the PDL, general metabolic activity, and rate of fiber synthesis were assessed during the first 72 hours after an elastic wedge was placed between the first and second maxillary molar. No significant differences were found in metabolic activity on the pressure or tension side and the amount of tooth displacement was found to be nearly ten times the measured change in the PDL. This suggests that bending of bone is also important.

Another study highlighting the importance of strain within the alveolar bone examined orthodontic tooth movement in five *maccaca fascicularis* monkeys, showing

formation of woven bone and increased bone density at a distance from the alveolus (Melsen, 1999). Melsen hypothesized that direct resorption is due to unloading of the pressure placed on bone by the PDL, while indirect resorption (undermining resorption) is due to sterile necrosis. Since all these reactions are consistent with Wolff's Law, it also helps explain the formation of woven bone, since the alveolar wall is flexed under loading. Williams and Murphy took histological samples from two selected cases in which large amounts of alveolar expansion was accomplished using a fixed "alveolar development appliance," showing new formation of woven bone (Williams & Murphy, 2008).

Overall, it can be concluded that both pressure changes within the PDL and within alveolar bone are important in orthodontic tooth movement. Unfortunately, the exact loading achieved by orthodontic appliances and the exact reaction of the tissue is nearly impossible to non-destructively evaluate *in vivo*.

I.iii. Properties of the periodontal ligament (PDL)

Multiple studies have examined the mechanical properties of the PDL, eventually leading to complex viscoelastic models for PDL behavior under load (Poppe et al., 2002; Toms et al., 2002; Toms & Eberhardt, 2003; Nekouzadeh et al., 2007; Slomka et al., 2008; Zhao et al., 2008; Qian et al., 2009). The most simple assumption is bilinear behavior with two different Young's Moduli assigned to the PDL (Poppe et al., 2002; Natali et al., 2004). Linear viscoelastic models are slightly more complex, with the viscoelastic behavior directly proportional to the applied load. This has been show in the literature using two elastic spring constants and a damping constant, which must be defined (Slomka et al., 2008). Viscoelastic models with higher complexity include many more terms and constants that must be defined,

4

such as a third-order generalized Mooney-Rivlin model (Qian et al., 2009), a three-parameter Maxwell model (Qian et al., 2009), or a linear convolution integral model (Nekouzadeh et al., 2007). The computational requirements of these more complex models place them beyond the scope of the current study.

High stress to a tooth causes undermining resorption. Thus, when the tooth begins movement again, it becomes rather loose in the socket (Reitan, 1967). Clinicians qualitatively observe this change, but no studies have yet precisely calculated this change in mobility during orthodontics. Therefore, accurate computer modeling of the PDL becomes challenging, as discussed in detail later.

I.iv. Influence of force magnitude and duration on tooth movement

Clinicians generally closely manage force levels during orthodontic treatment. However, the last systematic review of the literature stated that "no evidence-based force level could be recommended for the optimal efficiency in clinical orthodontics" (Ren et al., 2003).

Many clinical studies have been done to examine the influence of force magnitude in orthodontic treatment (Hixon et al., 1970; Boester & Johnston, 1974; Andreasen & Zwanziger, 1980; Ren et al., 2003; Hayashi et al., 2006). Although experienced clinicians have recommended force levels for specific movements (Table 2), there is conflicting scientific evidence as to what is considered an ideal force for movement (Figure 1) (Ren et al., 2004), and how teeth respond to different force levels (Quinn & Yoshikawa, 1985). In addition, many studies limited their measurements of tooth movement to a single measure in a horizontal direction (Andreasen & Zwanziger, 1980; Hixon et al., 1970). While the

experimental setups in these studies were optimized to minimize side effects, tipping and

rotations were likely not fully eliminated.

Table 2: Summary of guidelines for recommended force levels for orthodontic movement. Adapted from Proffit 4th Ed (Proffit et al., 2007) *Note, these are merely guidelines, as proper scientific evidence is still lacking.

Type of movement	Force (gm)
Tipping	35-60
Bodily movement (translation)	70-120
Root uprighting	50-100
Rotation	35-60
Extrusion	35-60
Intrusion	10-20
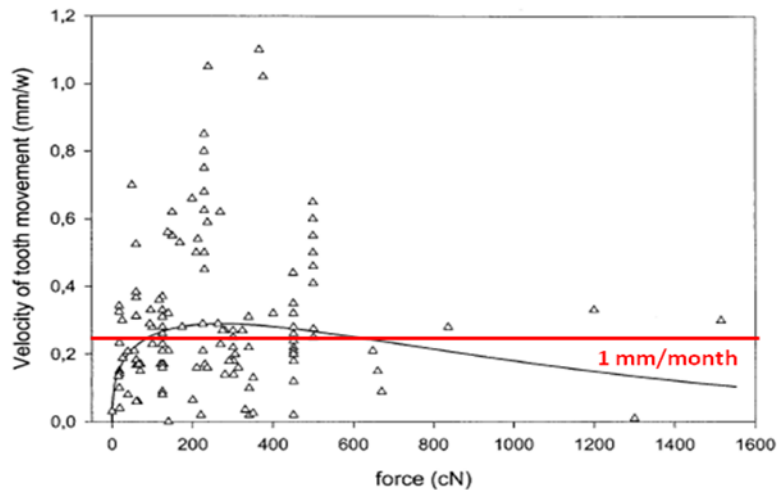
Figure 1: Summary of clinical data for velocity of tooth movement versus force (Ren et al., 2004).

I.v. Current mechanical prediction of orthodontic loading and its limitations

From a mechanical perspective, orthodontic force systems can be very complex,

typically including 14 teeth and brackets per arch. With this many deflections in an

archwire, the force system becomes statically indeterminate, so a clinician cannot accurately

predict force levels using free-body diagrams and the principles of statics. Additionally, the contribution of friction and binding to the force system is difficult to predict.

As previously discussed, Ren et al. (2003) concluded in a recent systematic review that no ideal force level could be recommended in orthodontics based on the current literature. This may be due to the fact that current literature typically records merely the magnitude of space closure that results from an applied force level. Closer examination of the interaction between orthodontic force and tooth movement requires knowledge of how applied force creates stress and strain in the surrounding tissue, and full understanding of how the tooth moves in three planes of space under the applied load. Careful clinical studies and detailed impressions can record detailed tooth movement, but non-destructive *in vivo* techniques for measuring stress and strain in the PDL and surrounding bone do not exist.

An engineering technique known as finite element analysis (FEA), which uses the principles of solid mechanics on a virtual model, has been developed that can bridge this gap. This technique is growing in popularity in orthodontics, due to its ability to show internal strains and to solve statically indeterminate force systems (Nikolai, 1975; Poppe et al., 2002; Cattaneo et al., 2005; 2009a; 2009b; Hohmann et al., 2009). However, the predictions from FEA depend greatly on the assumptions made in creating the model, especially properties of the PDL, contact conditions, and boundary conditions (Cattaneo et al., 2009a).

I.vi. Finite element analysis

Although direct measurements cannot be taken *in vivo* at any point within a biological structure, the theorems of solid mechanics and elasticity theory allow calculation of internal stresses if the loading, geometry, and material properties are known. The computational

technique that can accomplish this is known at finite element analysis (FEA). This technique

divides a virtual structure into discrete elements. Specific material properties are applied,

boundary conditions are set, and approximate solutions can be found using the Ritz method

of numerical analysis (Jones et al., 2001). This method can directly calculate approximate

solutions for the complex matrix of partial differential equations and associated boundary

conditions set during FEA. The solution includes calculated stress and strain at any point

within the geometry.

Although this technique was originally employed for relatively simple two-

dimensional (2D) objects, recent advances and technological improvements have allowed for

more complex, three-dimensional (3D) geometries to be analyzed. The technique is growing

in popularity in dentistry since its introduction by Farah in 1973 (Farah et al., 1973).

Currently, multiple complex dental models have been published, showing dramatic

improvements over the roughly meshed 2D initial models. Recent advancements in

orthodontic FEA fall under two broad categories: improved modeling of biological structures

and improved modeling of orthodontic appliances.

Multiple researchers have worked on improved modeling of biological structures.

Probably the most significant studies were the series of papers published by Cattaneo

between 2005 and 2009 (Cattaneo et al., 2005; 2008; 2009a; 2009b).   In the initial study,

sequential 2D layers from a μCT scan (37 micron voxel size) were stacked to create a high

quality 3D model of two maxillary anterior teeth. Additionally, the internal trabeculation of

the alveolar bone was traced – allowing separate material properties to be assigned to the

high and low density areas. The final model was meshed using 10-node tetrahedral elements,

yielding a final mesh with 197,186 elements and 253,309 nodes. Using this model, three

different PDL properties were examined: a low stiffness linear modulus (0.044 MPa), a high

stiffness linear modulus (0.17 MPa), and a non-linear modulus that was nearly zero under

compression (Figure 2). The resulting stress in various levels of the PDL and alveolar bone

was vastly influenced by whether a density-based modulus for bone utilizing the traced

internal structure or a single averaged modulus for bone was used. Additionally, the different

PDL assumptions were also found to vastly influence the resulting stress in the PDL and

bone.
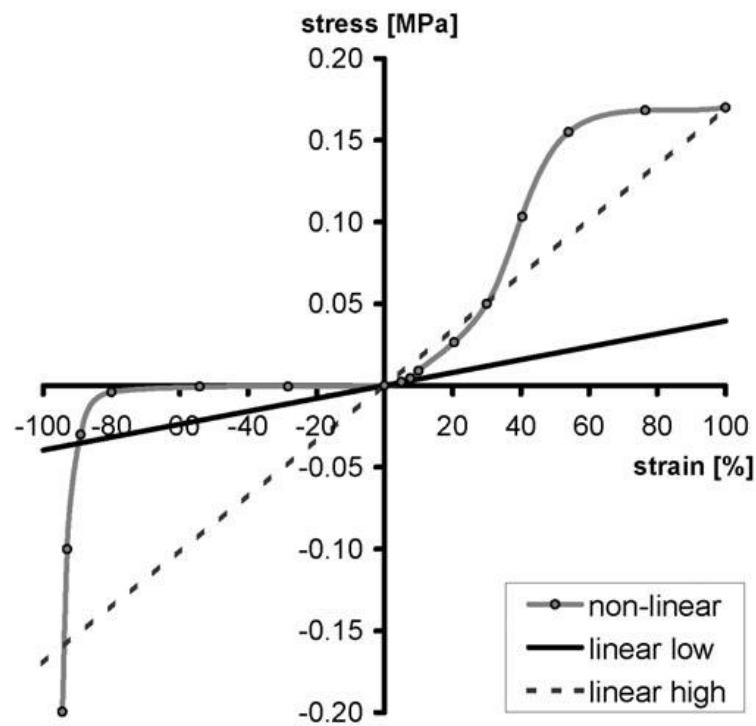
Figure 2: Different values for the PDL elastic modulus modeled by Cattaneo et al. (2004).
Note the non-linear modulus showing minimal PDL stiffness in compression.

Continued research on the previous two-tooth model further examined the effects of

moment-to-force (M/F) ratios on the stress and strain generated in the PDL (Cattaneo et al.,

2008). The results of the study were unable to confirm the traditional M/F ratios predicted to

produce bodily movement based on the length of the tooth root. Interestingly, it found that

the required M/F ratio to produce bodily movement varied by force level. This result

appeared to defy standard mechanical principles, but makes sense in terms of the non-linear PDL behavior used in the study (Figure 2), with minimal PDL stiffness initially in compression.

The final study published by Catteneo's group investigated the response of anterior and posterior teeth under different loading conditions (Cattaneo et al., 2009b). Uncontrolled tipping, translation, and occlusal forces were tested separately on a two-tooth anterior and two-tooth posterior model. The traditional theory of distinct pressure and tension zones causing bone resorption and deposition, respectively, was not observed. Very little compressive stress was seen until the dentin nearly was touching the alveolar bone. However, this was due to the nonlinear assumption used in the study, with a very low Young's Modulus for the PDL until the two surfaces were nearly touching. Interestingly, little data on PDL strain was reported, which may have been more appropriate on the pressure side. Additionally, the authors tested a separate model using a generic block of bone as opposed to accurate geometry. They reported a significantly different stress distribution, highlighting the importance of anatomically accurate models.

In another study advancing the ability of FEA to model biological complexity, Jones et al attempted to correlate the *in vivo* tooth displacement allowed by the PDL with FEA properties (Jones et al., 2001). The clinical study was run very well, using a laser to measure tooth displacement in ten healthy volunteers with 0.39 N of load placed on the facial surface of the central incisor. Measurements were taken every 0.01 seconds, but the study was only run for one minute (10 seconds of pre-loading, 30 seconds of loading, and 20 seconds of relaxation), so the full extent of changes during orthodontic tooth movement was not observed. The initial displacement of the central incisor was correlated to a FEA model with

an approximate modulus of elasticity of 1 N/mm^2 (1 MPa) and a Poisson's Ratio of 0.45 for the PDL. The FEA was conducted using a generic model with a fairly rough mesh, but this remains one of the few studies to correlate *in vivo* findings with FEA results. Since correlation with *in vivo* findings is essential to verifying the accuracy of FEA assumptions, this study remains valuable.

No previous studies analyzing orthodontic loading of the dentition using FEA have confirmed that true orthodontic loading can be modeled without the inclusion of accurate orthodontic appliances, yet accurate appliances are found infrequently in the literature. Several studies have examined torque control and center of resistance of incisors by placing loads directly onto the tooth structure, using a rough mesh, and keeping teeth bonded relative to each other (Reimann et al., 2007; Liang et al., 2009). Some recent studies have added tooth attachments, although frequently they did not accurately mimic orthodontic brackets, but merely incorporated generic rectangular blocks (Field et al., 2009).

It appears from the results of recent studies that adding complexity and some appliance geometry will clearly influence results, but care must be taken to closely analyze how the appliances are used. A recent study using a rough bracket design compared orthodontic tooth loading using a single tooth and using a three-tooth model, finding significant differences in stress and strain distribution with the three-tooth model (Field et al., 2009). This highlights the importance of mimicking at least the closest neighboring tooth when applying orthodontic forces, which some studies ignore. One recent study even shows a visually pleasing full maxillary model, yet analysis of miniscrew loading was done using a bulk block of bone without accurate geometry (Jasmine et al., 2012).

11

When examining FEA solutions, it is imperative to examine the mesh convergence as well. Unfortunately, few studies have examined this in dentistry and no studies have examined the effects of mesh density in orthodontics. Two dental articles highlight the issues of using a single mesh size (Schmidt et al., 2009; Bright & Rayfield, 2011). Schmidt el al found dramatic issues with convergence of the maximum von-Mises stress when examining orthodontic miniscrews using implicit calculations (Schmidt et al., 2009). Convergence using the explicit solver, however, was obtained relatively quickly. Pull-out velocity of the miniscrew was found to influence mesh convergence, but density had a negligible effect. Bright and Rayfield examined a domestic pig skull meshed to 18 different densities (Bright & Rayfield, 2011). Forces were applied to the model at the insertion points of the temporalis and masseter muscles, modeling muscle loading of the skull structure. Linear and quadratic tetrahedral elements were both used and did not significantly alter the rate of convergence. Convergence typically occurred to within 5% by a 0.92 mm mesh sizing (total of 1,750,000 elements), but in some occasions occurred with as rough as a 2 mm mesh density (250,000 elements). Models with insufficient mesh density underestimated strain and displacement, leading to inaccurate results and conclusions. Both studies agree that mesh convergence is acceptable if < 5% variation occurs with further mesh refinements.

Despite these significant improvements, no current model combines accurate dental anatomy for the complete dentition with detailed orthodontic appliances allowing various contact conditions. Without this combination, these models still fall short of the complexity required for comprehensively examining orthodontic tooth movement. Therefore, we aim to create a model combining accurate anatomy, orthodontic appliances, adequate mesh density and accurate boundary conditions to model orthodontic loading.

I.vii. Well-controlled clinical data on canine retraction.

Well controlled clinical data was obtained by Hayashi at the Health Sciences University of Hokkaido, Japan. (Hayashi et al., 2006) This study consisted of 10 patients (4 males, 6 females, 19.4 – 29.2 years old), who required upper premolar extractions and retraction of maxillary canines with absolute anchorage. Osseointegrated midpalatal implants (Institute Straumann AG, Waldenburg, Switzerland) were used to provide anchorage. The implant was connected to the maxillary first molars through a 1.2 mm^2 (~0.048" diameter) transpalatal arch with three steel ball bearings for fixed reference points throughout treatment (Figure 3).
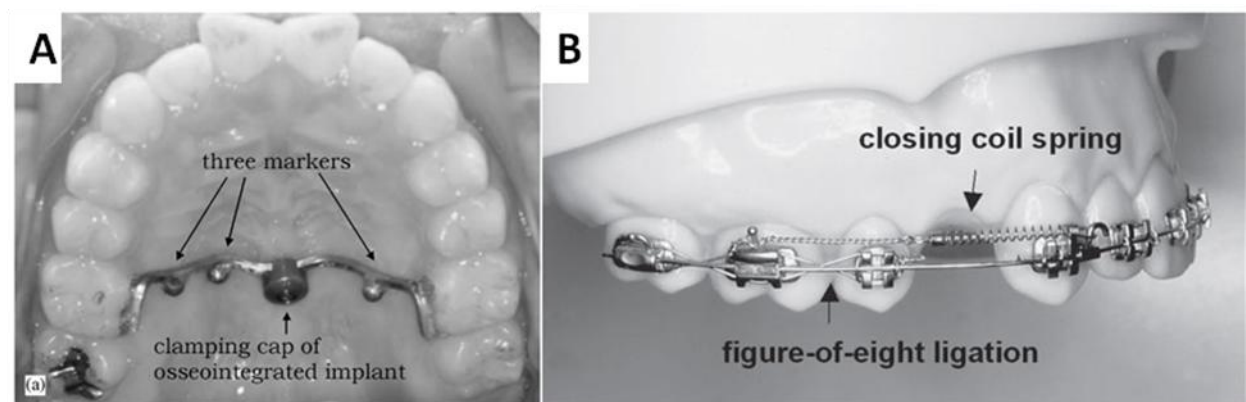
Figure 3: A. Clinical setup in Hayashi study (2006), with TPA placed with fixed reference points. B. Side view of clinical setup showing activation of NiTi coil spring.

Sliding mechanics were used for space closure. A 0.018" stainless steel continuous archwire with a NiTi closed-coil spring (Sentalloy, Tomy International Inc, Tokyo, Japan) was used on all patients. The coil was placed from the maxillary first molar to maxillary canine bilaterally. On the right side, a 0.5N (black) coil was used, while a 1N (blue) coil was placed on the left side. The force level of each spring was confirmed with a dial tension

gauge (Mitutoyo, Kawasaki, Japan). Each week the springs were reactivated to 12 mm to

keep a constant force on the canine (either 0.5N or 1N).

Along with reactivating the appliances, hydrophilic vinyl polysiloxane impressions

(JM Silicone, J. Morita, Tokyo, Japan) were taken every week. They were poured in die

stone (Noritake super rock, J.Morita, Tokyo, Japan) and scanned with a slit laser beam

(VMS-150RD, UNISN, Osako, Japan) to provide 3D digital models of the maxillary arch.

The movement of the canine was measured from these virtual models using two different

systems (Figure 4). In the XYZ system, the translation and rotation in all three planes of

space (X, Y, and Z) were calculated as seen in Figure 4a. This method is relatively easy to

understand for clinicians, as it highlights the movements and side effects in each direction.

The other method calculated the finite helical axis (FHA) of the movement, as shown in

Figure 4b. This is essentially the "center of rotation" for a 3D object. The calculated

parameters are the direction vector of the helical axis (v_x, v_y, and v_z), the rotation around the

axis (θ), the translation around the axis (t), and the distance from the axis to the object (d).

Therefore, it provides excellent biomechanical analysis of tooth movement, yet is more

difficult for clinicians to quickly understand.
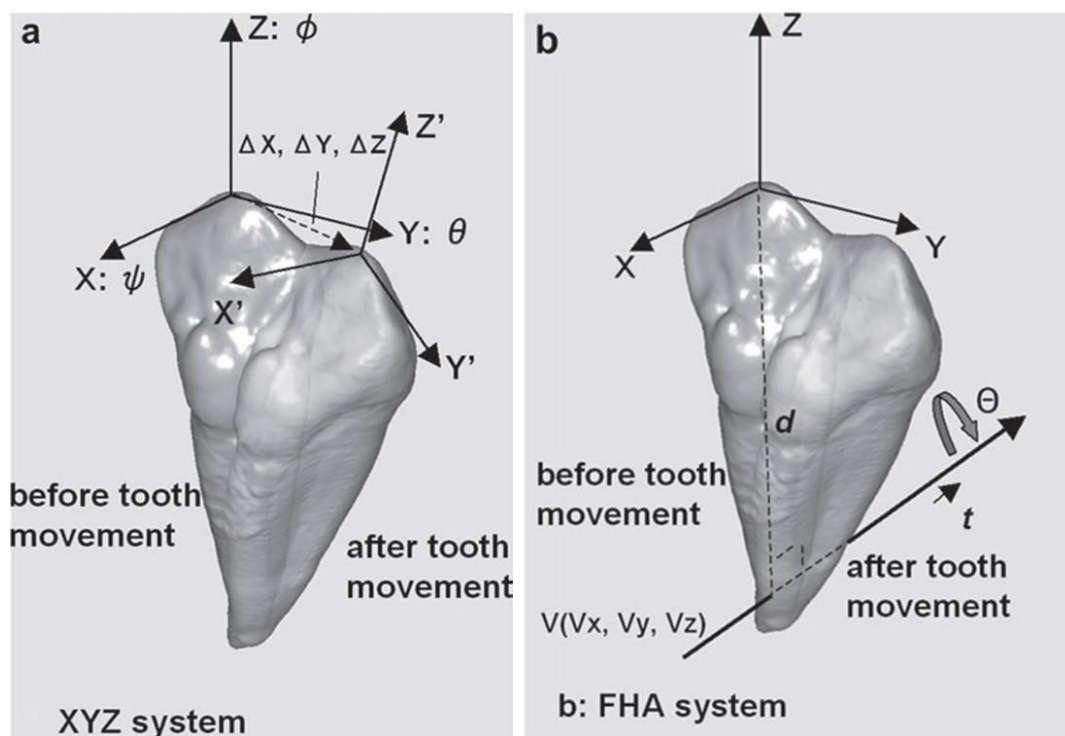
Figure 4: The XYZ system (A) and FHA system (B) used by Hayashi to calculate tooth movement and side effects during canine retraction (Hayashi, Uechi, Lee, & Mizoguchi, 2007).

The results from this study are shown in Table 3 (XYZ system) and Table 4 (FHA system). No difference in the amount of distal movement was seen between the 0.5N and 1N group. However, this study found increased distal tipping in the 1N group. Additionally, looking at the direction vector of the FHA, significant differences were seen in v_x and v_y, which essentially corresponds to tipping and flaring of the canine. These results clearly illustrated a biomechanical difference in retraction with 0.5N versus 1N of force.

Table 3: XYZ clinical data from Hayashi et al (Hayashi et al., 2007)

XYZ system parameters	0.5 N		1.0 N		P	
	Mean	SD	Mean	SD		
Distal Movement of canine crown tip (mm)	3.16	0.60	3.39	0.70	0.236	NS
Tipping angle ψ of canine (degrees)	6.99	2.10	8.22	2.23	0.048	*
Flaring angle θ	-1.39	2.12	-1.54	1.22	0.583	NS
Rotation angle φ of canine (degrees)	4.11	4.79	4.30	7.62	0.824	NS

*$P < 0.05$.   NS, not significant.

Table 4: Finite Helical Axis (FHA) data from Hayashi et al (Hayashi et al., 2007).

FHA system parameters	0.5 N		1.0 N		P	
	Mean	SD	Mean	SD		
Distal Movement of canine crown tip (mm)	3.17	0.60	3.38	0.71	0.199	NS
Rotation around the FHA θ (degrees)	12.24	2.14	12.91	2.30	0.478	NS
Translation along the FHA t (mm)	0.37	0.17	0.29	0.13	0.223	NS
Shortest distance from the space coordinate origin to the FHA d (mm)	14.63	7.54	14.74	8.01	0.877	NS
Direction vector of the FHA v_x	-0.25	0.22	-0.57	0.20	0.048	*
Direction vector of the FHA v_y	0.61	0.21	0.37	0.22	0.042	*
Direction vector of the FHA v_z	0.61	0.29	0.58	0.30	0.234	NS

*$P < 0.05$.   NS, not significant.

Although this study provides excellent controlled clinical data, these results do not provide data on the stress and strain within the PDL and alveolar bone. Therefore, comparing this data with an accurate FEM could further improve our understanding of orthodontic tooth movement.

I.viii. Hypothesis

We hypothesize that biomechanical parameters calculated from a finite element model of sufficient complexity can be correlated to well-controlled clinical data for tooth movement.

This study focused on four specific aims:

1. To create a complete maxillary biomechanical model capable of analyzing orthodontic canine retraction using absolute anchorage.

2. To isolate a workable substructural model for comparison to a complete maxillary model.

3. To determine the effects of model size, mesh sizing, accurate orthodontic appliances, and periodontal ligament linear elastic modulus on the resulting finite element predictions.

4. To compare calculated tooth movement during initial loading with controlled clinical data provided by Hayashi.

II. METHODS AND MATERIALS

II.i. Creation of a complete maxillary biomechanical model.

Construction of a working finite element model involves many steps and is especially difficult for organic objects. Many engineering models, such as cars or bridge trusses, can be directly created in a computer-engineering design (CAD) program. However, organic structures are typically too complex to be created *de novo* in a CAD program. Rather, they must be reverse engineered by digitization of the organic structure itself. Currently, computed tomography (CT) scans are the ideal method of acquiring this data. Optical laser scans are also common, but will only capture surface data.

For this study, accurate geometry for maxillary teeth was generated from micro-computed tomography (µCT) scans of previously extracted teeth without any unusual geometry, previous restorations, or decay present. The pulp, dentin, and enamel outlines were identified on sequential slices of the µCT scan and then stacked to create a solid body. The geometry of the supporting bone was determined from a previously obtained human cone-beam computed tomography (CBCT) scan with no evident bony pathology. Again, by examining sequential slices, the maxilla was differentiated into cortical bone, trabecular bone, and sinus.

Following this segmentation, additional steps are required to prepare a model for CAD programs. FEA requires closed solid bodies – in other words, each part of the model should be able to hold water. Typical CT segmentations yield polygon surfaces with

18

irregularities and potential holes. A program capable of manipulating these polygons and creating solid CAD bodies is required, such as Geomagic (Geomagic USA, Morrisville, NC, USA)

Although segmentations may initially appear very accurate (Figure 5a), there are often many small irregularities that must be addressed (Figure 5b). Obviously, organic objects will have natural irregularities that may be important to maintain, but defects from the scanning and segmentation process must be removed. Automated processes in Geomagic such as "mesh doctor" can identify problematic areas (Figure 5b) and fix many minor problems. For larger defects, defeaturing may be required. Defeaturing involves removal of problematic geometry and recreating the surface morphology based on the surrounding surface topology. When used on small areas of irregularity, this technique may be highly effective, but should be limited to small regions to avoid loss of important topology. Once the gaps in the surface have been filled, some degree of smoothing is typically beneficial. Excess surface detail that will not affect results only increases the file size, meshing times, mesh density, and solution times. To improve surfacing, a surface mesh on the order of 200,000 polygons is recommended. Geomagic has a tool ("optimize for surfacing") that redistributes the polygons nodes on the surface to create a more ideal distribution for surfacing (Figure 5c). Following these optimization steps, it is important to compare the final surface to the initial surface to verify that no significant changes were made. Further discussion of geometry manipulation in Geomagic can be found in Appendix 1.
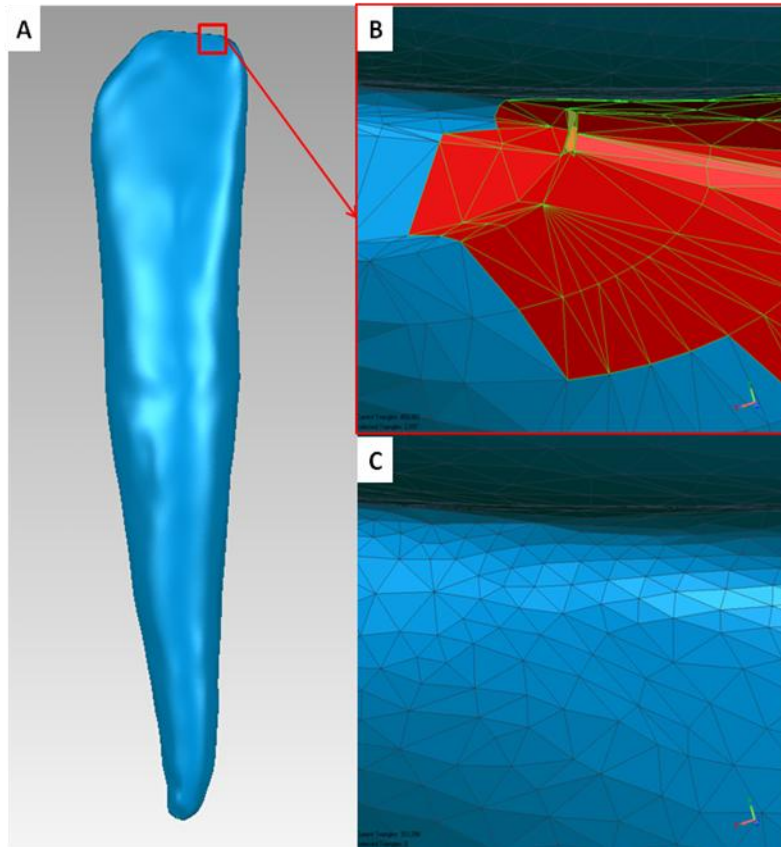
Figure 5: Although initial geometry following segmentation can appear smooth (A), many small defects are present that Geomagic will highlight in red using "mesh doctor" as potentially problematic (B). Following closing gaps, smoothing, minor defeaturing, and optimization for surfacing, the polygon mesh is greatly improved (C).

With the optimized surfaces prepared using the previous steps, closed solid bodies can be created. Although the final bodies with proper interior and exterior surfaces can be created at this stage, we have observed that closing each exterior surface independently and using Boolean subtraction in the CAD program typically improves results (see Appendix 2 for more details). For example, this forces the interior surface of the enamel to precisely match the exterior of the dentin. If the Boolean operations are done prior to surfacing rather that in the CAD program, minor differences in creating the NURB (non-uniform rational B-splines) mathematical approximation of the surfaces may affect the connectivity of the objects. Some research labs (e.g. Bright and Rayfield 2011) will simply transfer the polygon

surfaces over to a FEA program for analysis without using a CAD program. This can be very

effective for relatively simple models, but when multiple solid bodies are included and

various mesh densities are required this process becomes cumbersome.

To use a CAD program with organic structures, a mathematical approximation of the

surface must be generated from the polygon mesh surface. This is typically done with

NURB surfaces, so the solid can be saved as in a standard .iges or .step file format. This

process involves multiple steps – laying out patches, creating grids within these patches,

optimizing the surface detail with grids, and finally creating the NURB surface (Figure 6,

discussed in detail in Appendix 1). Surfacing must be done carefully, as incorrectly laying

out the patches on the surface or not allowing sufficient detail may severely distort the

surface. In the end, the surfaced body should be free of problematic geometry, such as sliver

faces, small faces, or small edges.
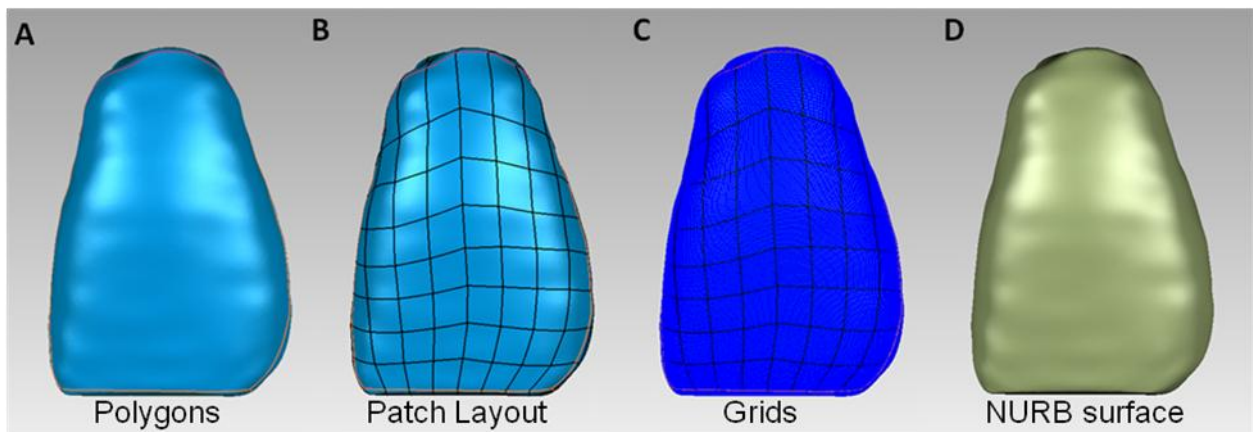
Figure 6: Process of NURB surface generation using Geomagic. A. Contour lines are
defined that follow the natural geometry - in this case, line angles were used. B. Patches
were constructed and shuffled to create a clean grid pattern. C. Grids were created within
each patch. D. NURB surfaces are created by placing control points along the created grids.

It is suggested that these NURB surface bodies be imported into a true CAD program

for preparation. FE software or other platforms with limited CAD tools typically do not

provide the full range of features required to manipulate these complicated organic models.

Therefore, the use of a genuine CAD program is typically preferred for detailed characterization of the material and its contact correlation with surrounding structures. In this study, Solidworks 2010 (Solidworks Corp., Concord, MA, USA) was utilized for all CAD manipulation of the model – further details may be found in Appendix 2.

To model the appliances, 0° CAD brackets with accurate geometry will be placed on the facial surfaces of the teeth. A straight wire was placed through the brackets and virtual coil springs (0.5N and 1 N) to retract the canine were modeled by forces applied to the canine and molar bracket hooks. The interface between the wire and bracket was set to a contact mode, which is more difficult to model virtually than a bonded contact due to non-linear behavior and lack of corresponding nodes across the interface. However, it more accurately describes the interaction clinically. No previous studies could be found where this has been done for a half-maxilla model.

Figure 7 portrays the final half maxilla model, which incorporates the design features described above. Although Figure 7 initially appears similar to other finite element models shown in the literature, it provides several significant advantages over previous model designs, including:

- It contains minimal problematic geometry. There are no sliver faces (very small in one dimension), small edges (less than expected mesh size), flipped normals, or gaps. This enhances reliable meshing with various mesh sizes.

- An ability to manipulate contact conditions and boundary conditions. The assembled model contains 43 separate bodies with numerous interfaces still present – not a single part. This allows a finite element program to manipulate these interfaces and add nonlinear contact conditions (friction or frictionless contacts, not just bonded).

- Ideal connectivity. Bodies were created to ensure ideal contact conditions as summarized in Table 5.
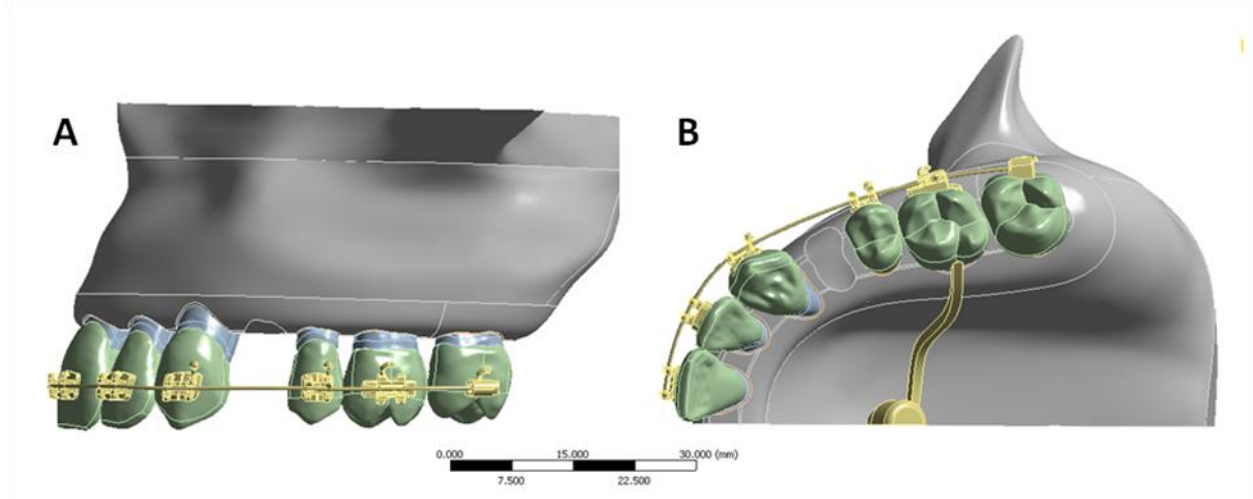
Figure 7: Final half maxilla model created after smoothing and surfacing in Geomagic and CAD manipulation in Solidworks. Note the significant improvements of this model noted in the text.

Table 5: Description of techniques used to ensure ideal connectivity of the model.

Interface	Technique used to create interface	Potential Error
Enamel/Dentin	Boolean subtraction	None
Enamel/Enamel (Interproximal regions)	Visual removal of overlap in Geomagic	No Penetration, Minimal Gap
Dentin/Pulp	Boolean subtraction	None
Dentin/PDL	Boolean subtraction	None
PDL/Cortical Bone	Internal cortical surfaced used for PDL	None
Cortical Bone/Trabecular Bone/Sinus	Trabecular bone remade using internal surfaces of cortical bone and sinus	None
Bone/Palatal Miniscrew	Boolean subtraction	None
Palatal Miniscrew/TPA/ First Molar Enamel	Wire extruded into miniscrew and enamel, then Boolean subtraction	None
Bracket/Enamel	Bracket base extruded into enamel, then Boolean subtraction	None
Bracket/Wire	Wire created using bracket geometry, but allowing slot of wire	No Penetration, Minimal Gap

Once the biomechanical model geometry was finalized in a CAD program, it was transferred to FEA software. For this study, ANSYS Workbench 13.0 (Swanson Analysis

23

Inc., Huston, PA, USA) was used for the FEA software. One desirable feature of this

software is that it has a direct import tool from Solidworks, so no model detail is lost by

saving into a different file format. Once in ANSYS, the model must be divided into a finite

number of elements, known as the mesh, which can be analyzed. The model was meshed

using 10-node tetrahedral h-elements (ANSYS solid 187), with an 8-node swept hexahedral

mesh for the wire. Mesh parameters used for the complete model are shown in Table 6, and

the created mesh is shown in Figure 8.

Table 6: Mesh sizing used for complete half maxilla model.

Part	Body mesh sizing (mm)
Cortical bone, trabecular bone, miniscrew, TPA, and sinus	2.0
Brackets and wire	0.2
Enamel, dentin, pulp, and PDL	0.8
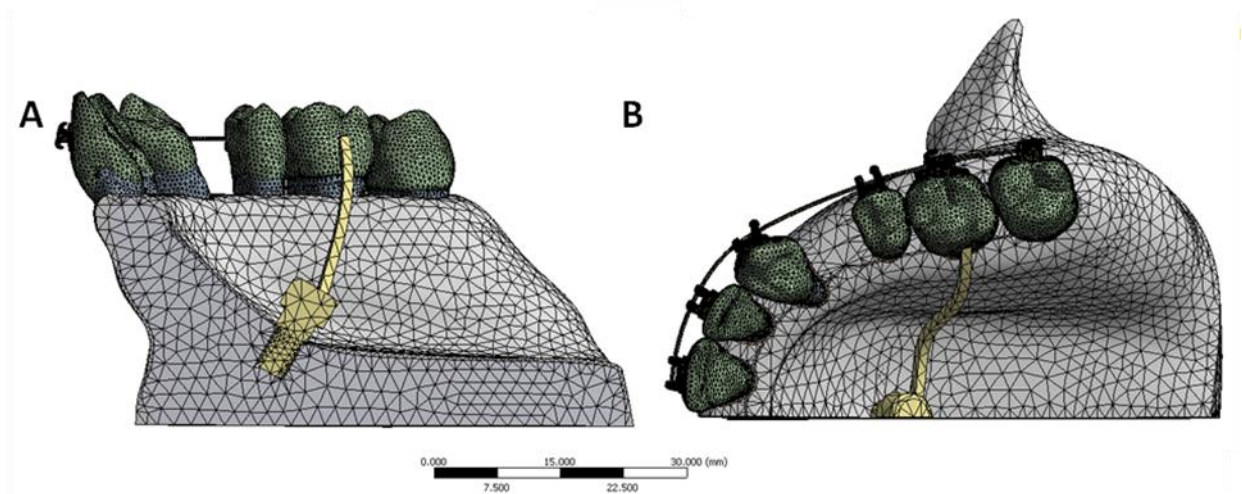
Figure 8: Visual representation of the final mesh for the full maxillary model.

Finally, adequate boundary conditions, material properties, and contact conditions

must be set to obtain a biologically realistic solution for the model. In this case, a fixed

support (allowing no translation or rotation) was applied to the mirror plane at the midline of

the model (Figure 9). Additionally, the mesial surface of the wire was fixed in the x-

dimension to prevent the wire from travelling. This boundary condition for the wire most

24

closely mimics a wire clinically that cannot travel around the arch perimeter but otherwise is unrestrained except for the brackets.

Reported material properties for cortical bone, trabecular bone, periosteum, gingiva, enamel, and dentin were applied to the finite element model (Table 7).   The most difficult material to accurately model is the PDL. Assuming a linear, isotropic response uses the least computing power, but the PDL is actually a viscoelastic material. Previous studies have shown significant differences by using a non-linear response (Cattaneo et al., 2009b). Various assumptions for the PDL elastic modulus were tested to balance accuracy with realistic computational requirements (Table 8) (Poppe et al., 2002; Nekouzadeh et al., 2007; Qian et al., 2009). The various tests performed are described in further detail in Section II.iii.

Table 7: Material Properties for all materials in the model, except the PDL described in Table 8. Both the Poisson's ratio and Young's Modulus (Elastic Modulus, E) are reported. (Bourauel et al., 1999; Jones et al., 2001; Poppe et al., 2002; Toms et al., 2002; Toms et al., 2002; Toms & Eberhardt, 2003; Ziegler, Keilig, Kawarizadeh, Jager, & Bourauel, 2005)

	Poisson's Ratio (v)	Young's Modulus (GPa)
Enamel	0.41	80
Dentin	0.31	18
Pulp	0.30	0.175
Cortical Bone	0.31	13.7
Trabecular Bone	0.30	1.37
Steel	0.30	200
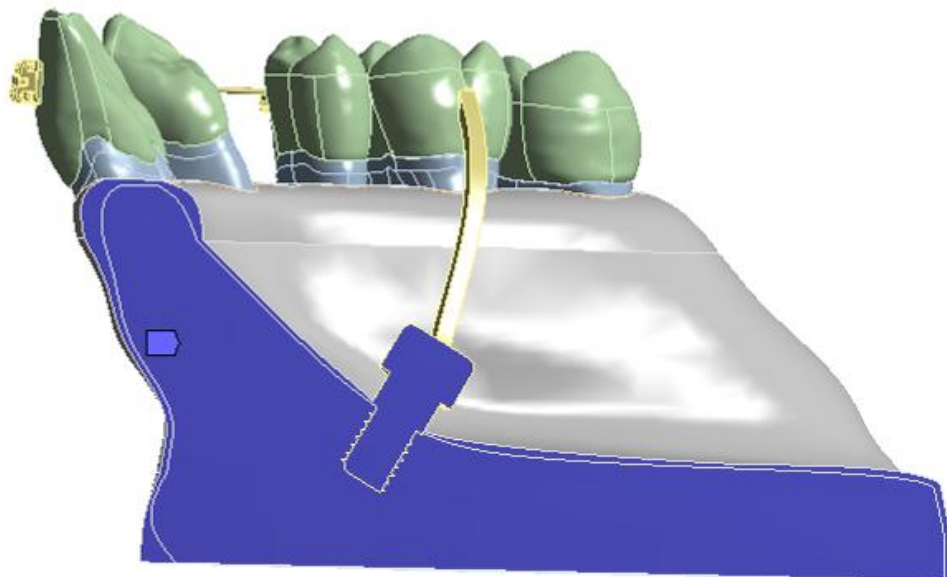
Figure 9: Boundary conditions on the model – showing a fixed support placed on the central mirror plane. The mesial of the wire was also fixed in the x-dimension (unable to cross midline), but no other boundary conditions were applied.

The model was solved under large-displacement assumptions. Post-processing was done to calculate equivalent (von-Mises) stress, equivalent (von-Mises) strain, maximum displacement, resultant force and moment on the canine, and the displacement of 5 different points on the canine crown (Figure 10).
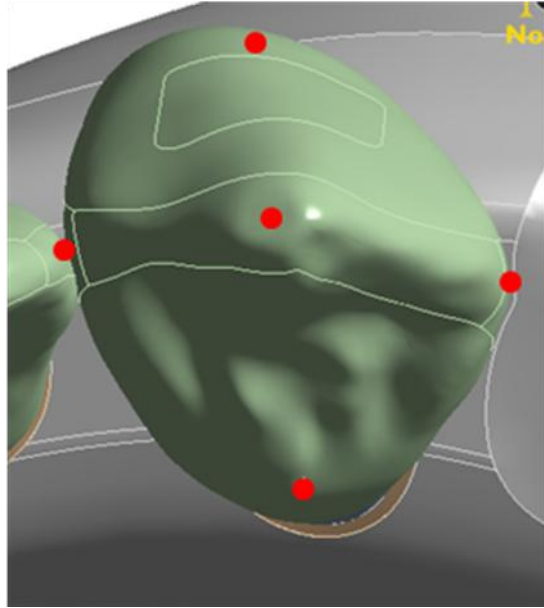
Figure 10: Five displacement probes set on the canine crown to record displacement of various regions of the tooth.

II.ii. Isolation of a two-tooth substructural model

An ideal FE model should represent all essential geometry while eliminating unneeded geometry to reduce the computational requirements. Therefore, a substructural two-tooth model was generated from the half maxilla model to examine whether a limited model can provide adequate information on initial orthodontic tooth loading. This model is shown in Figure 11, with fixed boundary conditions set at both the mesially and distally sectioned surfaces.
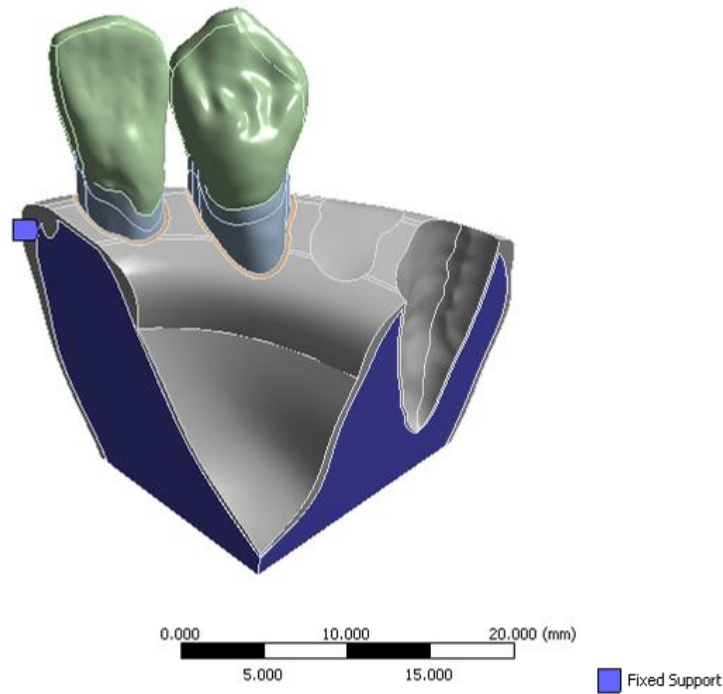
Figure 11: Limited-scope model with two teeth and fixed supports applied at both sectioned surfaces. In this model, the wire was suppressed.

A limited model does allow further manipulation of the mesh density. As previously discussed, the sizing of the mesh elements may have a profound impact on the final results. For that reason, an initial mesh was generated using the same sizing as the complete model, but a higher mesh density was generated for the limited model (Figure 12). This mesh was generated by simply applying a contact sizing of 0.2 mm at the contacts between the PDL and cortical bone, and allowing the program flexibility to accommodate the remaining mesh sizing. This resulted in a mesh with a PDL multiple elements thick – the first found in published literature.
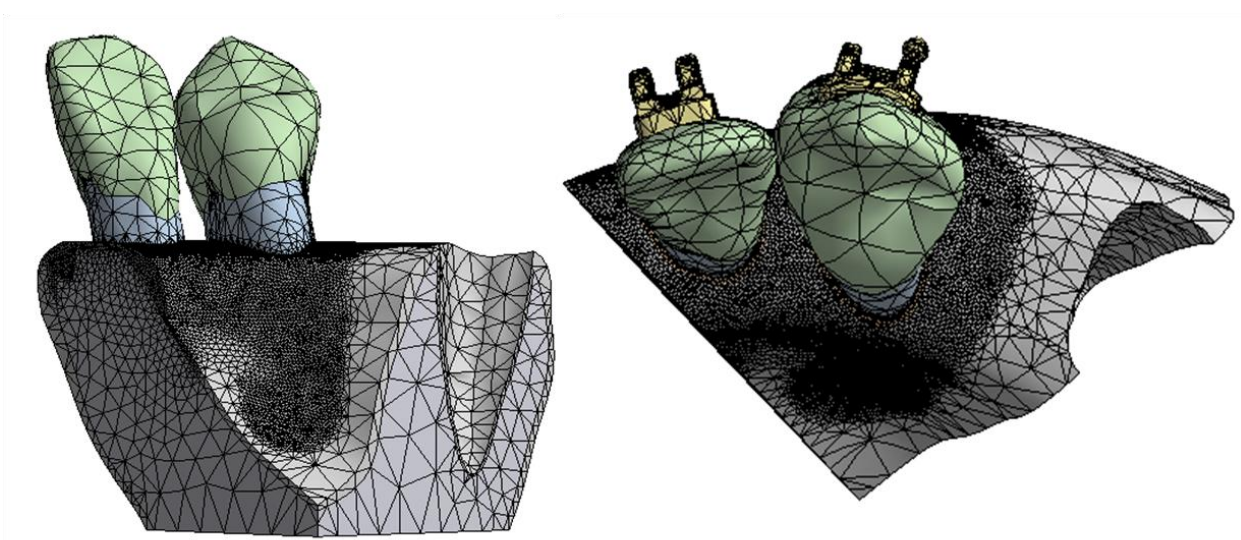
Figure 12: Fine mesh for the limited model, generated with a 0.2mm contact sizing between the dentin and cortical bone.

II.iii. Effects of model size, mesh density, PDL properties, and accurate orthodontic appliances.

Four different parameters were varied to examine their effects on the final FEA results. The first parameter analyzed was model size. The complete half maxilla model (Section II.i.) was solved and the final displacement, maximum stress, and maximum strain were compared to the substructural two-tooth model (Section II.ii).

Next, the effect of mesh sizing was examined. Substructural models were solved using both a coarse and fine mesh size as described above. If a certain model would not solve due to computational requirement, all models of increased complexity were excluded.

Finally, many published values have been used to model the PDL (Cattaneo et al., 2005; Chen et al., 2005). Table 8 shows the four values used in this study.

Table 8: Different Poisson's Ratio (v) and Young's Modulus (E) Values used for the PDL

	v	E (MPa)
Chen et al.	0.30	1750
Intermediate Value	0.30	17.5
Catteneo - high	0.30	0.175
Catteneo - low	0.30	0.044

Finally, the complete model and substructural model were both generated with full

orthodontic appliances and a passive 0.018" SS wire, but each model was run both with the

wire in place and after suppressing the wire (fully removing the wire from the FE analysis).

This tested whether placing accurate orthodontic appliances significantly altered FEA results.

II.iv. Comparison of FEA results with clinical data

Solutions were obtained in initial loading during sliding mechanics under 0.5 N and

1.0 N force. Differences between these two models were compared both qualitatively and

quantitatively. Visually, strain distributions were compared between simulations and the

movements found in the clinical data by Hayashi presented in Section I.vii.

The resulting data also was quantitatively referenced to the clinical data from

Hayashi. Since the FEA only obtains a solution during initial loading, the XYZ data

obtained after weeks of clinical loading could not easily be compared. However, the FHA

direction vector provides data on the biomechanical direction of movement and was therefore

used for comparison.

III. Results

III.i. Specific Aim 1: Creation of a complete maxillary biomechanical model

The specific aim of creating a full maxillary biomechanical model capable of

analyzing orthodontic canine retraction using absolute anchorage was achieved. This

complete model was named the FJORD model (Full Jaw Orthodontic Dentition model, UNC

copyright, Ko Lab 2011). Forty-three solid bodies were resurfaced, confirming seamless

interfaces. This model properly integrates with current versions of Solidworks (Version

2010) and ANSYS (Version 13.0) with no reported error messages during transfer. Although

the entire model was too large to be considered a single multi-body part that can undergo

conformal meshing (meshing all aspects of the model at one time, given coincident nodes at

interfaces), the 43 solid bodies were able to be grouped into 8 multi-body parts: each tooth

(with pulp, dentin, enamel, bracket, and PDL), the surrounding bone, and the archwire.

Interfaces between bodies were checked, showing no significant gaps or penetration – except

where clinically realistic gaps were desired between the bracket and wire (frequently referred

to as slop).   Mesh variations and non-linear interface conditions (e.g. friction and

frictionless) are supported with the model. Solutions were able to converge for a variety of

test conditions as discussed in Section III.iii. Figure 13 shows a typical displacement color

map when retracting the canine with 1.0 N of force.

Figure 13: Solved full half maxilla model showing total deformation during canine retraction with 1.0 N of force. Model was solved with an 0.018" SS archwire with frictionless interfaces. Note the minimal deformation of the molar, indicating successful anchorage with the palatal implant.

Converged FE solutions also include a full stress and strain components for each node – these results can be displayed graphically. Figure 14 shows von-Mises (equivalent) elastic strain over the whole model, showing increased strain on the canine and molar hooks where the model was loaded and also within the canine PDL. Minimal strain was seen in the molar PDL, as would be expected with the presence of the transpalatal arch to the palatal miniscrew. This model was run under 1.0 N of retraction force and a PDL stiffness of 1750 MPa.
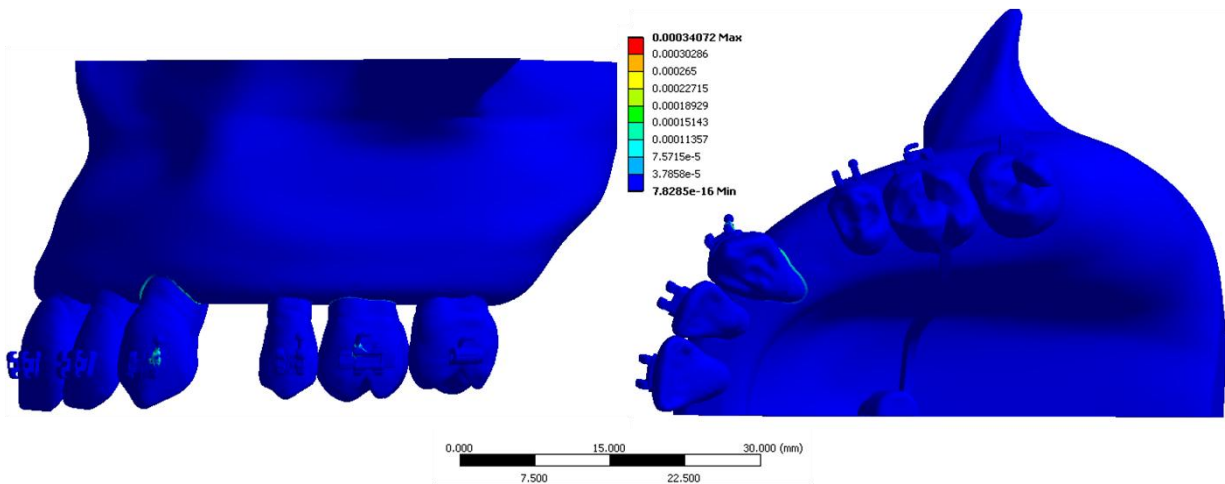
Figure 14: Equivalent (von-Mises) elastic strain in the full model during retraction with 1.0 N of force. PDL stiffness was set at 1750 MPa. (No archwire was included as the wire did not engage at this PDL stiffness).

Individual bodies can also be examined after the model has solved. Figure 15 displays von-Mises (A), maximum (B), and minimum strain (C) in the canine PDL. These results were taken from the same model as Figure 14 - run under 1.0 N of retraction force and a PDL stiffness of 1750 MPa. Strain is seen on both sides of the PDL when looking at the equivalent strain, but tension is occurring on the mesial (Figure 15B) and compression on the distal (Figure 15C).
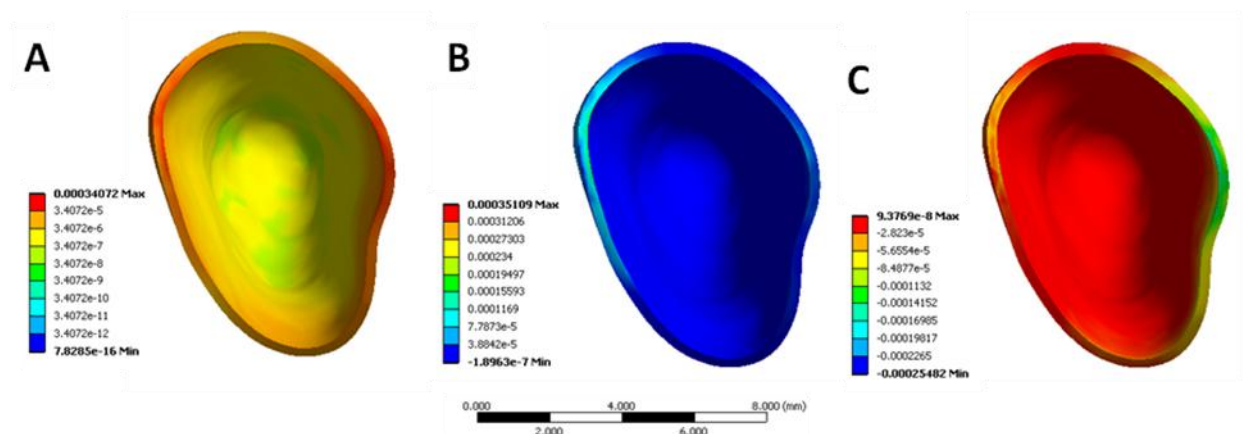
Figure 15: Equivalent (von-Mises) elastic strain (A), maximum elastic strain (B), and minimum elastic strain (C) within the canine PDL during retraction with 1.0 N of force. PDL stiffness was set at 1750 MPa.

III.ii. Specific Aim 2: Isolation of a two-tooth substructural model

The two-tooth substructure model isolated from the complete half maxilla model allows more complex analysis of canine movement, such as variations to PDL stiffness, mesh density, and contact conditions.   While the full model was unable to converge on a solution when using a PDL stiffness <175 kPa, this substructure model was able to converge using a stiffness of only 44 kPa and have sufficient computational resources (16GB) to solve at a higher mesh. This model, including especially the fine PDL mesh, is shown in Figure 16.
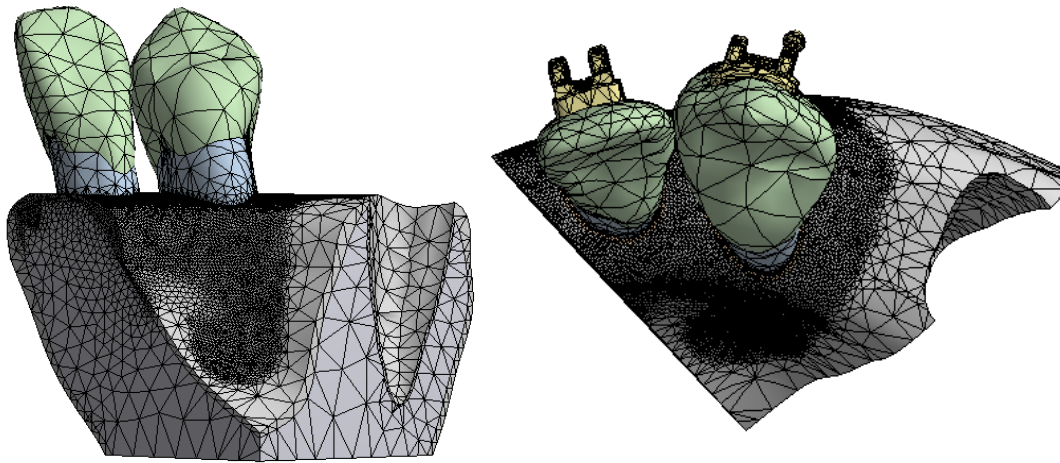
Figure 16: Isolated two-tooth substructure from the full half maxilla model, demonstrating the fine PDL mesh size.

III.iii. Specific Aim 3: Effects of model size, mesh density, PDL properties, and accurate orthodontic appliances

Table 9 shows models tested with variations in mesh density, PDL properties, and orthodontic appliances. Solution time varied, with multiple comprehensive models unable to converge on a solution. High mesh density, low PDL stiffness, and the presence of orthodontic appliances all increased the computation burden and more frequently led to failure to converge on a solution.   These finding were unsurprising: high mesh density increases the number of nodes and therefore the dimension of the global matrix, low PDL

stiffness leads to greater deformation of the tooth, and additional appliances and interfaces

will demand greater computational resources. Interestingly, orthodontic appliances produced

almost no increase in solution time with a PDL modulus of 1,750 MPa, quadrupled solution

time at 17.5 MPa, and increased over twenty times at 0.0175 MPa. Figure 17 shows that the

canine does not tip enough to engage a round 0.018" archwire with any PDL stiffness, but a

large rectangular wire (0.022 x 0.020") will engage at a 17.5 MPa stiffness (Note that

archwire width was only 0.020" due to passive steel ligatures already in place on the

brackets). Engagement of the archwire dramatically increased computational requirements.

Also of note was the fact that the high density mesh with the isolated two-tooth model had

faster solution times than a course mesh on the complete model.

Table 9: Chart of time (seconds) required for models to converge, with models unable to converge marked with "DNC" (Did not converge).

Elastic Modulus Pa	Complete Model Coarse Mesh	Complete Model Coarse - Wire	Complete Model Fine Mesh	Partial Model Coarse Mesh	Partial Model Coarse - Wire	Partial Model Fine Mesh
1.75E+09	3531 s	3590 s	DNC	181 s	254 s	1023 s
1.75E+07	6190 s	25456 s	DNC	499 s	685 s	2419 s
1.75E+05	DNC	DNC	DNC	1943 s	117117 s	4429 s
4.40E+04	DNC	DNC	DNC	3962 s	70140 s	DNC
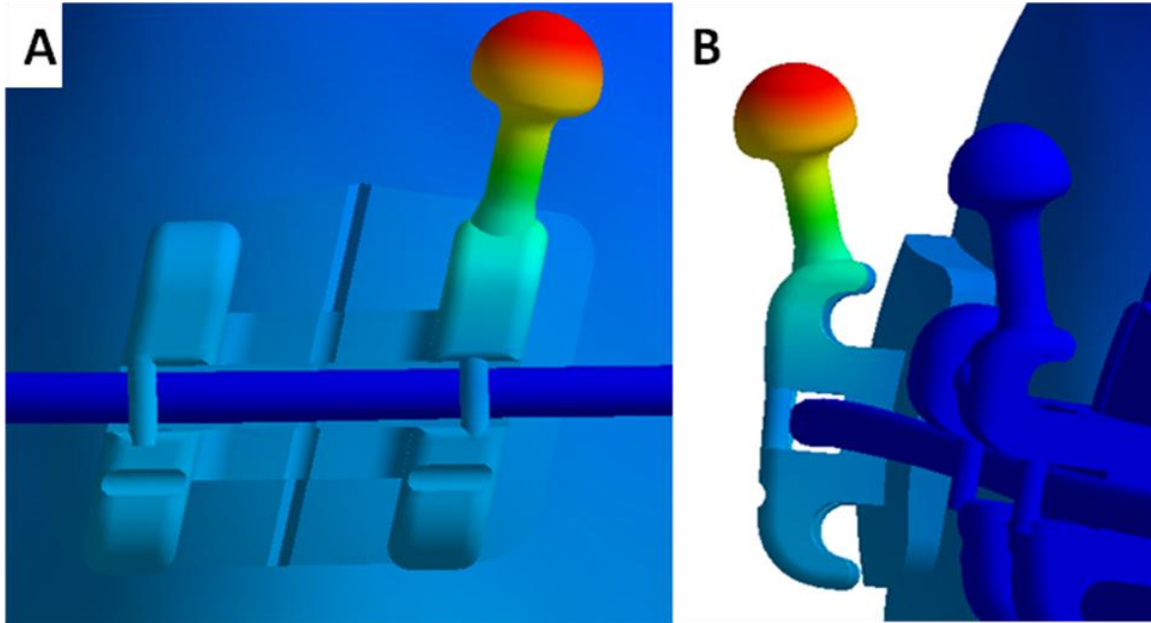
Figure 17: Facial (A) and distal (B) view of the tipping of the maxillary canine under 1.0 N of force with a PDL stiffness of 1750 MPa. Note no engagement of the archwire due to insufficient initial tipping.

Although adding complexity to the model increases solution time, these added complexities should be included if they create significant changes to the prediction of clinical outcomes. Typically, in FEA, results between two models are considered equivalent if they vary by <5% (Schmidt et al., 2009; Bright & Rayfield, 2011). Therefore, added mesh refinement, model size, and appliances that do not change the results by >5% are not necessary to include for accurate results. Table 10 compares a fine mesh to a coarse mesh for displacement in the substructure model, showing significant variations for nearly all testing conditions (all except the cusp tip displacement with a 1750 MPa PDL stiffness). Additionally, the maximum stress and maximum strain during the same simulations are shown in Table 11, with significant variations occurring for all test conditions. Therefore, mesh density can greatly influence results and fine meshes should be tested when performing FEA on orthodontic loading conditions.

Table 10: Comparison of a coarse mesh (CM) with a fine mesh (FM) in the two-tooth limited model of canine retraction with four different values for linear elastic modulus (E). Maximum displacement (Dmax) and overall displacement of the canine cusp tip (Cusp) are included.

PDL E (MPa)	Dmax CM - mm	Dmax FM - mm	%	Cusp CM - mm	Cusp FM - mm	%
1750	2.84E-03	2.60E-03	**9.48**	4.85E-04	4.86E-04	**-0.06**
17.5	4.74E-03	4.28E-03	**10.67**	2.43E-03	2.24E-03	**8.44**
0.0175	0.16115	0.13362	**20.60**	0.14051	0.11508	**22.10**
0.0044	0.62956	0.56455	**11.52**	0.5489	UNCONVERGED	

Table 11: Comparison of a coarse mesh (CM) with a fine mesh (FM) in the two-tooth limited model of canine retraction with four different values for linear elastic modulus (E). Maximum stress (Stress max) and maximum strain (Strain max) of the canine cusp tip are included.

PDL E (MPa)	Stress max CM - MPa	Stress Max FM - MPa	%	Strain max CM	Strain max FM	%
1750	79.296	53.961	**-46.95**	3.96E-04	2.70E-04	**-46.95**
17.5	79.296	53.961	**-46.95**	3.71E-03	4.16E-03	**10.65**
0.0175	79.295	53.961	**-46.95**	0.28709	0.30673	**6.40**
0.0044	79.293	UNCONVERGED		1.085	UNCONVERGED	

Additional comparisons were also performed on the effects of model size. The two-tooth substructure model was compared to the complete six-tooth half maxilla model for a variety of testing conditions. Table 12 compares the differences in maximum displacement and cusp tip displacement, while Table 13 compares maximum stress and maximum strain. Interestingly, when examining only displacement, results from the limited model appear relatively accurate – only the displacement of the canine cusp tip in the 17.5 MPa PDL modulus model varied by > 5%. However, stress and strain results did vary >5% for all test conditions. Therefore, the use of a full model is supported when examining stress and strain within the model, but may not be needed to accurately solve for displacement. To compare our results with the displacement found by Hayashi, the use of a limited model appears justified. The deviations seen in Table 12 and 13 are notably smaller compared to Table 10 and 11, which shows that results were less affected by model size compared to mesh density.

Therefore, if computational resources are limited, it would appear that a slightly smaller

model with a finer mesh may provide more accurate results.

Table 12: Comparison of the two-tooth partial model (PM) and the six-tooth half maxilla (HM) for modeling canine retraction with two different values for linear elastic modulus (E). Maximum displacement (Dmax) and overall displacement of the canine cusp tip (Cusp) are included.

PDL E (MPa)	Dmax PM - mm	Dmax HM - mm	%	Cusp PM - mm	Cusp HM - mm	%
1750	2.84E-03	2.84E-03	0.06	4.85E-04	4.98E-04	-2.61
17.5	4.74E-03	4.97E-03	-4.66	2.43E-03	2.69E-03	-9.76

Table 13: Comparison of a two-tooth partial model (PM) and a six-tooth half maxilla (HM) for modeling canine retraction with two different values for linear elastic modulus (E). Maximum stress (Stress max) and maximum strain (Strain max) of the canine cusp tip are included.

PDL E (MPa)	Stress max PM - MPa	Stress Max HM - MPa	%	Strain max PM	Strain max HM	%
1750	79.296	68.144	16.37	3.96E-04	3.41E-04	16.37
17.5	79.296	68.143	16.37	3.71E-03	3.49E-03	6.47

Solutions obtained using models with accurate orthodontic appliances were also

compared to models without orthodontic archwires in place. It was found that for a PDL

stiffness $\geq$17.5MPa, no bracket-to-wire interaction occurred, so modeling the appliances was

not required if testing a high stiffness PDL during initial loading. In fact, when the original

0.018" stainless steel archwire was placed in the model, it did not engage the brackets under

any loading conditions tested. When moving to the larger rectangular wire, engagement did

occur with a PDL stiffness of either 0.044 MPa or 0.175 MPa.

Without orthodontic archwires in place, the resultant force and moment within the

PDL were calculated under 0.5 N, 1.0 N, and 2.0 N of canine retraction force. Not

surprisingly, although the magnitude of the resultant force varied, the direction was

unaffected by force level (See Figure 18).
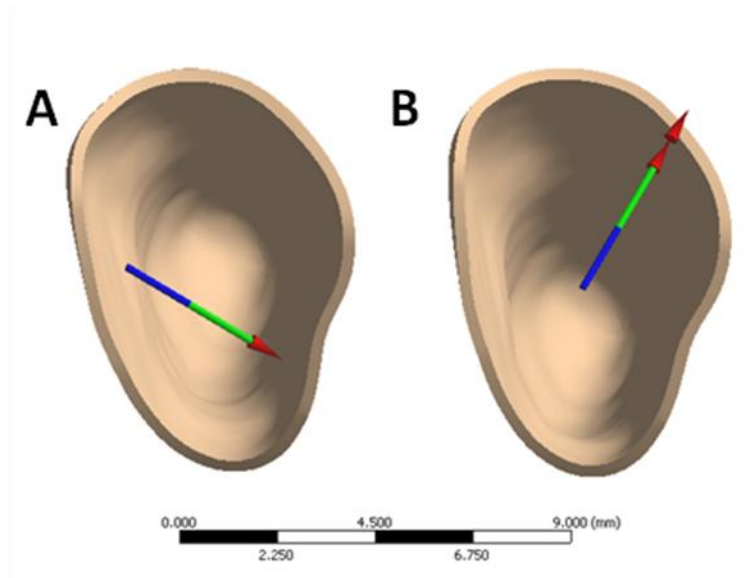
Figure 18: Resultant force (A) and moment (B) felt by the PDL during canine retraction at any force level without orthodontic appliances. This shows a resultant force in the PDL predominantly in the distal direction. The resultant moment shows tipping and rotation are both occurring. *Note: These directions are identical at any force level, as opposed to Figure 19 and 20 with orthodontic appliances.

However, when orthodontic appliances were modeling and the PDL stiffness was reduced below 0.175 MPa so the bracket engaged the wire, resultant force and moment direction varied with force application (Figure 19 and 20). Figure 19 shows a subtle difference in the direction of the resultant force felt by the PDL during retraction, with the 1.0 N force not inclined quite as far apically. The resultant moments, which closely mimic the direction vector of the FHA, show a more apparent difference. The resultant moment is less inclined to the distal under 1.0 N of force, showing less apparent flaring side effects.
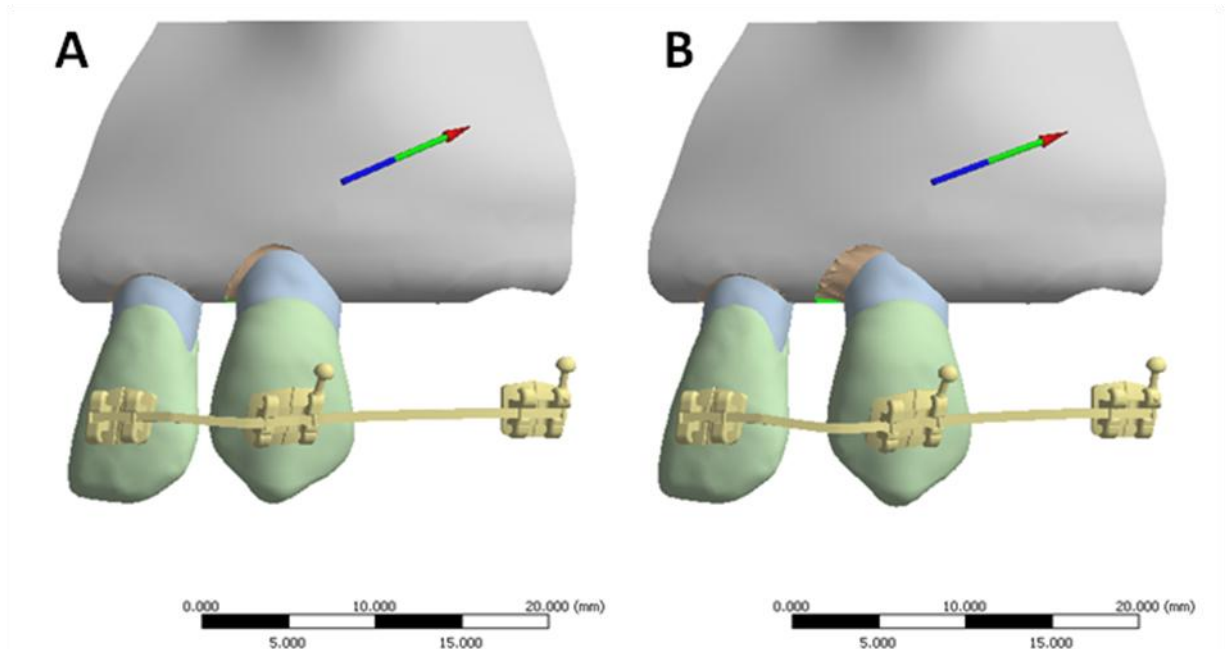
Figure 19: Resultant force during canine retraction with 0.5 N (A) and 1.0 N (B) when modeling orthodontic appliances.
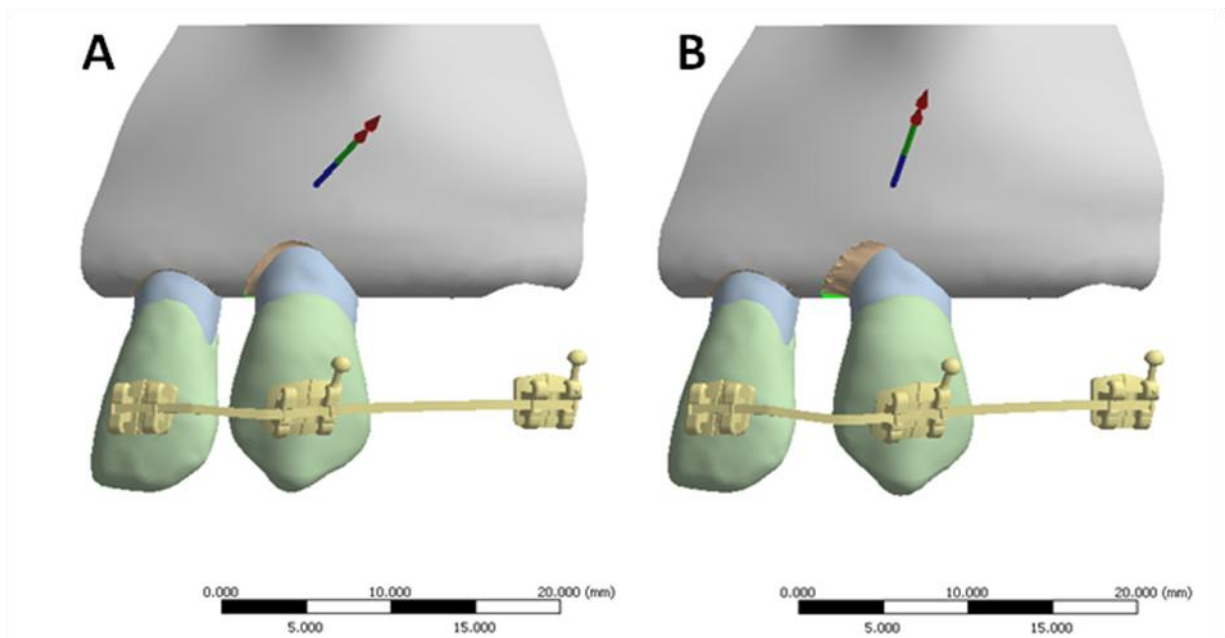
Figure 20: Resultant moment during canine retraction with 0.5 N (A) and 1.0 N (B) when modeling orthodontic appliances (PDL=0.175 MPa)

III.iv. Specific Aim 4: Comparison with clinical data

One significant clinical finding by Hayashi was that the finite helical axis direction was affected by the retraction force (Hayashi et al., 2007). This finding was supported by

FEA, as shown in Figure 19 and 20. Table 14 shows the FHA parameters calculated by

Hayashi, as well as results found in this study. Interestingly, the values for v_z were roughly

similar, corresponding to the degree of rotation present. However, the values for v_x and v_y

were quite different from the data found clinically. The overall degree of rotation about the

FHA was ~1% of rotation found in the clinical data. Therefore, properly modeling the

resultant direction of tooth movement requires remodeling of the FE model.

Table 14: Comparison of the FHA clinical data for canine retraction provided by Hayashi
and the generated results from FEA under 0.5 N and 1.0 N of load.

FHA system parameters	0.5 N		1 N		P		0.5 N	1 N
	Mean	SD	Mean	SD			FEA	FEA
Distal movement of canine crown tip (mm)	3.17	0.6	3.38	0.71	0.199	NS	0.0215	0.0685
Rotation around the FHA θ (degrees)	12.24	2.14	12.91	2.3	0.478	NS	-0.275	-0.226
Translation along the FHA t (mm)	0.37	0.17	0.29	0.13	0.223	NS	0	0
Shortest distance from the space coordinate origin to the FHA d (mm)	14.63	7.54	14.74	8.01	0.877	NS		
Direction vector of the FHA v_x	-0.25	0.22	-0.57	0.2	0.048	*	0.731	0.680
Direction vector of the FHA v_y	0.61	0.21	0.37	0.22	0.042	*	-0.127	-0.0864
Direction vector of the FHA v_z	0.61	0.29	0.58	0.3	0.234	*	0.671	0.728

*$P < 0.05$, NS = Not Significant

IV. DISCUSSION

IV.i. Comparison of Results to Previous Literature

This study provides the first known report in the literature of a complete maxillary biomechanical model combining high-quality tooth geometry and accurate orthodontic appliance placement, while maintaining independent anatomy (enamel, dentine, pulp, PDL, and alveolar bone can all be separately manipulated) and high-quality interfaces capable of mesh size variations and interface manipulation (e.g. bonded contacts, frictionless contacts).

Cattaneo et al. has shown the importance of high-quality μCT scans of the dentition and creation of a high-quality virtual model (Cattaneo et al., 2005; 2008; 2009a; 2009b), yet point forces and moments are not capable of representing the wide variety of tooth loading conditions available with the FJORD model. Additionally, these studies included only two teeth, while our results highlighted differences when moving to a full half maxilla with contact interfaces between neighboring teeth.

Reimann et al. presented a model with full maxillary bone and four incisors, yet rectangular blocks were used as brackets, bonded contact conditions were used, and the mesh density was relatively rough (Reimann et al., 2007). Very similar issues are seen in more recent publications (Field et al., 2009; Hohmann et al., 2009; Liang et al., 2009; Ammar et al., 2011; Jasmine et al., 2012). No previous study could be located where mesh density was increased to inflate the PDL thickness to multiple layered elements. In our results using an

average PDL stiffness of 0.175 MPa (the high stiffness PDL model described by Cattaneo, 2005), increasing the mesh density of the PDL altered displacement results by 20.6%, stress by 47.0% and strain by 6.4%. Less than 5% variation is typically required to assume model convergence and therefore accurate results. Therefore, a single element thickness in the PDL was not sufficient for mesh convergence in this study.

The current comprehensive FJORD model is the first reported model to provide sufficient anatomical accuracy for reliable biomechanical modeling of a full jaw, while maintaining independent CAD bodies capable of variations in meshing. Our results show, however, that high density meshes demand substantial computational resources when implemented on a full model. This led to many results being generated through the use of a limited two-tooth model. However, as opposed to other limited models published in the literature, the accuracy of our limited model was demonstrated through comparison with the comprehensive model.

IV.ii. FEA versus Laboratory Testing

Some authors have criticized the use of finite element modeling in orthodontics due to lack of complete validation for each model and loading condition. While model validation is important, the mechanical principles underlying the analysis are mathematically valid (Timoshenko & Goodier, 1951; Lanczos, 1962;). Therefore, it is important to examine the assumptions made and the interaction of mesh density (mathematical convergence), but once these assumptions are validated, the technique can be widely applied in orthodontics. Accurate assumptions have been validated for many non-biological applications, such as in the automotive and aeronautic industries, where a majority of current design testing for these

industries is first performed with computer simulations. This is extremely effective for the automotive and aeronautic industries due to the high cost of producing designs for laboratory testing. In orthodontics, the progression to computer modeling is also extremely important, as it is the only way to examine biological structures and internal stresses without destructive evaluation of tissues.

A currently advocated laboratory technique for quantification of resulting forces from a statically indeterminate system uses force and torque transducers attached to brackets in an orthodontic arch (Badawi et al., 2009). While this method can provide a great deal of valuable information on resultant forces and moments, it does have major limitations. The first concern is the absence of biological tissues from the analysis, especially the PDL. Without the PDL, it is impossible to extrapolate the data to the human conditions of tooth movement. Therefore, the effects of initial displacement of the teeth under loading and the long-term viscoelastic effects within the PDL cannot be examined.

The second major concern using a laboratory model is that currently available force and torque transducers still are relatively large when compared to orthodontic brackets. Therefore, the transducers must be placed a distance away with a cantilever arm to the bracket (Figure 21). This cantilever arm is affected by loading and the deformation (although small) must be accurately characterized. Additionally, even with the setup seen in Figure 21, the interbracket distances are not identical to *in vivo* conditions (all blocks are 10mm in width and have space between them), which can significantly influence results. Specifically, changes in the interbracket distance affect strength inversely, springiness to the third power, and range to the second power of the length ratio.

Figure 21: Laboratory model used by Badawi et al (Badawi et al., 2009).

Finally, the greatest limitation of this technique is that even if forces and moment can be accurately determined, the resulting stress and strain within the tissue cannot be calculated. As discussed in Section I, further advancements in orthodontics require more accurate characterization of the effect of loading. Only calculation of internal stress and strain will be able to separate the effects of PDL and alveolar bone loading, determine how specific stress and strain corresponds to biological response, and how this affects tooth movement.

Full validation of FEA in orthodontics is ongoing, but a great deal of progress has been made by several investigators. Jones et al. compared initial loading of an incisor with a FE model of an incisor, showing an appropriate elastic modulus of 1 MPa and Poisson's Ratio of 0.45 (Jones et al., 2001). Catteneo et al. explored the importance of non-linear viscoelastic effects and accurate representation of alveolar bone anatomy (Cattaneo et al., 2009b). The importance of modeling multiple teeth was shown by Field et al (Field et al., 2009). Our findings highlight the importance of accurate appliances and proper mesh density, supporting initial work by Schmidt et al and Bright et al (Schmidt et al., 2009; Bright & Rayfield, 2011). The combined outcomes of these previous research projects provide

45

excellent guidelines for creation of FE models capable of producing data translatable to clinical application.

IV.iii. Current Limitations and Further Improvements

Although the FJORD model is a significant improvement in orthodontic FEM, limitations still exist. One of the primary limitations is current computational resources. In the 1970s and 1980s, 3D modeling was rarely performed due to computational demands. The vast improvement in computer speed and memory in the last few decades has allowed the development of accurate 3D models capable of modeling non-linear surface interactions. Despite these improvements, fine mesh sizes and comprehensive models can quickly strain computational resources. As processor speed, available RAM, and ability for parallel processing improves, model complexity can be further improved. It is important to note that the goal of FEA is not creation of the most complex model. Limited models are important, but must be validated against more complex ones to ensure no loss of accuracy. The current literature in orthodontics and this study both support the development of additional model complexity, as variation with further refinement still appears significant.

Degrees of Freedom

Mesh density is one area that further computational resources could improve. An additional model that further inflates the PDL mesh to three or four elements should be tested to ensure that a two element thickness is sufficient for accuracy. Additionally, ANSYS does not currently support the entire half maxilla as one multibody part, which allows matched nodes at the interfaces. Therefore, the bracket, enamel, dentin, pulp, and PDL of each tooth

were combined into a multi-body part, while the cortical bone, trabecular bone, and sinus

formed an additional part. This improved the mesh, but still leaves unmatched nodes at the

interface between the PDL and cortical bone. When it attempts to create shared nodes at this

interface, it effectively required the computer to mesh all parts simultaneously, which quickly

exceeds the computational ability of our computer. Figure 22A shows minor variations that

occur within the PDL when this occurs.   Using a limited model, the computational ability is

not exceeded, allowing matched nodes as seen in Figure 22B. Further improvements in

computational ability and software capabilities may soon solve this issue.
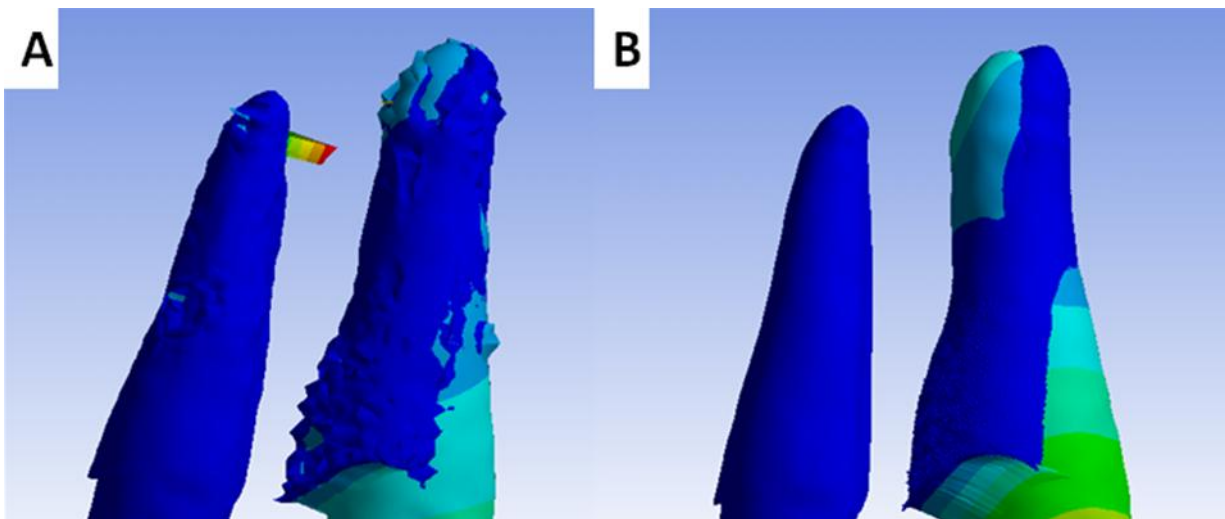
Figure 22: A. Variations in the PDL surface arising from unmatched nodes. B. Smooth
surface if the nodes are matched.

Contact Interfaces

An additional area where computational resources are strained is during modeling of

non-linear surface interactions, especially frictional contacts. Bonded interfaces have low

computational requirements, but have limited use when examining a full range of orthodontic

loading. Frictionless contacts require more computational power, but were able to be utilized

in this study. In a limited model, frictional contacts could be solved using a frictional

coefficient of 0.2. However, increasing this coefficient or the size of the model led to unconverged solutions.

Another difficulty with current FEA modeling is a limited ability to model active ligation. The current study uses passive stainless steel ties on the mesial and distal to hold the wire into the slot. However, current tools in Solidworks do not allow the user to specify direct contact between the wire and ligature, nor a specific gap. Therefore, the ligatures are visually placed with minimal gap. Although reasonably accurate, some variation in placement undoubtedly exists. Moving from passive ligation to active ligation introduces a great deal of added complexity. (A relatively simple method of applying a seating force on the wire at each bracket could be used. However, this force remains constant during modeling regardless the position of the wire to the base of the bracket, which does not accurately represent what occurs in a clinical situation.) In order to create a true active appliance, the birth-death technique introduced by Canales et al. must be utilized (Canales et al., In preparation). This greatly increases complexity and had not been previously attempted in the literature.

PDL

Finally, the ultimate goal in modeling orthodontic tooth movement is to add actual remodeling into the simulation. Currently, only initial loading can be examined, but calculating changes in stress and strain during canine retraction would be a significant contribution to our understanding of tooth movement. However, this requires not only moving the tooth based on the loading conditions, but also properly manipulating the PDL and bone with the tooth structure. The complexity of these changes, the need for clinical data

to validate the amount of actual remodeling based on the applied load, and the computation

requirements mean that an accurate model of orthodontic remodeling still requires a great

deal of further investigation.

V. CONCLUSIONS

1. A comprehensive biomechanical model of the maxilla was developed capable of convergence under a variety of loading conditions.

2. A limited two-tooth model was extracted from the comprehensive model, allowing more complex simulations to converge with shorter solution times. However, predicted stress and strain values deviated from the full model by up to 16.4%.

3. Models with a single element PDL thickness were not fully converged, with up to 22% variation seen in displacement and 47% seen in stress when moving up to a fine mesh density with a two element PDL thickness.

4. The PDL elastic modulus significantly influenced the initial displacement, which can be used to partially describe the viscoelastic behavior of the PDL.

5. The inclusion of orthodontic appliances supported the finding by Hayashi that a biomechanical difference exists between canine retraction with 0.5 N and 1.0 N of force. However, the results could not be directly correlated, highlighting the need for a model incorporating remodeling.

APPENDIX 1
GEOMAGIC

i. Importing into Geomagic

Geomagic Studio is a powerful tool to accurately manipulate 3D scans into CAD

models. In order to manipulate objects in Geomagic, the geometry must be imported from an

external file. This could be an .stl file generated directly from a 3D scan, but for the

purposes of this study, .iges files were used since the geometry had already been converted to

a CAD object previously. The .iges file type is one of the earliest developed file structures

that is currently used – this provides a robust format, but lacks support for many complex

functions (e.g. maintaining hierarchy, support for complex multibody parts). The dentin for

the UL2 and for the UL5 both did not transfer properly using .iges, but the geometry was

accurately transferred through the use of a .step file (a newer file version which interestingly

had issues with multiple other surfaces in the model).

CAD files, such as .iges or .step, are displayed under the "CAD" tab once they are

imported into Geomagic. Since Geomagic is not a CAD program with multiple functions for

surfaced objects, the first step is converting the geometry to a polygon model (Figure 23).

ii. Manipulation of the Polygon Model

Once converted to a polygon model, there are often numerous unneeded boundaries.

These extra boundaries can be removed and the interior surface can be cut into a new body as

described in Figure 24. The final result of these steps is seen in Figure 25.
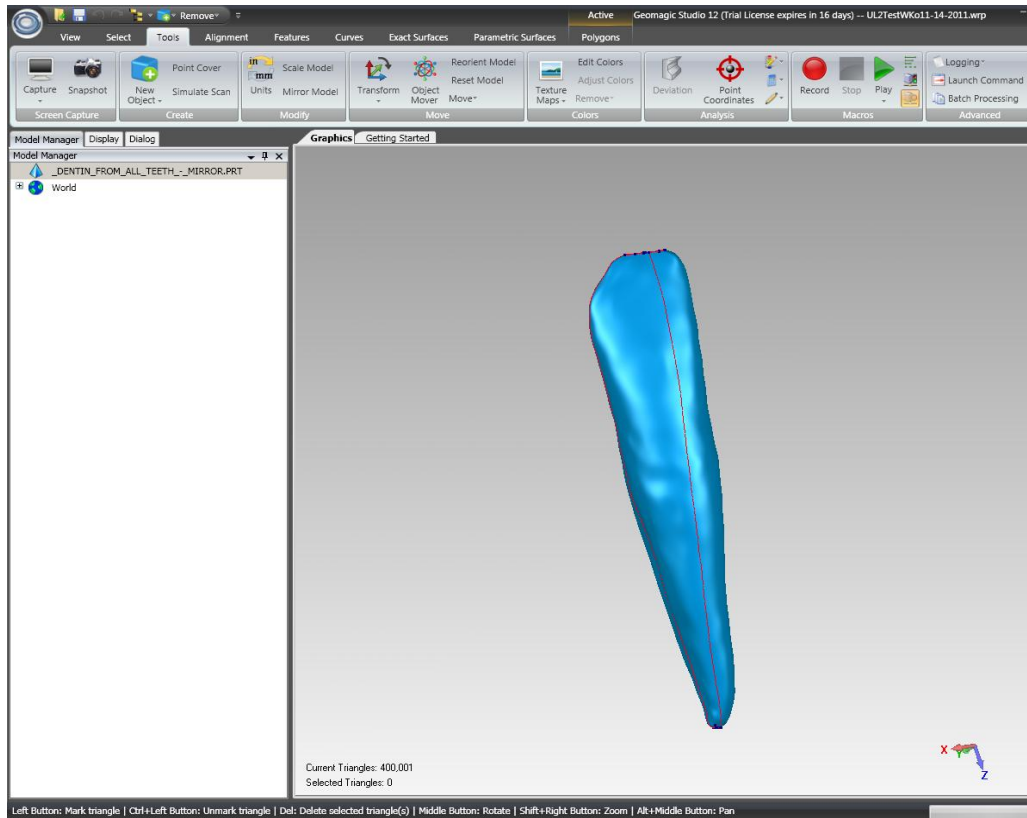
Figure 23: Polygon model of UL2 in Geomagic directly after importing from STEP file and converting to polygons.

Figure 24: To remove extra boundaries, first the click "Remove" under the "Boundary tab" and select "Clear Subdivision Points" (A). Next, select "Remove Boundary" and select any unwanted boundaries. Typically, it helpful to leave the apex boundary, because then the bounded components can be selected (B). This can highlight the entire interior surface, which then can be moved into a new object, by selecting "New Object" -> "From selection". (C)
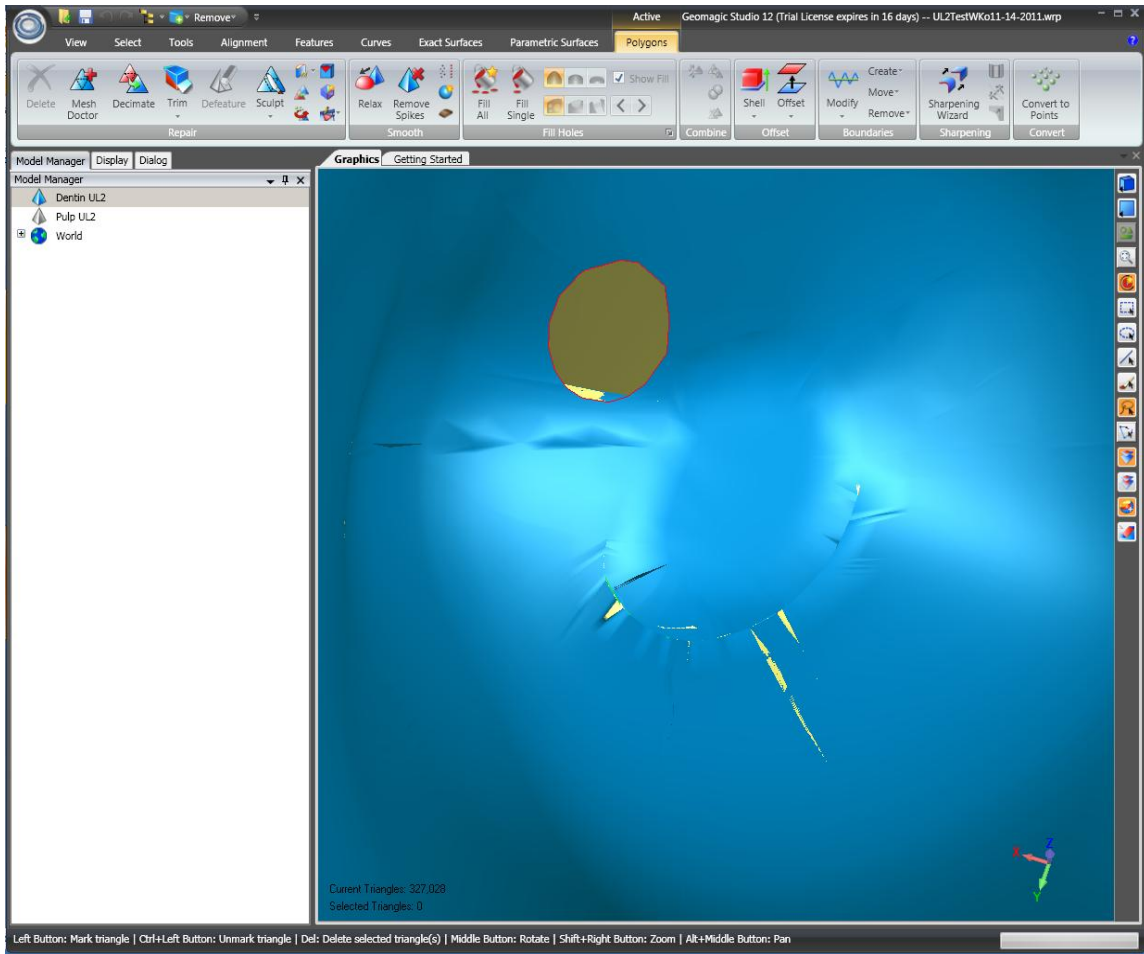
Figure 25: Interior surface cut into a new object (PulpUL2) and the exterior dentin selected. Note: This view highlights that although the overall view may look nice, defects exist that must be repaired.

Once the interior surface is cut away, typically it is preferred to fill the apex. This can be done by selecting "Fill single", highlighting the option to fill by using the surrounding surface normals, and then selecting the open apex (Figure 26). In addition, it may be useful to select "Fill All" as well to ensure the surface is closed.
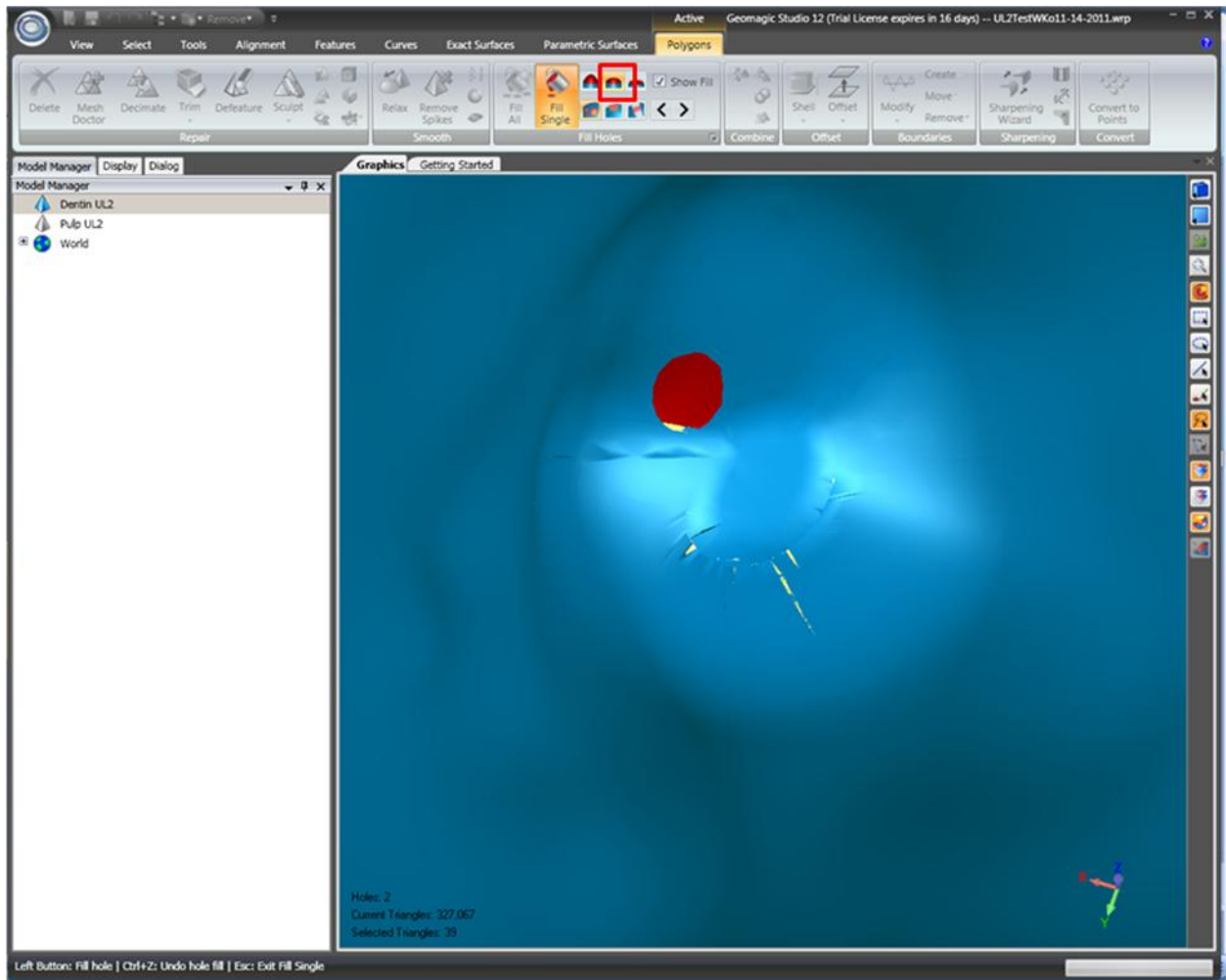
Figure 26: Filling an open hole in Geomagic. Select "Fill single", select the middle option (highlighted by a red square for emphasis) that fills the void by using the surrounding surface normals, and click the hole that needs to be filled. Pressing Esc will exit the menu.

Although Figure 23 looks smooth and complete, Figure 26 shows that rough areas exist with regions where the surface normal is reversed (yellow polygons). A Geomagic tool known as "Mesh Doctor" will highlight problematic areas (Figure 27). While the Mesh Doctor tool has automated repair tool, often quickly defeaturing the most problematic areas will improve the result (Figure 28).
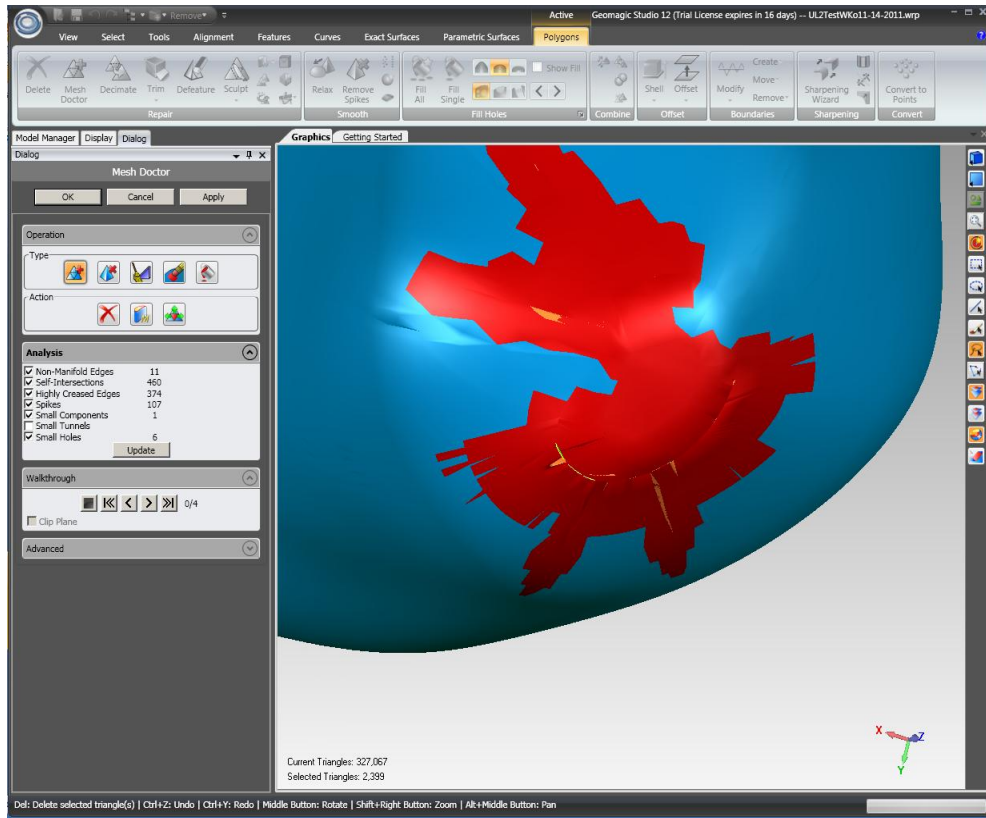
Figure 27: The "Mesh Doctor" tool highlights problematic geometry and offers automated repair options.
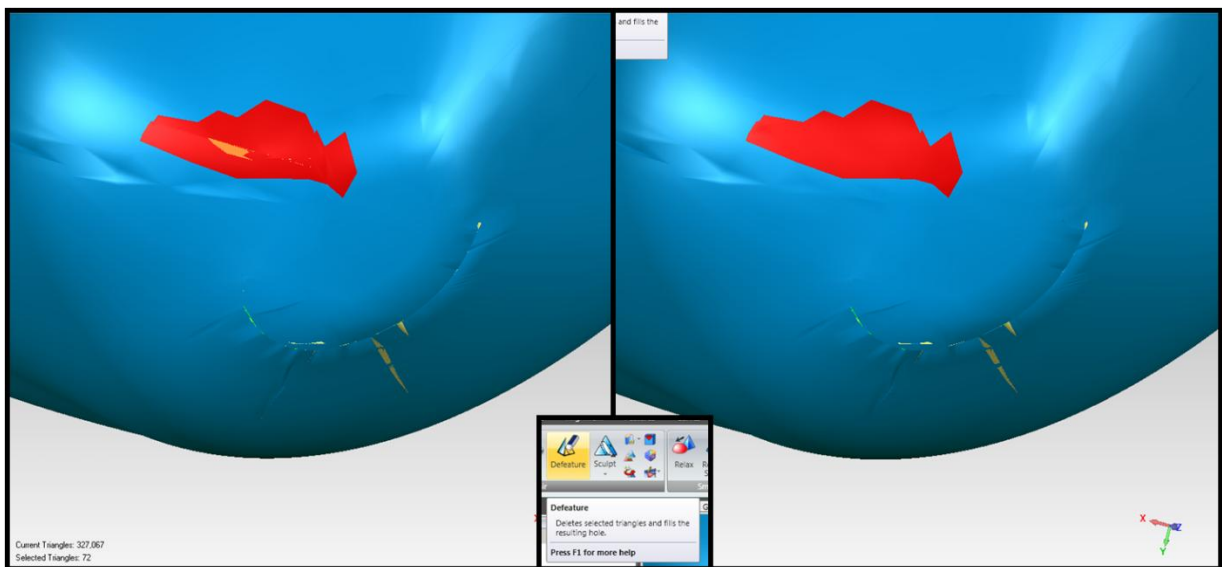
Figure 28: Defeaturing removes selected polygons and recreates the surface using the surrounding geometry. This work well to get rid of extremely rough geometry, but selection of too large of an area can cause a loss in accuracy of the model.

Once rough areas are defeatured, mesh doctor can be used to automatically repair minor issues. The goal at the end of this stage is to have no errors occur under the "Analysis" box of mesh doctor (Figure 29). Despite no problematic polygons, the geometry is still not fully prepared for surfacing. Under the "Display" menu on the left there is an option to display "Edges". After clicking this option, it is evident that many polygons near the incisal edge are skewed and larger than the average polygons in the body. To fix the issue with the large polygons, the polygons can be selected and the "Refine Polygons" tool is selected to increase polygon density (Figure 30). At this stage, the number of polygons in the overall model should be on the order of 200,000 to 400,000.
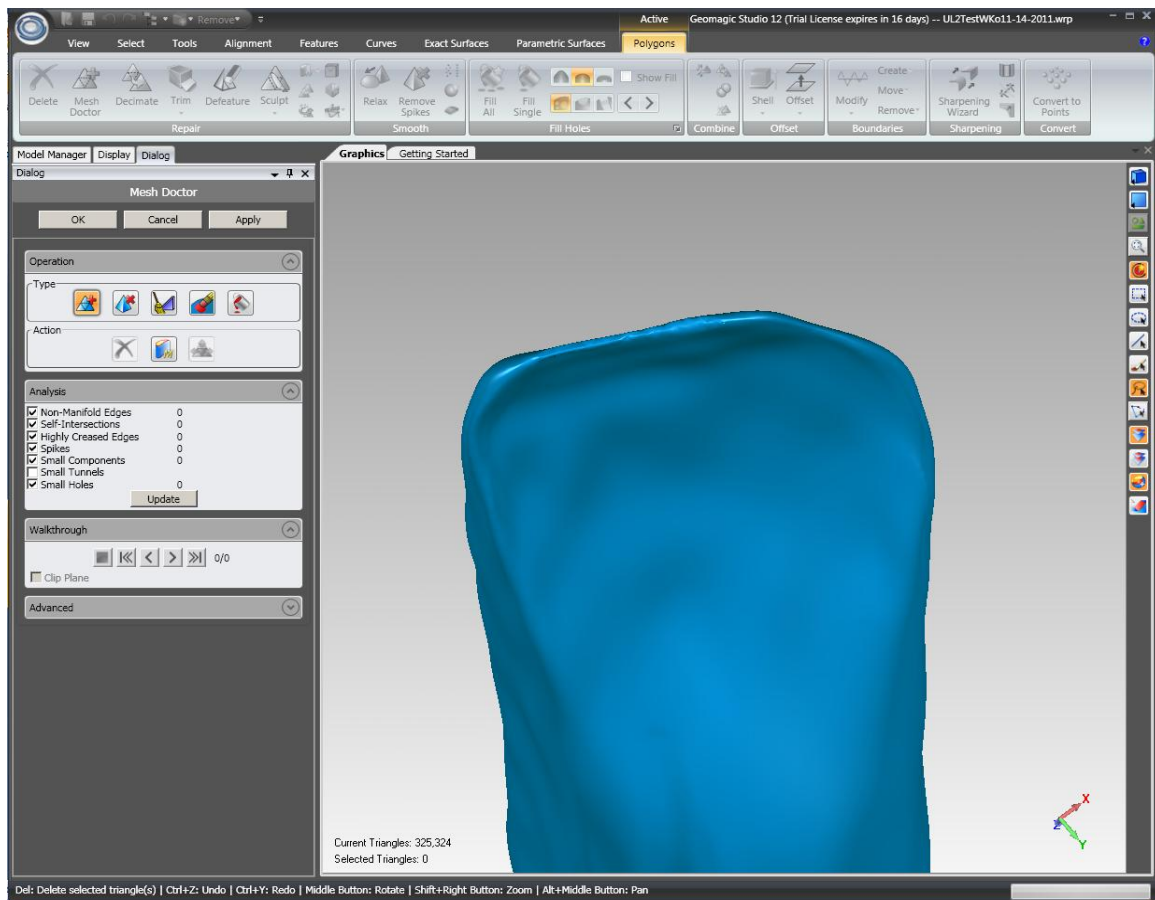
Figure 29: Ideal output from Mesh Doctor with no errors found.
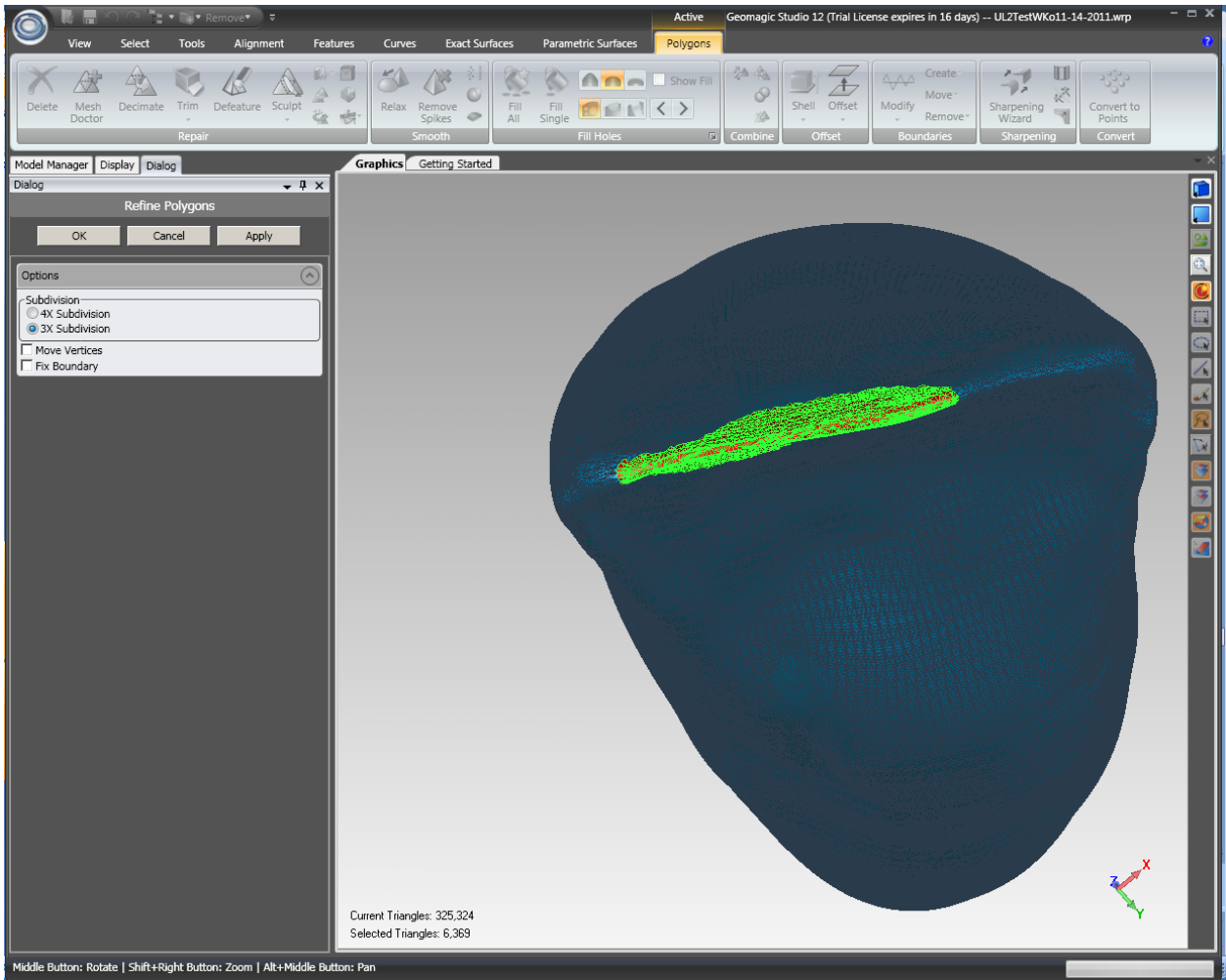
Figure 30: These selected polygons near the incisal edge are large and skewed. The "Refine Polygons" menu is open to create additional polygons in this area to improve the surface mesh.

After modifying the polygon size, the surface can be smoothed through the use of the "QuickSmooth" command under the "Smooth" menu. Finally, the "Enhance Mesh for Surfacing" tool is used to create an ideal polygon distribution for surfacing (Figure 31). Geomagic support recommends a 10% increase in polygon size to handle any additional polygons that need to be created for a smooth surface.   Figure 31 shows a reasonable final polygon surface, with non-skewed elements and a slightly increased density around the high-curvature incisal edge.
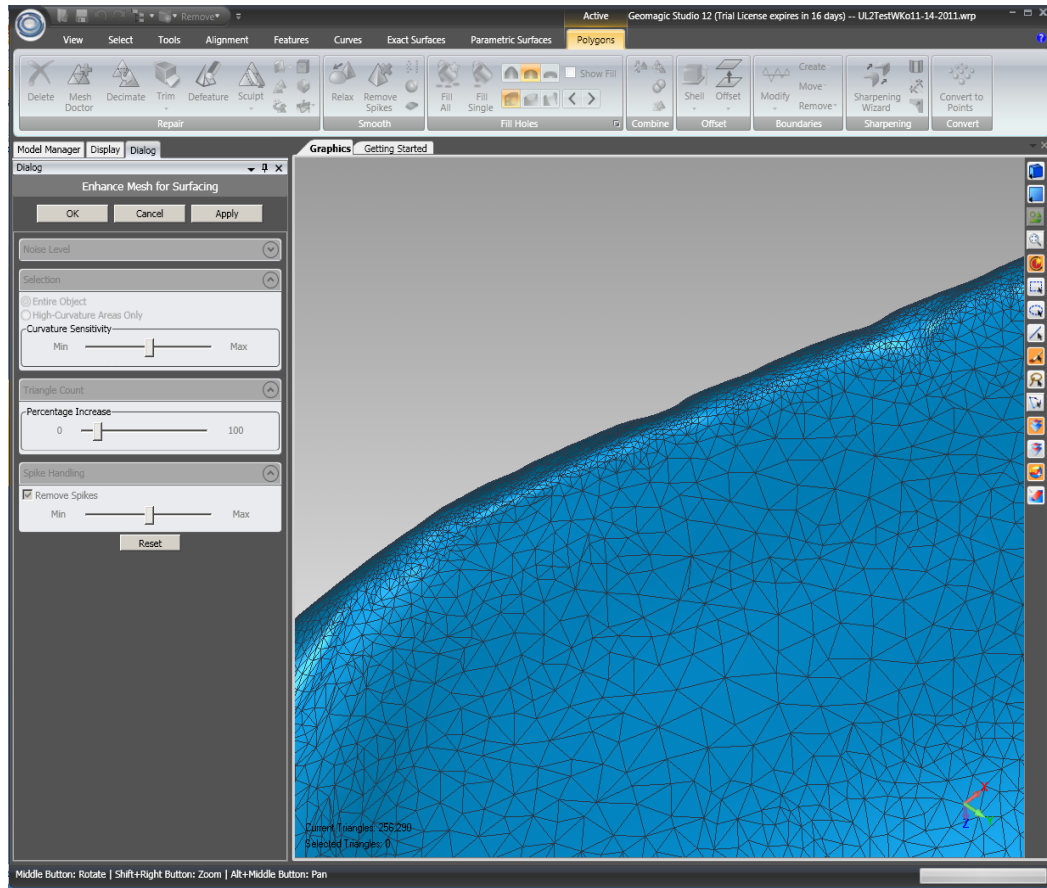
Figure 31: "Enhance Mesh for Surfacing" tool that creates an ideal mesh distribution to create non-skewed elements to assist with ideal surfacing.

iii. NURB Surfacing

At this point, the polygon model is ready for NURB (Non-Uniform Rational B-spline) surfacing. To summarize, the object should be a smooth, continuous, closed surface made of non-skewed polygons. All surface normals should be facing the exterior (denoted by a blue surface in Geomagic) and the model should contain approximately 200,000 to 400,000 polygons. In case the polygon model requires further manipulation, it would be wise to save the file separately at this point and also create a copy of the object in the workflow. At this point, select the "Exact Surfacing" tab and click "Exact Surfacing" under the "Start" region to the left of the tool bar (Figure 32). Notice the icon next to object changes and new workflow items are available in "Exact Surfaces."
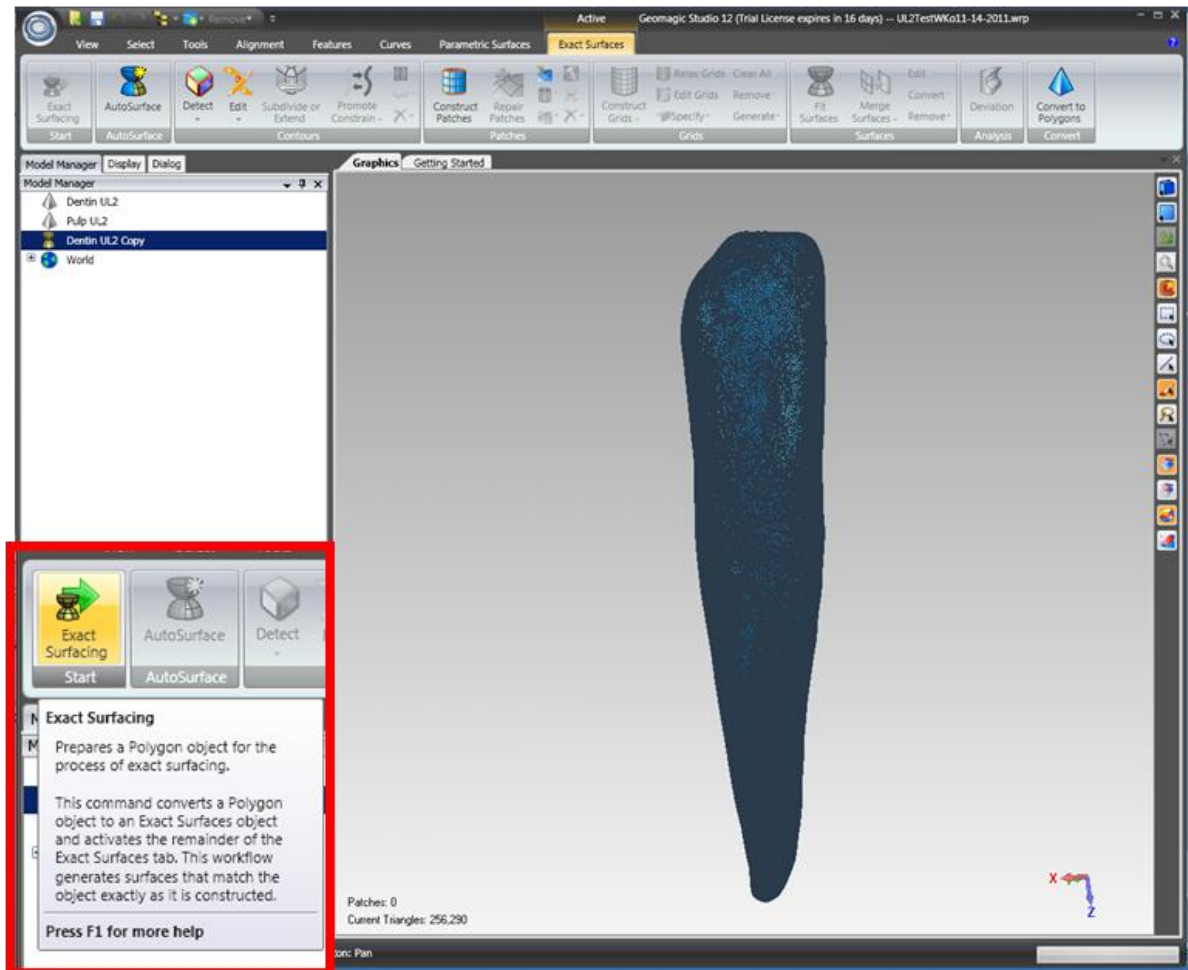
Figure 32: Object copied and moved into "Exact Surfacing". Initially, the menu has only the first box available, as shown in the red insert, but the rest of the options become available once "Exact Surfacing" is clicked.

At this point, the first available option is for autosurfacing. Autosurfacing techniques are frequently used, but Figure 33 shows some issues that occur during autosurfacing. Figure 33-B shows the auto-detected contour lines, which clearly do not follow the true contours of this object. Based on these contour lines, a total of 302 patches are created for this surface. These patches become unique faces in Solidworks (although some time consuming techniques can be used in Solidworks to partially reduce this number), which leads to a complex FEA model. Most problematic, the odd layout of the faces do not line up with any

anatomic interfaces, so the cementoenamel junction (CEJ) may oddly intersect these faces

and cause problematic geometry (specifically small edges and sliver faces).
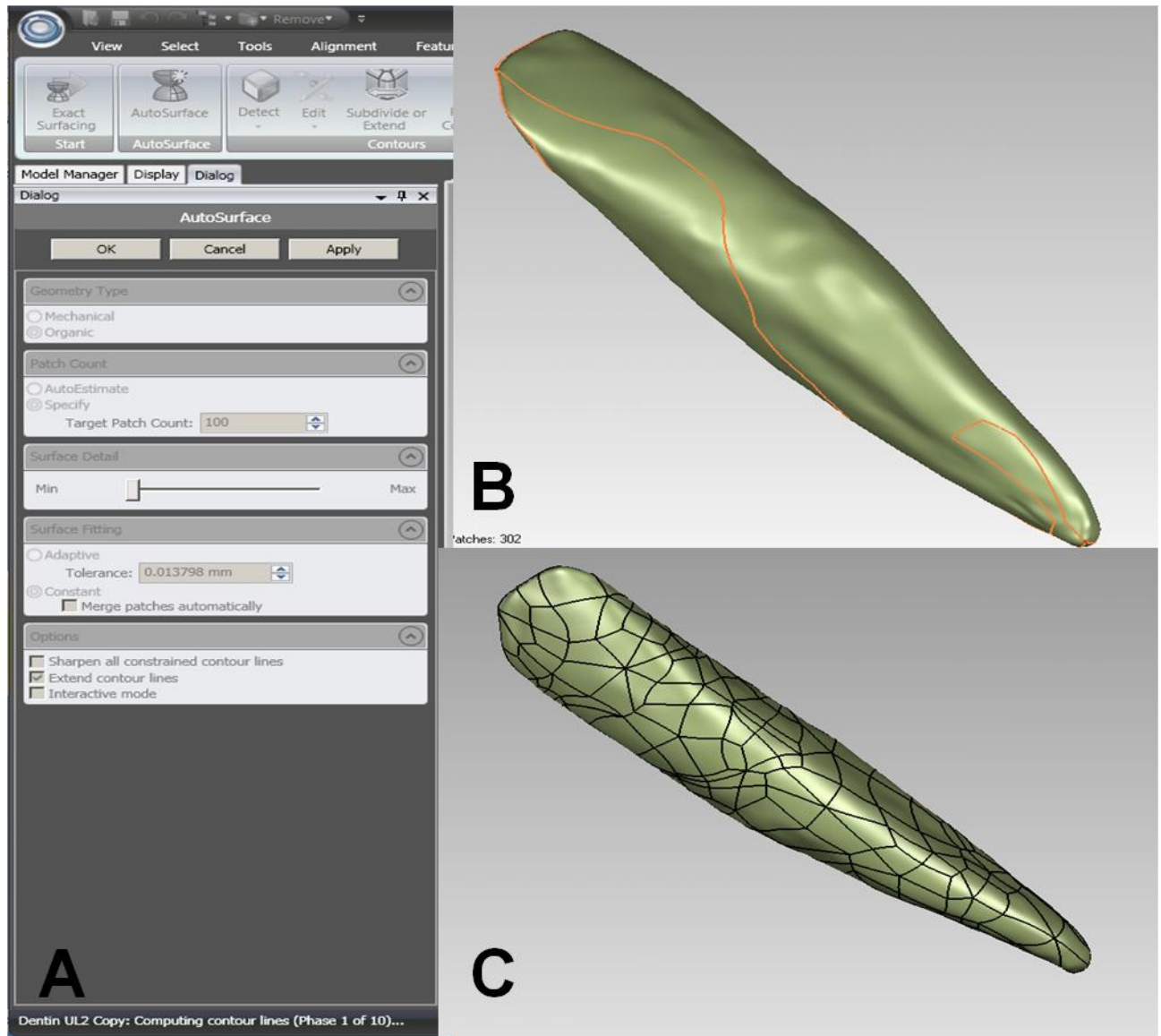
Figure 33: Autosurfacing in Geomagic. The menu screen is shown (A), as well as an example of automatically generated contour line (B) and patches (C) that can be problematic.

Due to the advantages in FEA with accurate patch layouts, a manual approach to

surfacing was chosen over the automated method. The remaining menu items in the "Exact

Surfacing" menu provide a workflow for how to manually surface an object. First, contour

lines must be created. There is a "Detect" option, but that uses the same automated method

that does not work well for the dentition. Ideal contour lines provide a framework of the object that can be filled with finer patches in the following steps. The following considerations were found to be important for creating a contour layout:

- Grid patch layouts frequently work best for creation of a small number of final faces, so creation of quadrilaterals with roughly right angles is ideal.

- Contour lines should follow the prominent geometry of the object. For example, tooth objects generally resemble a cylinder, so circular bands around the tooth are appropriate. However, line crossing the incisal edge of marginal ridges obliquely should be avoided.

- Red points are created at intersections and areas were high amounts of curvature change are detected. These points are given higher priority and there will always be two patches between each two red points. Therefore, if there are red points created that should not receive increased priority, they can be demoted by holding Ctrl and clicking them.

- Ctrl can promote or demote points, while shift deletes them.

- Once the final layout is created, save the file separately, as sometimes it does not allow alterations once the patches have been generated once (even if they are deleted).

Figure 34A give an example of an adequate contour layout for the upper left lateral incisor dentin. Note that some variation is acceptable, but this layout divides the surface into rough quadrilaterals with angles near 90 degrees. Additionally, the sharp transition at the incisal edge has contour lines near the region of transition (to closely monitor the patch layout), but not directly over it (which may need to a non-continuous surface).
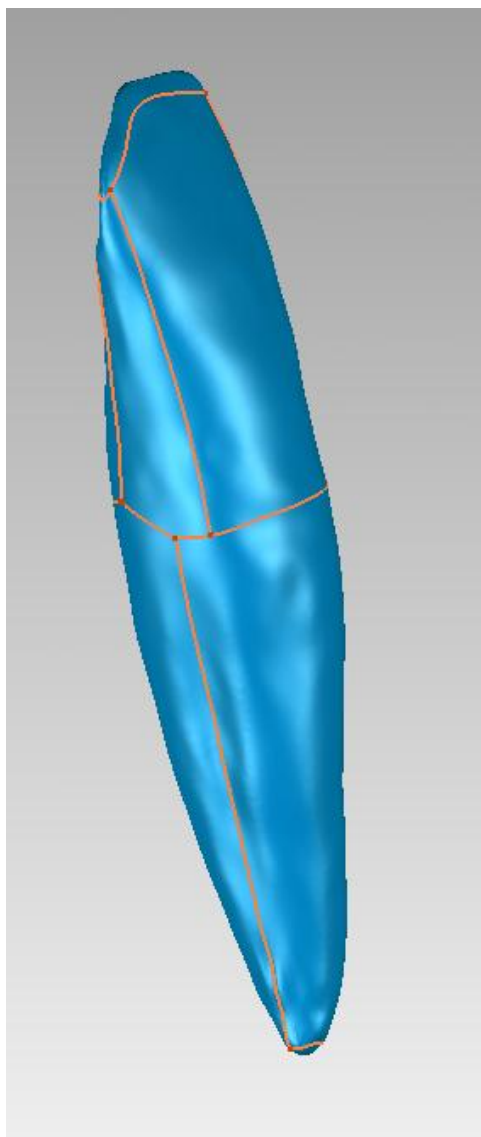
Figure 34: Contour lines for the upper left lateral incisor dentin.

At this point, it is worth summarizing the remaining steps before fully considering

issues in each area. Figure 35 shows the menus involved in these steps. First, the contour

lines are used to create a patch layout. This is automatically performed at the start, but

typically should be modified using the "Shuffle Patch" command to give a grid layout

wherever possible (Figure 36). Next, grids must be constructed using the patch layout. This

should yield a very detailed grid of the entire surface. If some areas are not finely covered or

the program highlights red regions, some detail has been lost. Finally, "Fit surfaces" is

clicked to create the NURB surfaces and the "Merge Surfaces" command can be used to automatically merge patches into a more reasonable number of faces for FEA. For the purposes of this study, typically around 10-20 faces were required. Fewer faces are preferred, but the original CAD objects had only two faces, which led to issues in FE modeling.
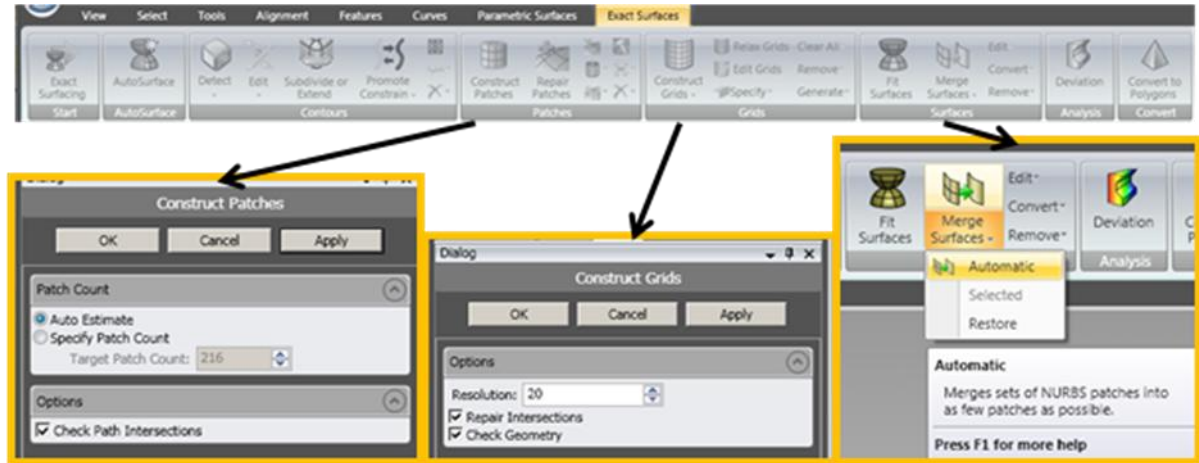
Figure 35: Summary of surfacing steps from construction of patches to construction of grids to merging of final surfaces.

If the contour lines are not fully closed, some problematic patch layouts can occur, such as seen in Figure 37A. Additionally, if the patches are skewed, it may create grids that are intersecting, as seen in Figure 37B. Finally, Figure 38 shows a typical result is non-grid layouts have the faces merged – many faces still remain.
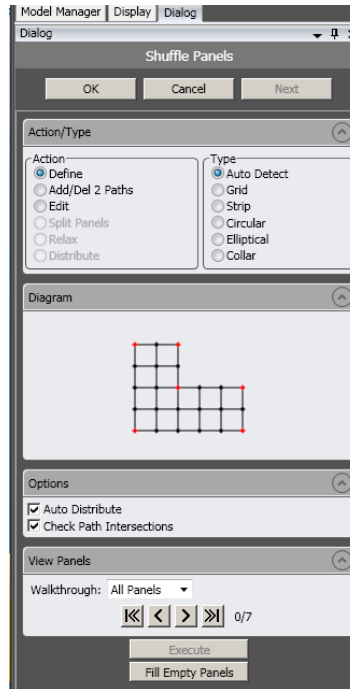
Figure 36: Shuffle patch menu, which allows selection of different regions defined by the contour lines, addition or deletion of the number of patches on edges (clicking on the edge adds or deletes two points, while clicking on the corner adds or deletes one points on each adjoining edge), or directly editing the points. The type of layout typically works best for reducing the number of faces if a "Grid" layout is selected.
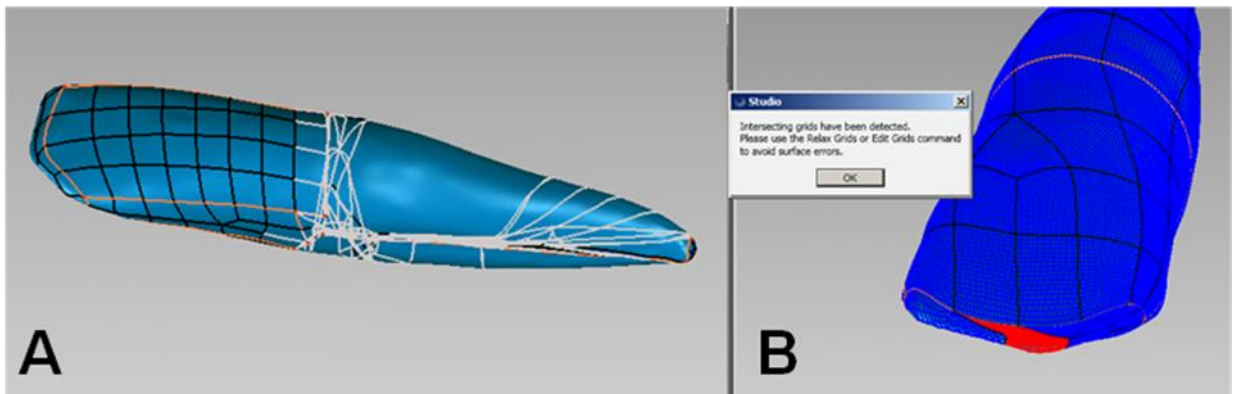
Figure 37: Potential errors in the surfacing process. A). Lack of closed contour lines leads to erratic patch layouts. B). Skewed patches may lead to intersecting grid lines.
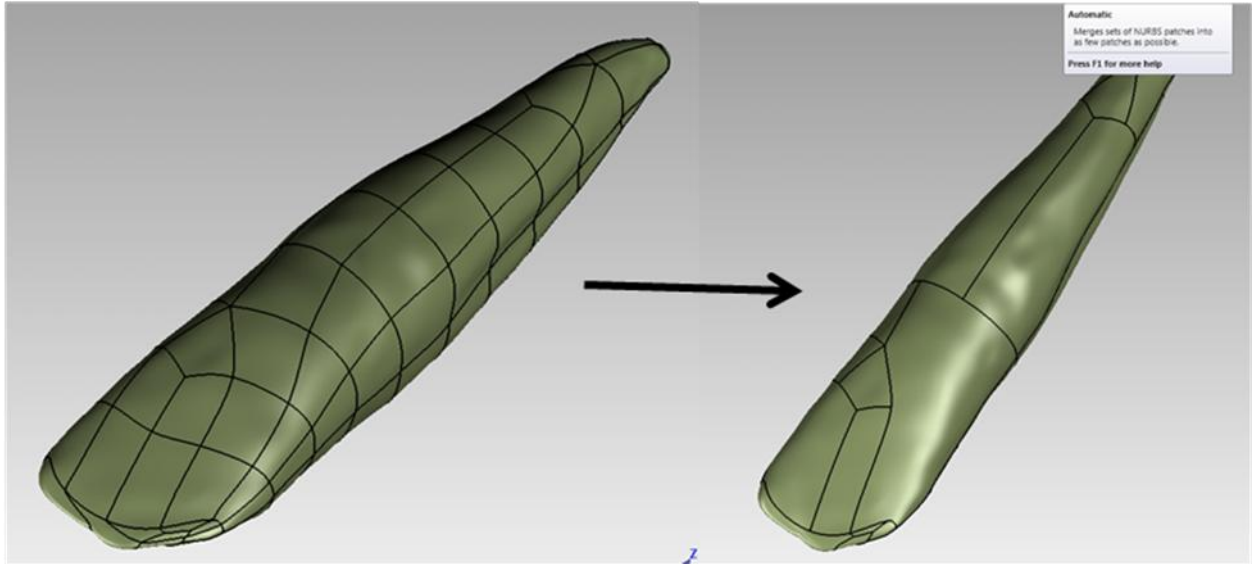
Figure 38: Demonstration of how a non-grid layout will not fully merge faces under "Merge Faces -> Automatic Merge"

The "Shuffle Patches" tool can be used to move to a simplified grid structure (Figure 39). A final grid appearance and final surface with the faces shown is seen in Figure 40, with 11 overall faces. Finally, a deviation analysis should be performed with the final surface and the initial input to assure that no undesired changes were made (Figure 41).
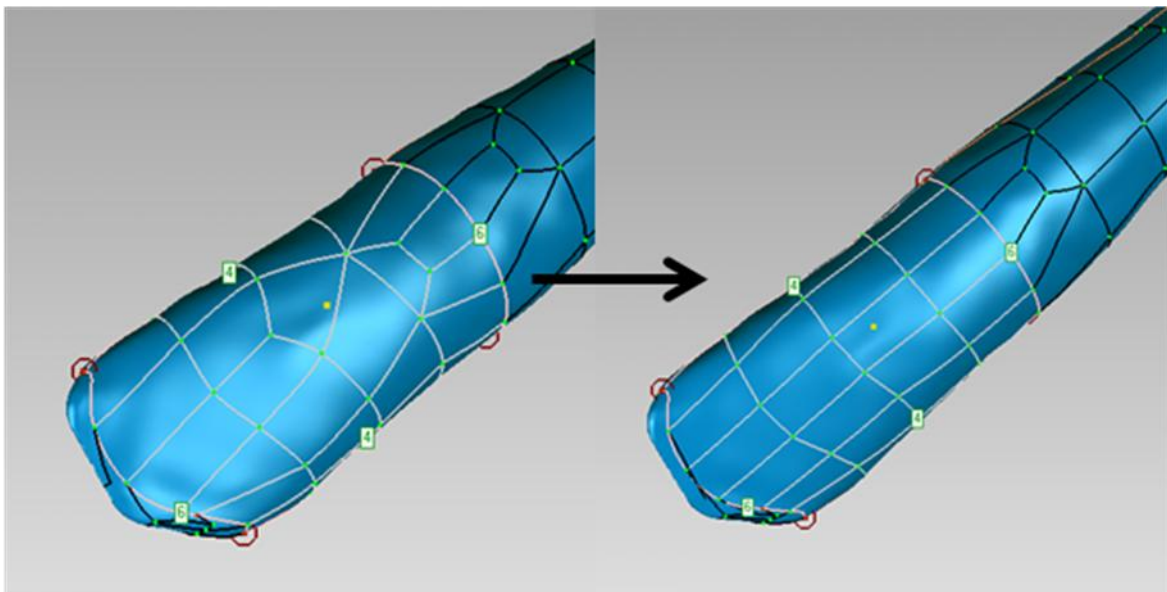
Figure 39: Simplification of a surface by using a grid layout.
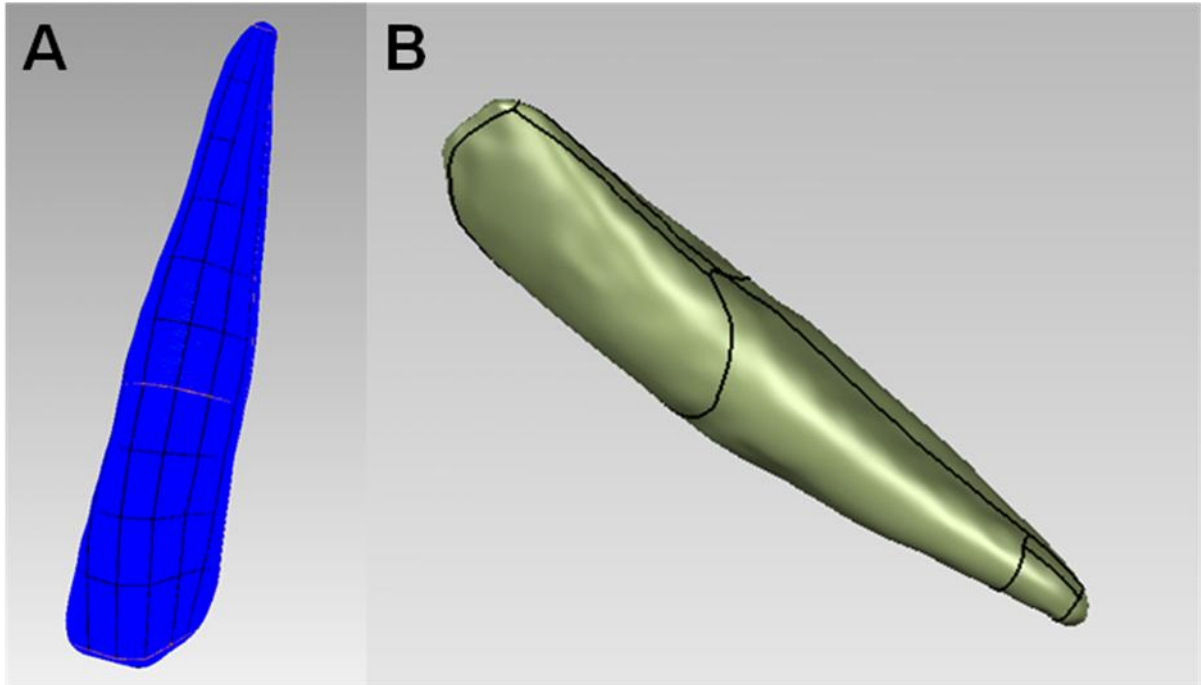
Figure 40: Ideal grid appearance (A) and final surface with 11 patches (B).
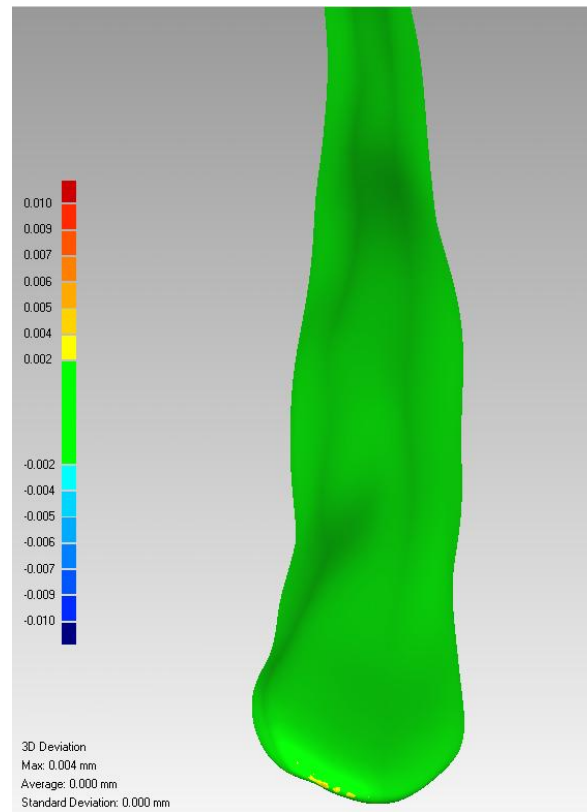
Figure 41: Deviation analysis between the initial upper left lateral incisor pulp and the final surface, demonstrating minimal undesired changes.

iv. Moving from individual objects to complex models

Proper surfacing of individual objects is important for FEA, but the most essential part of preparing complex models for FEA is ensuring proper connectivity. This is why only external surfaces were used in the previously surfacing steps – then the internal surface can be created by Boolean operations in Solidworks, ensuring an identical surface with identical faces. Figures 42 and 43 show a final setup of the upper left lateral incisor in Geomagic, including the following details:

- Enamel: The CEJ boundary is extended at least 0.5 mm before it is removed in order to assure an ideal interface is created when the dentin is cut away in Solidworks.

- Dentin: The apex is closed to allow a proper interface with the pulp. Additionally, the CEJ was changed to a separate curve object, moved 1 mm apically on the dentin, and projected onto the surface to mimic biological width. To smooth this curve, often it is necessary to hand-draw a spline on the surface that roughly follows the CEJ projection (Figure 44) This allows future creation of the PDL and also assures that faces do not abnormally intersect the CEJ.

- Pulp: The apex is further extruded 0.25 mm to assure that it extends through the apex and is able to be cut away by the surface of the dentin. (Figure 45)

Final surfaced bodies were saved into a STEP214 file format for importing into Solidworks.
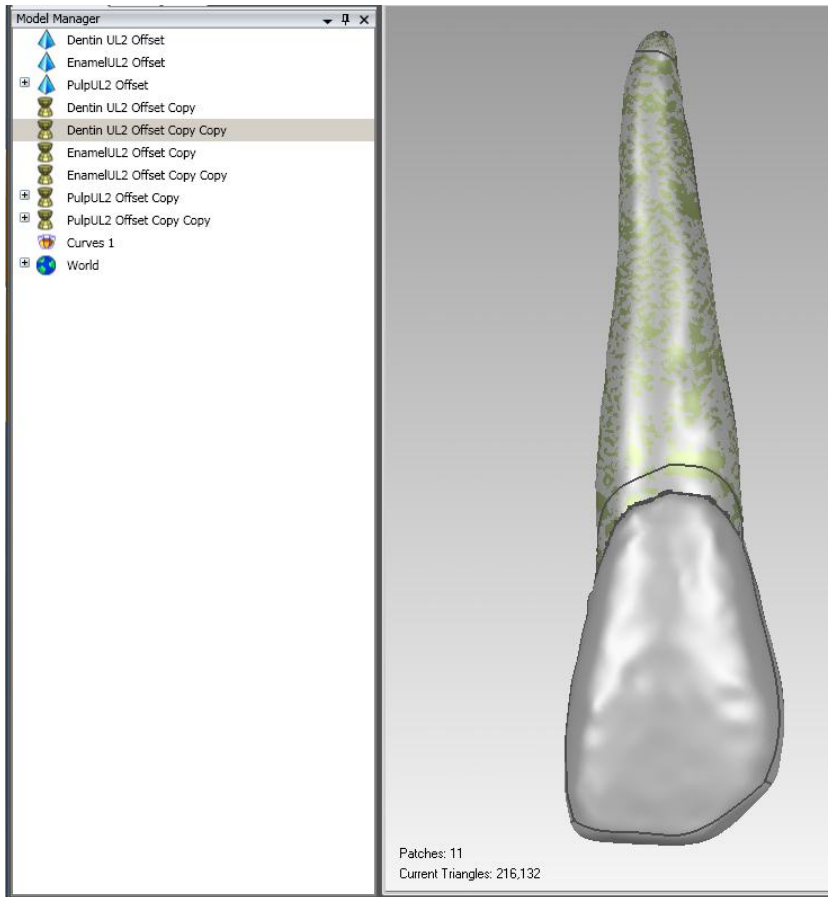
Figure 42: Overall appearance of the full model for the upper left lateral incisor. Note the preserved polygon models for manipulation if needed, the extra copy of the NURB surfacing workflow to recover any errors, and the CEJ curve ("Curves 1") that can be independently manipulated.
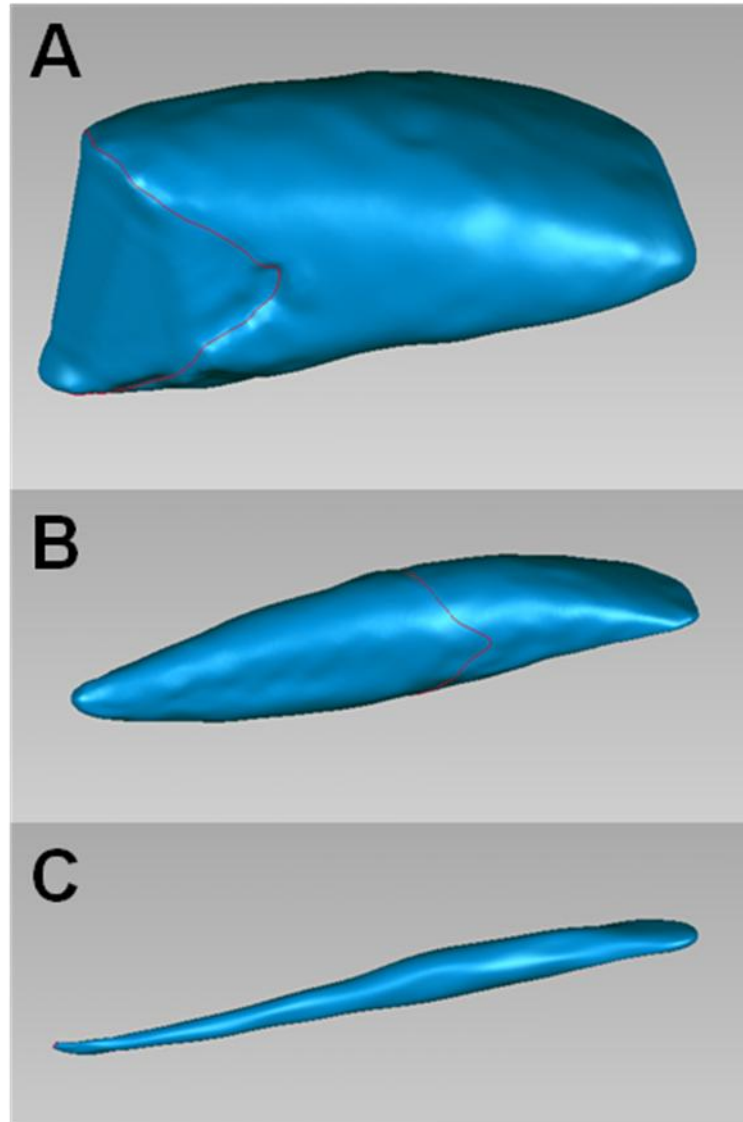
Figure 43: Final closed polygons models of the enamel (A), dentin (B), and pulp.
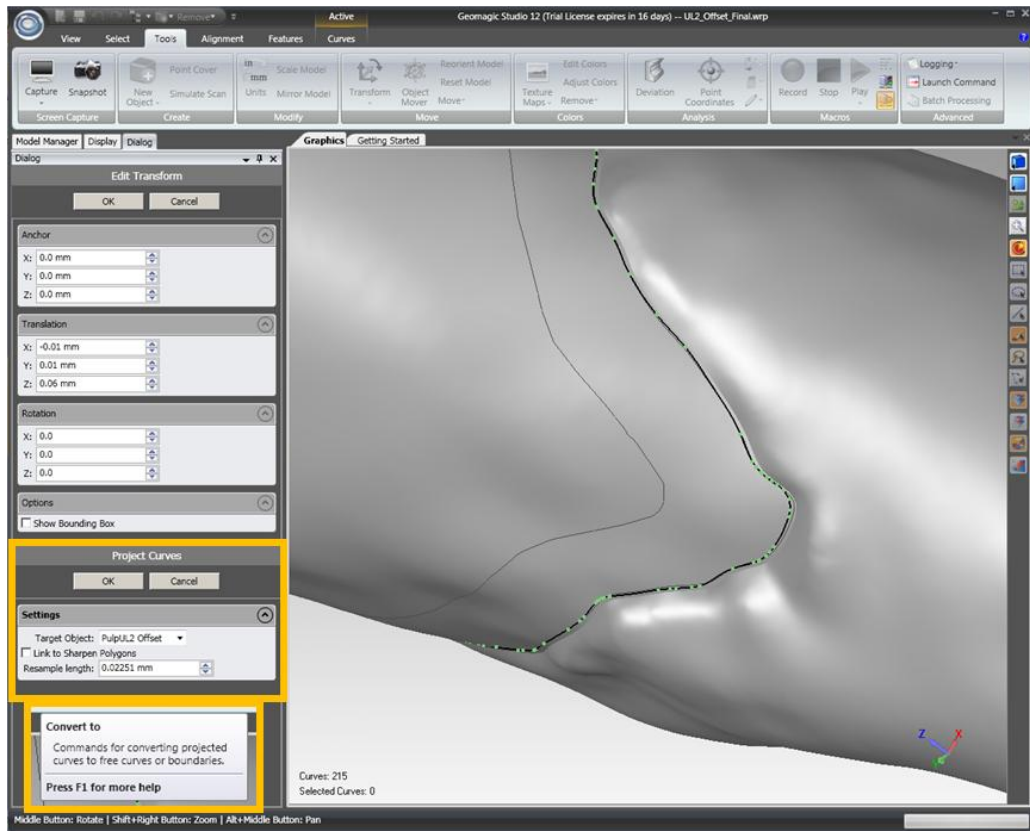
Figure 44: Independent manipulation of the CEJ boundary to create new curves. The "Edit Transform" option under "Tools" allows translation and rotation of the boundary. Using the "Project Curves" and "Convert to" -> "Boundary" options shown in the orange inserts allows the curve to be projected onto the dentin in another location.
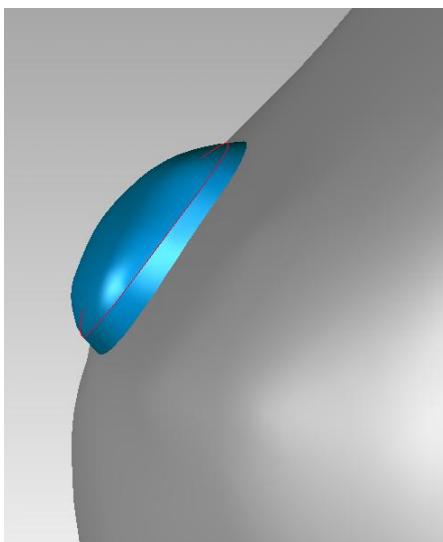
Figure 45: Extruded pulp through the dentin to allow Boolean operations in Solidworks.

ADDENDIX 2
SOLIDWORKS 2010

i. Importing objects from Geomagic

File -> Open -> selection STEP (.stp) file types and select bodies saved from

Geomagic.

Occasionally the program will prompt to repair a problematic face. Selecting "repair

all" typically works well and no further problems exist. Do not alter the location where the

body is imported (if the teeth are already in proper relationship with each other).

Save file as a .sldprt file, allowing further manipulation. For this study, these models

were saved as Dentin_UNCUT.sldprt, for example, to highlight the file was not yet ready for

FEA.

ii. Boolean operations.

The final enamel, dentin, and pulp were created from the following Booleans:

- Enamel: Subtraction of uncut dentin from the uncut enamel

- Dentin: Subtraction of the uncut pulp from the uncut dentin

- Pulp: Common body from the uncut pulp and uncut dentin

If this Boolean object is saved again as a .sldprt file, it will always load both previous

bodies and perform the Boolean object every time it is loaded. Since we are using many of

these Boolean objects, it is convenient to resave these as a separate geometry file. Parasolids

(.x_t) are the internal Solidworks geometry files, so no significant information is lost if these

bodies are first saved as a Parasolid file, reopened, then saved as a .sldprt file. These files

were saved as Dentin_CUT.sldprt, for example.

The final cut enamel, dentin, and pulp for each tooth were loaded together into a common

Solidworks part file, such as UL2.sldprt, which became the base tooth used for all combined

models in the future (Figure 46).
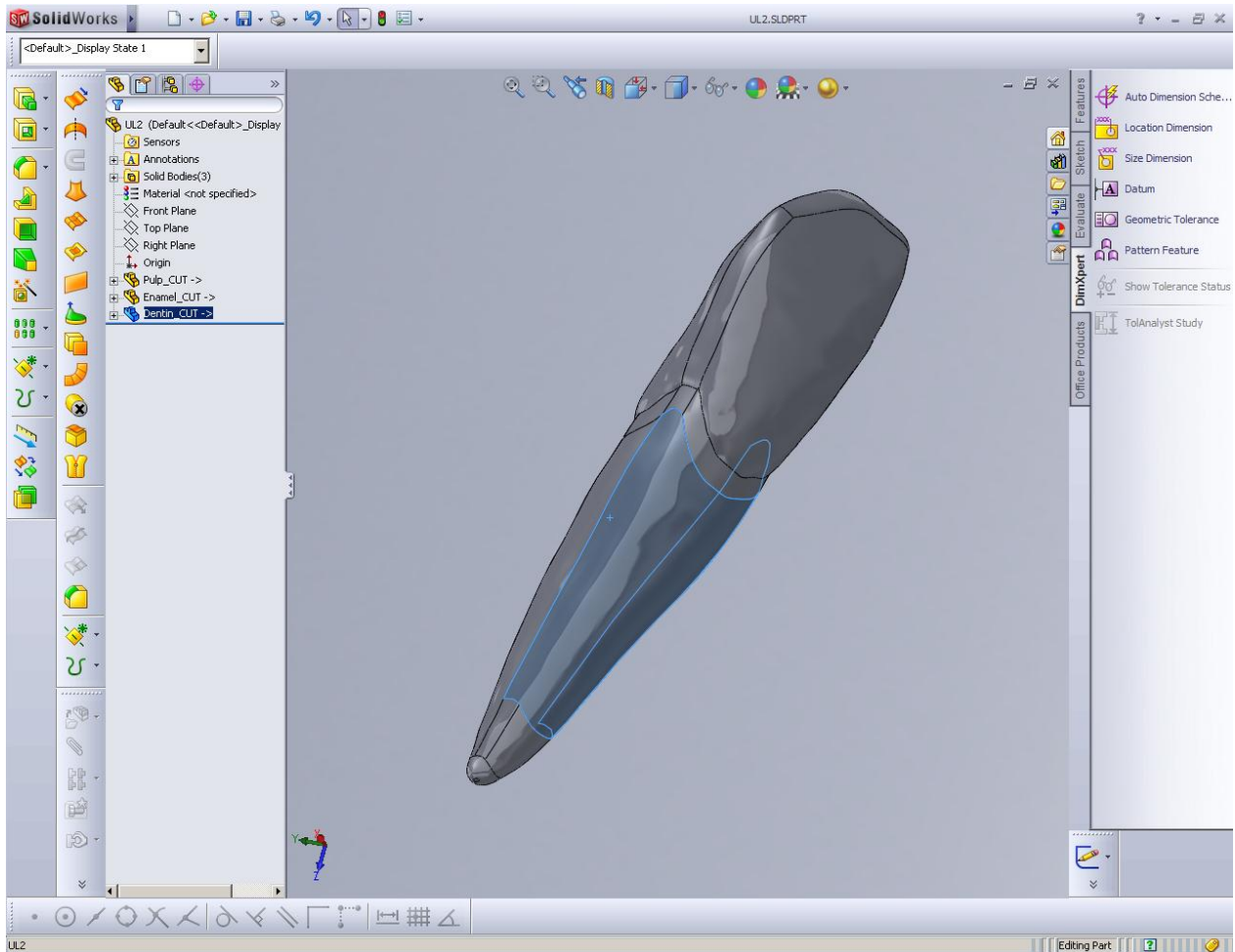
Figure 46: Final Solidworks part file with the cut enamel, dentin, and pulp of a single tooth.

iii. Creation of the PDL

Ideally, the biologic width of each tooth could be respected and the apical faces over

1mm below the CEJ could be thickened 0.25 mm to 0.5 mm to reproduce each individual

PDL. However, this study already had a scan of the maxillary trabecular bone and cortical

bone with the teeth placed within the structure. Therefore, it was decided to use the 0.25 mm

gap between the cortical bone and dentin of each tooth as the PDL, with the occlusal

boundary being the height of the existing alveolar bone. Note that on some occasions this

was significantly greater than 1mm and other occasions significantly less.

In order to create each PDL, the internal surfaces of the lamina dura were duplicated

from the cortical bone model, using the "Surface-Offset" command seen in Figure 47.   The

surface was merely duplicated, so an offset value of "0" was used. Next, using the "Surface

Fill" and "Surface Knit" commands, a closed solid was created by filling over the entire

occlusal portion of the surface (Figure 48A). Then, a Boolean operation was used to cut the

dentin of that tooth from pulp (Figure 48B). Note that either the uncut dentin must be used,

or the cut dentin and cut pulp.
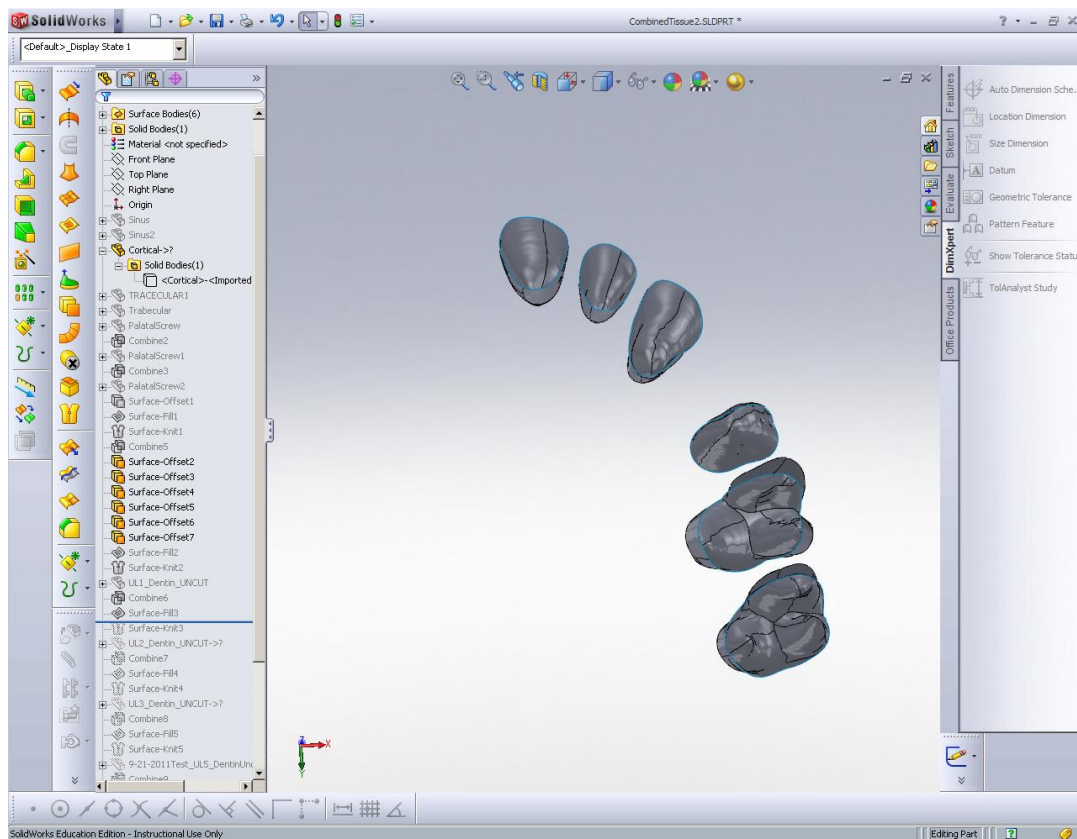
Figure 47: "Surface –Offset" command to create duplicates of the internal surfaces of the lamina dura.
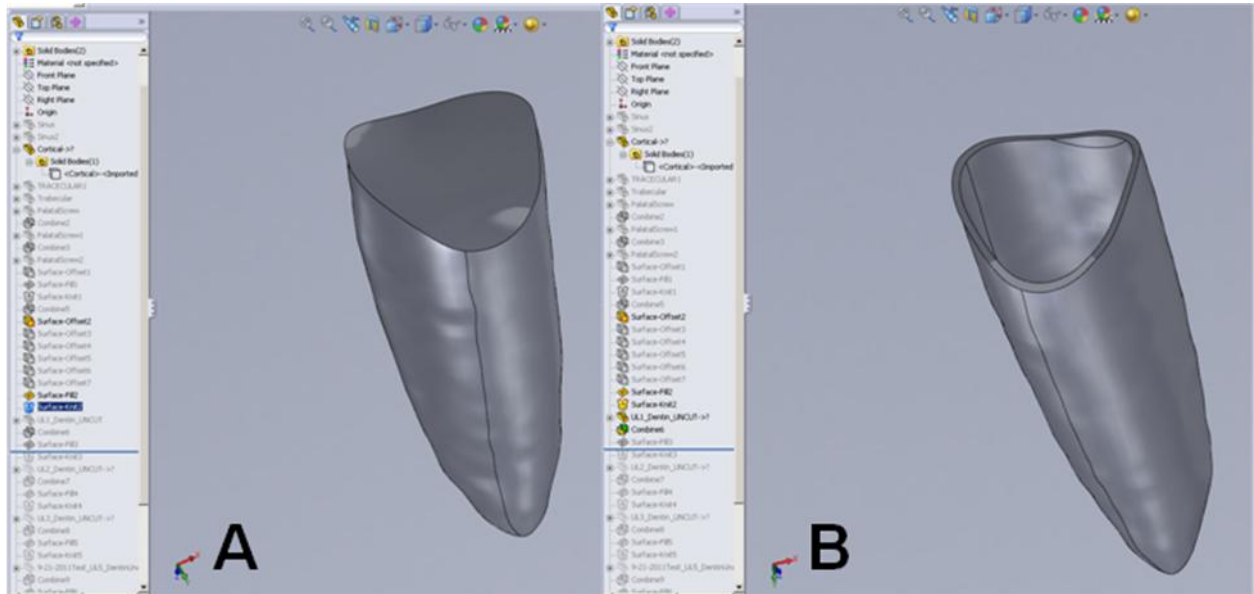
Figure 48: A: "Surface-fill" command and "Surface-Knit" command used to form a solid body. B: Final PDL with the dentin cut away from the previous body.

iv: Miscellaneous checks to ensure adequate connectivity

The follow manipulations were also performed to ensure connectivity:

- In a similar manner to how the PDL was created, the internal surfaces of the cortical bone and sinuses were duplicated and used to form a new solid body for the trabecular bone to ensure no gaps or penetration.

- Bracket bases were extended into the enamel, then cut to ensure good adaptation.

- The palatal miniscrew was cut from the cortical and trabecular bone.

- The transpalatal arch (TPA) was extruded at both ends and cut to ensure proper fit.

- All adjacent enamels surfaces were checked to ensure no overlap.

The final Solidworks model is shown in Figure 49.
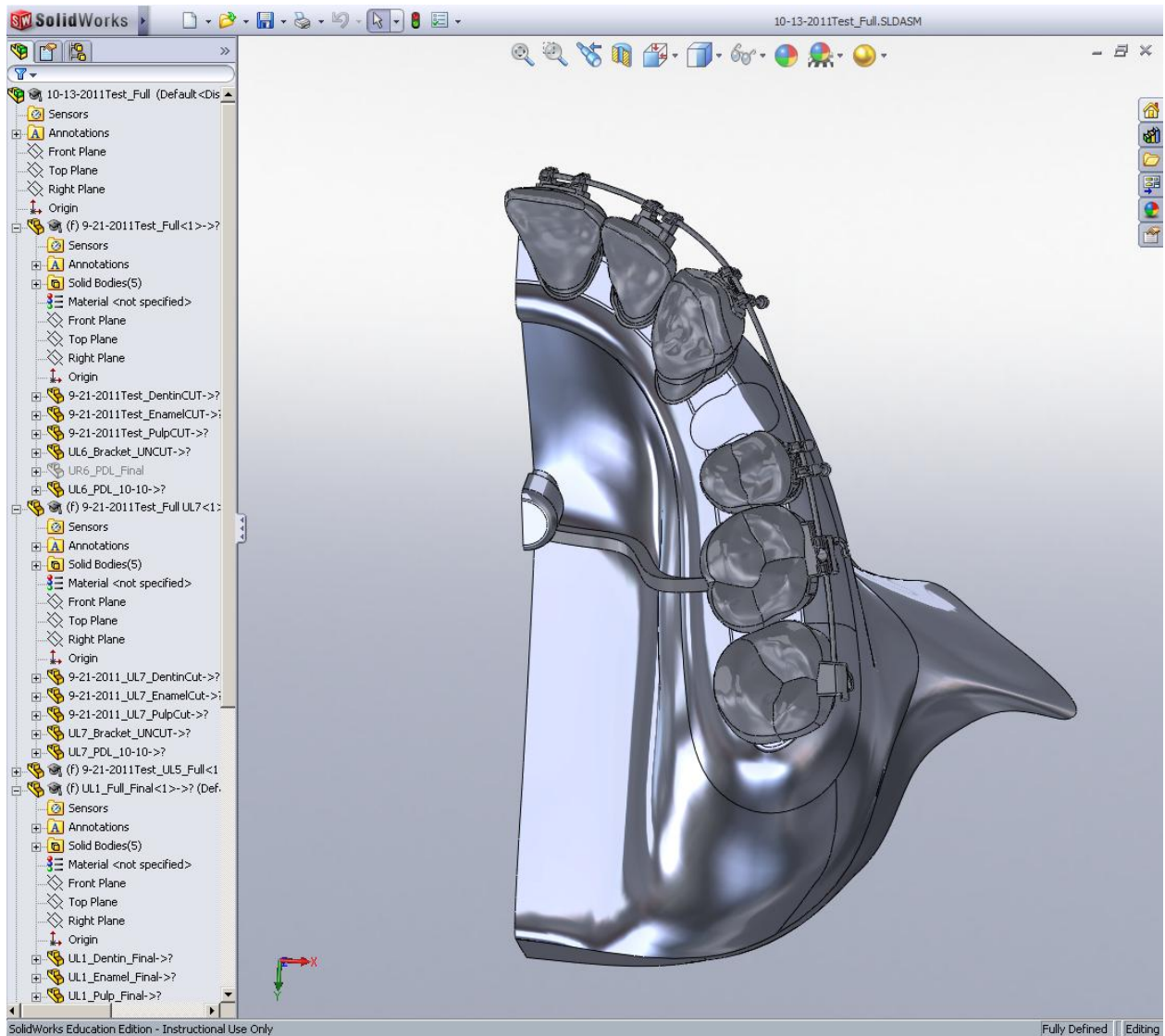
Figure 49: Final Solidworks model of the dentition with palatal miniscrew, brackets, and round wire.

If all the previous steps have been properly followed, this model should have

geometry with no small holes, gaps, sliver faces, or poor connectivity. This should allow the

geometry to be directly imported into Solidworks. If this fails for any reason, the file can be

saved as an IGES file (Figure 50):

- SolidWorks -> File -> Save as.

- Change file type to IGES (*.igs) and click options

- Change to "Manifold Solid B-rep Object" and change system preference to
  "ANSYS"
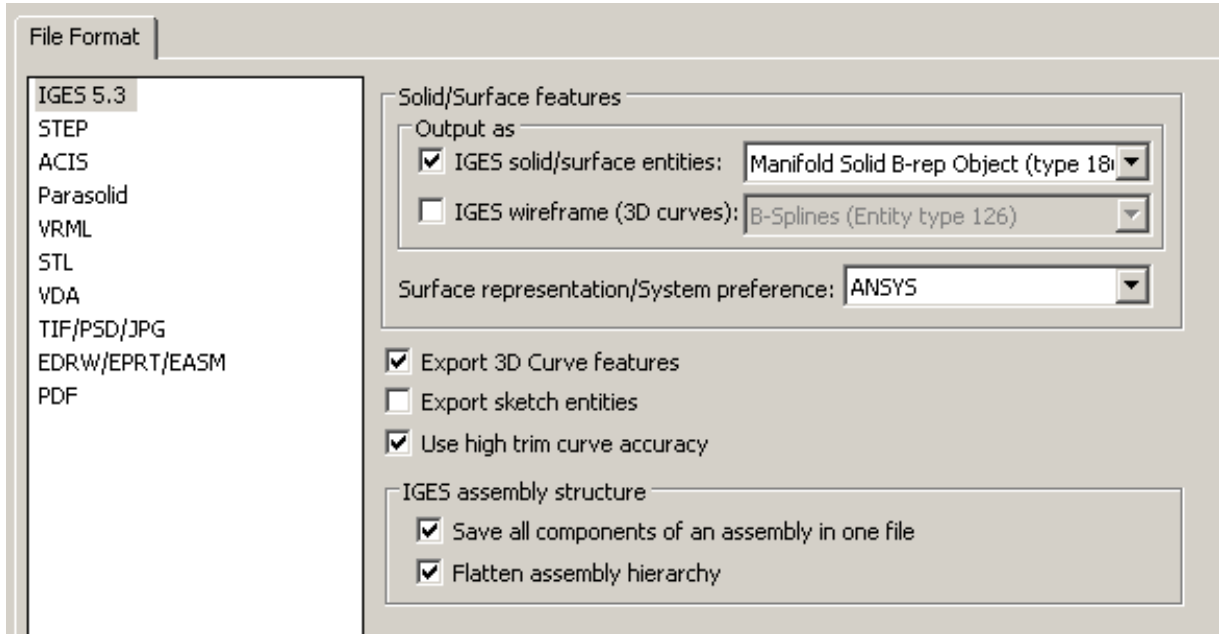
Figure 50: Correct options to save a Solidworks file as an IGES file for importing into ANSYS

ADDENDIX 3
ANSYS 12.1/13.0 /14.0

i. WorkBench:

To begin projects in ANSYS, load ANSYS WorkBench and select "New project". WorkBench combines multiple powerful FEA programs into one place and creates workflows to guide the user through an analysis. Drag over your planned design, which for the purposes of this study was "Static Structural" (Figure 51). Right click on geometry and select "Import geometry" and find your IGES file or SLDPRT file.

Points to know on the main WorkBench screen:

1. Static Structural will display a box with six components - the typical workflow a user will need to follow for running the simulation. Note: Green marks are good, yellow needs to be updated, and red are problematic.

2. Components from one system can be shared with a new system if it is dragged onto the screen.

3. Each of the six components can be double-clicked for editing, but this may occur in different programs (described below)

At this point, WorkBench will allow directly loading the CAD model into ANSYS Mechanical by clicking on "Model". First, first material properties should be added in "Engineering Data". However, in order to check the geometry, rename parts, group parts, or delete parts, Design Modeler should be loaded first by clicking on "Geometry".
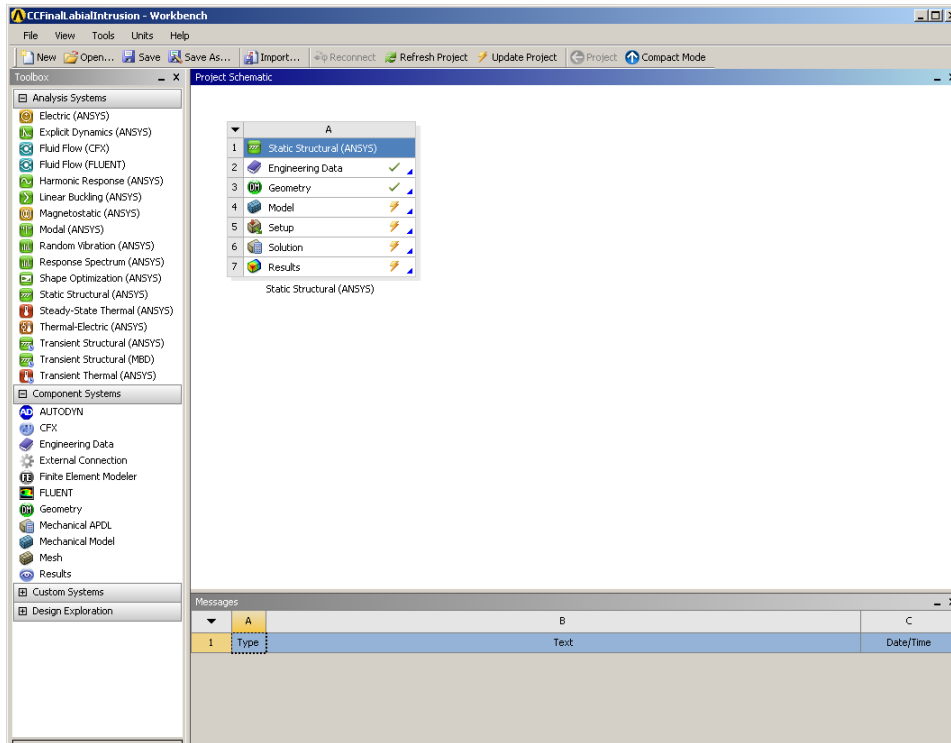
Figure 51: Main screen of ANSYS WorkBench, with a Static Structural workflow shown.

ii. Engineering Data

Any materials you want included other than stainless steel have to be added here

(Figure 52). Material properties for a typical organic model have been saved to a local

library in our lab. Click on "File", then "import engineering data", and select

"EngineeringData_new.xml" in D:\Users\Larson\Initial Half Maxilla Model - after the

library is loaded, the save icon needs to be selected on any materials used in the model.

If the material properties are not displayed, ensure that "Properties", "Outline",

"Table", and "Chart" options are selected under the "View" menu. Click "Return to Project"

on the top to go back.
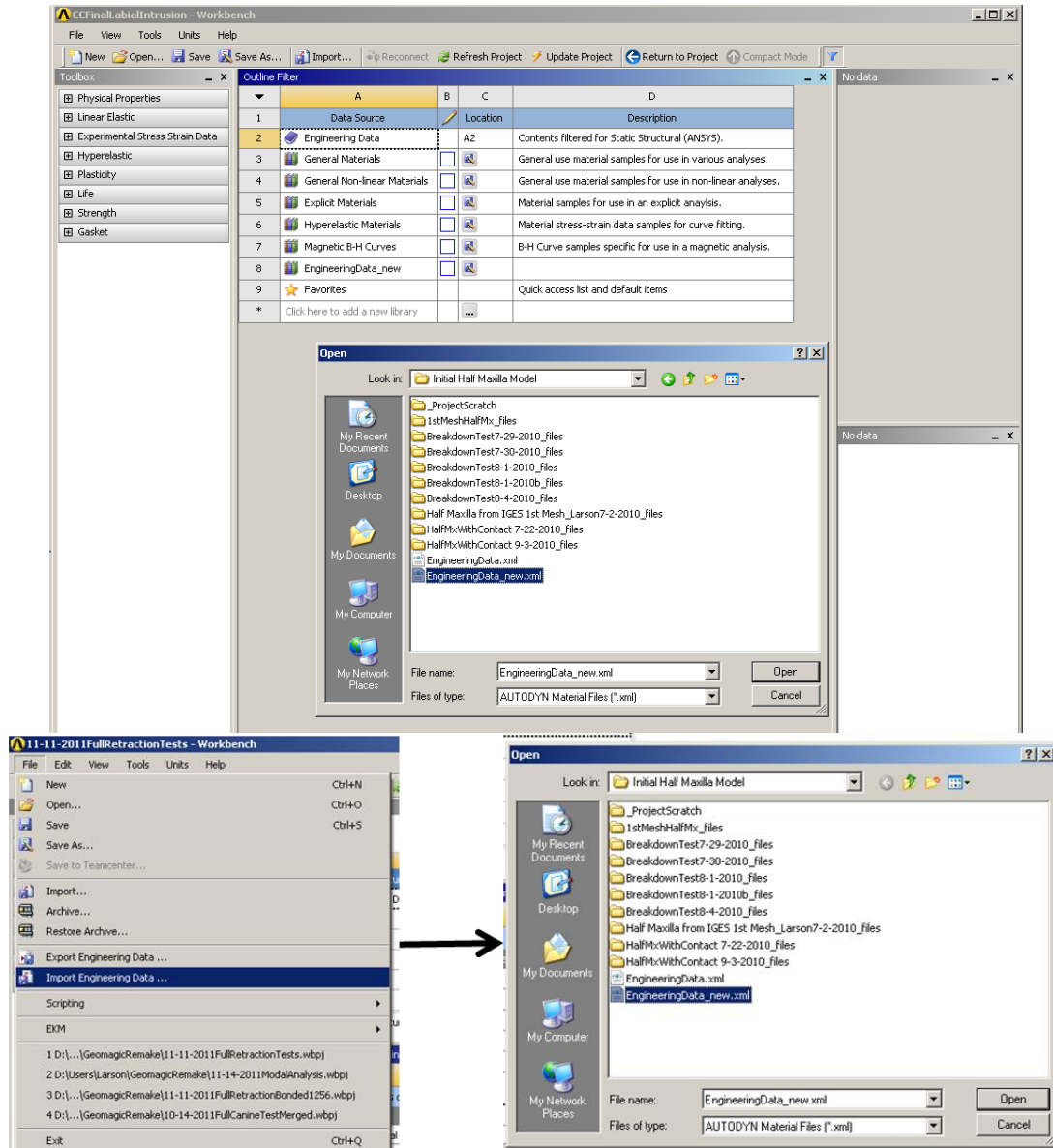
Figure 52: Importing previously saved engineering data to provide additional materials other than stainless steel.

iii. Design Modeler

The following items should be examined in DesignModeler:

- Import the geometry into DesignModeler by clicking "Generate" (Figure 53)

- Using the "Repair Geometry" tool, identify and fix any problematic geometry. For the previous labio-lingual model introduced by this lab, this involves suppressing all

bodies except for the lateral incisor dentin, selecting "repair faces", and fixing only the two smallest faces. The same should be done for the enamel of the lateral. For the updated geometry in the canine retraction model, no alterations are needed. (Repair edge and repair sliver were both used with default settings and fixed most problems. Repair face was used for the final problems - but must be performed careful. This feature will over simplify and create more problems if the default settings are used. For the labio-lingual model, it was effect to only select bodies with problematic geometry (namely, the lateral incisor dentin and enamel) and change max area to 1.3e-7.)

- Suppress any un-needed parts

- Group any bodies together that you would like to be considered one multibody part (Figure 54). Ideally, all bodies except for the wire should truly be merged together, but ANSYS does not load correctly the model correctly if they are all combined – both due to computational requirements and because the teeth are bonded to the PDL but not to each other (e.g. the central and lateral incisor enamel are not rigidly bonded, but are touching, which is difficult for the program to process as a single multi-body part). For the labio-lingual model, there were problems at the interface between the central incisor dentin and enamel, the central incisor and canine bracket and enamel, the gingival to the bone, and the PDL to the dentin of each tooth, so those bodies could not be combined. For the canine retraction model, typically each tooth is considered a unique part, and the PDL bodies are all combined with the surrounding bone.

- Close Design Modeler. This will take some time because it needs to save the geometry file, so do NOT force the program to close.
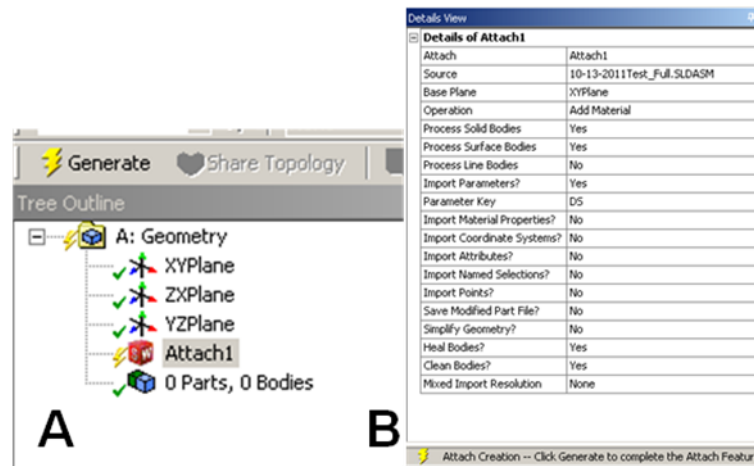
Figure 53: Selecting the geometry to import (A) and the options for attaching geometry (B). There should be only solid bodies to process, but "Process Surface Bodies" was also left on to help process any problematic geometry.
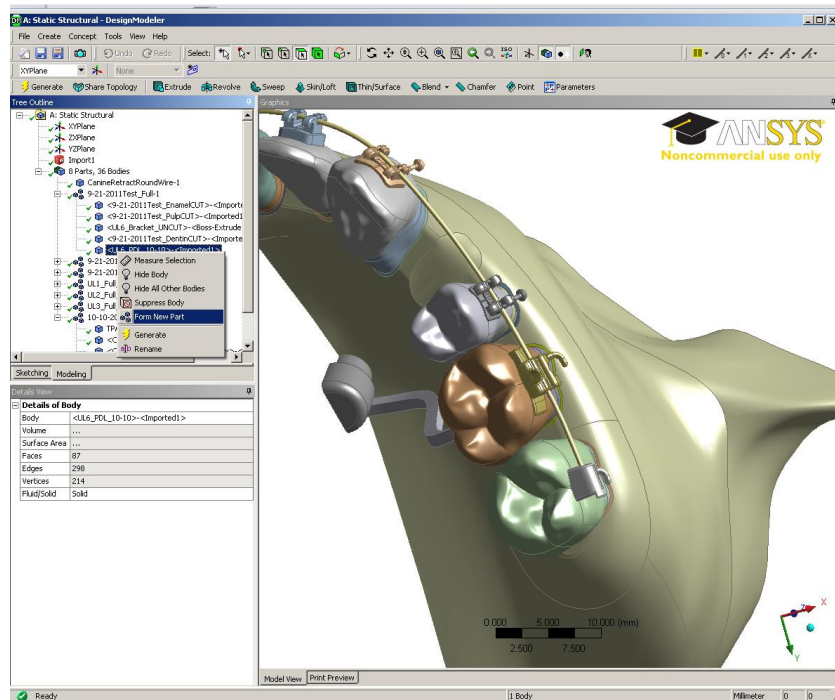
Figure 54: Using the "Form New Part" command by right clicking on a body to remove the PDL from the combined tooth part. This can also be used when selecting the PDL and the surrounding bone to combine them into one part.

81

iv. Mechanical

- Set material properties for each material under geometry (Figure 55).

- Any complex material properties (anisotropic, viscoelastic, etc) must be added with a "Command" object and coded.

- When selecting "Geometry," an option appears to display by "Material" under "Display style" (Figure 56).   This is a very effective check to ensure all the bodies were changed to the correct material property.
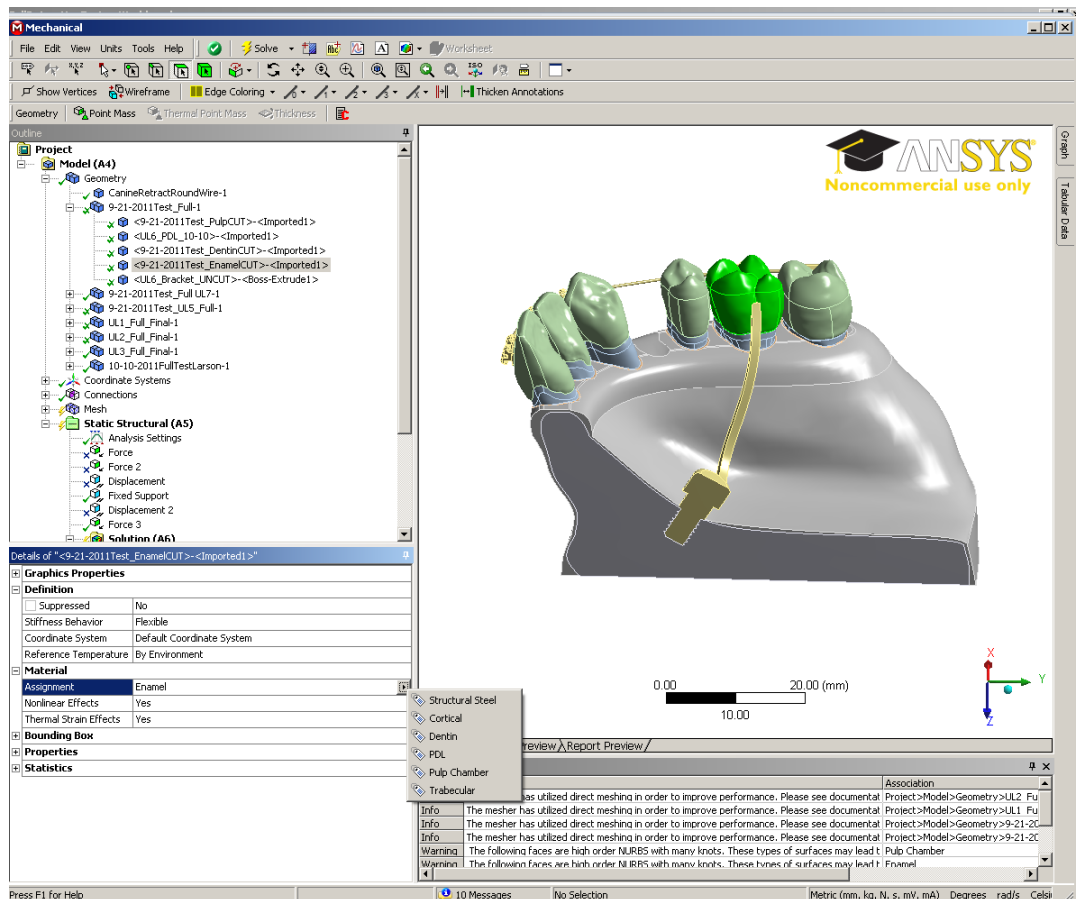
Figure 55: Assignment of material properties in Mechanical. Note: Properties must be added in "Engineering Data" prior to opening Mechanical
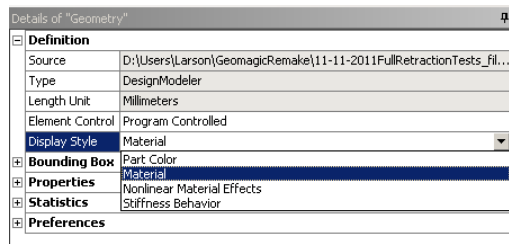
Figure 56: Displaying by material properties.

v. Contact Conditions

The next main menu in Mechanical is "Connections," which allows the manipulation of contact conditions between the bodies. (There is also a "Coordinate Systems" menu, but no local coordination systems were set for this study.) The connections under this menu are automatically detected when Mechanical is opened for the first time with new geometry. This automatic detection works well, but the connections should be checked as some problems do occur. Two common issues that occur are the following:

- Extra contact conditions between the cortical bone and some of the dentin bodies due to the minimal thickness of the PDL: This will not necessarily affect the solution, but will increase solution time since it will keep searching for interactions between these surfaces that never should touch.

- Lack of connection between an archwire and bracket when using the birth-death technique: Since the wire is often displaced from the bracket slow when using the birth-death technique, occasionally it will not properly detect the contact. This must be manually added to obtain accurate solutions.

Figure 57 shows a screenshot when selecting a contact and the proper menu to change the contact condition from a bonded contact to frictionless or frictional. For the purposes of this study, a frictionless contact condition was used, as frictional contacts require further investigation as to the proper frictional coefficient. Frictional coefficients from 0.03 – 0.2

frequently solved (0.2 solved in the labio-lingual model, but not in the canine retraction

model), yet a coefficient of 0.3 or greater did not converge on a solution. Also under this

menu are options to change the surfaces that are involved, the coefficient of friction (if

appropriate), penalties if the contact is penetrating, and the pinball region.
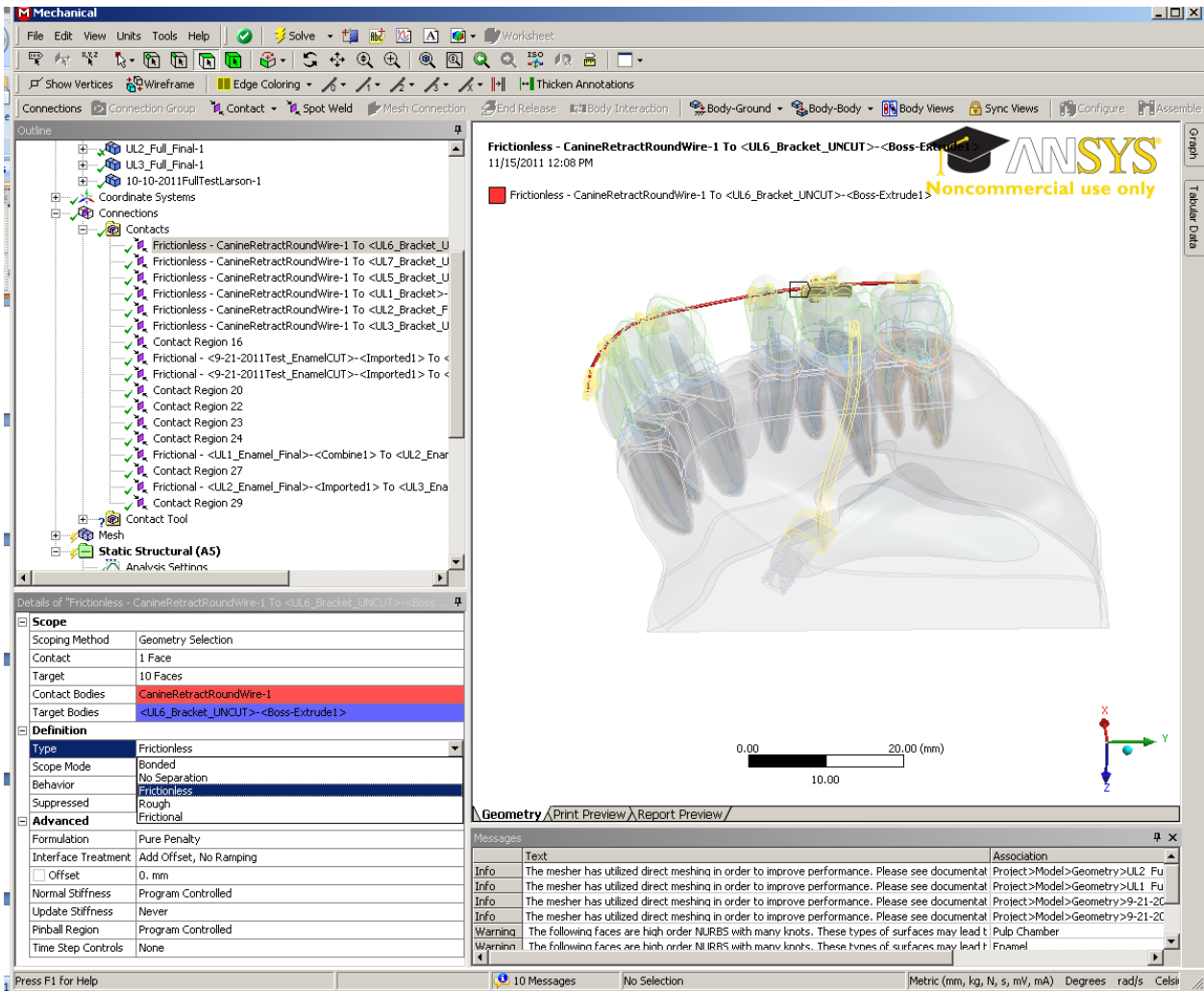
Figure 57: Screenshot of altering a contact condition in Mechanical. In this menu, the
pinball radius, interface treatment, stiffness, and surfaces involved can all be manipulated.

Another useful tool under the "Connections" menu is the "Contact Tool," which can

evaluate the initial contact conditions in the model. This can be very useful to check for

initial gaps or penetration of the contact surfaces. Note that some contact conditions are

more tolerant of initial penetration – for example, a bonded surface will merely remove any overlap.
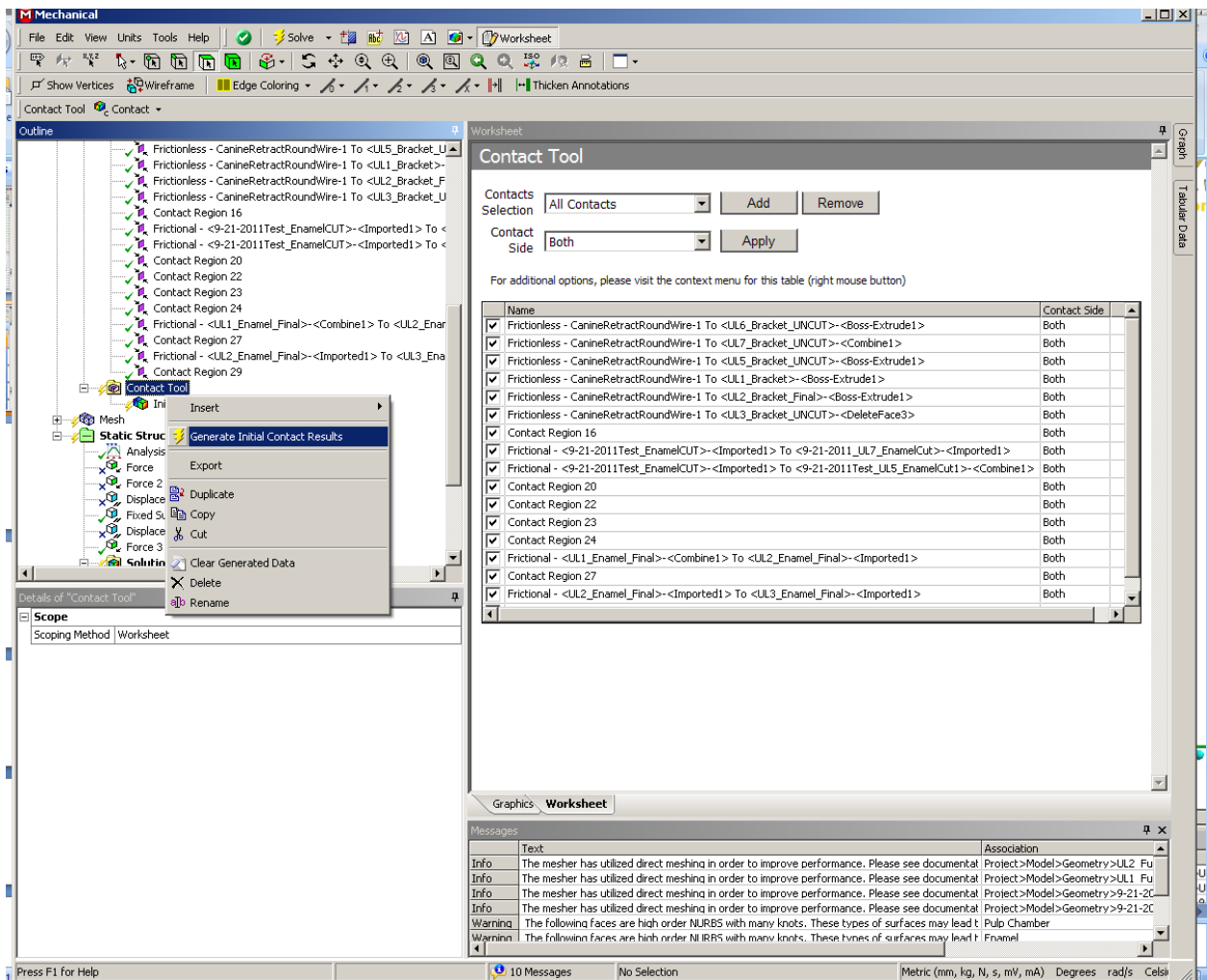
Figure 58: "Contact Tool" option that can be added under "Connection." This tool can generate the initial contact results and point out if any large gaps or penetration of the contact surfaces exist.

In order to model an active archwire (as done in the labio-lingual model), the birth-death technique must be utilized (Canales et al., in preparation). Technically, ANSYS supports a second method to engage an active arch – adding an initial offset to the contact under "interface treatment" – but solutions would not converge using this technique. The birth-death technique must be added through the use of a command object in Workbench. Here is an example of a typical implementation:

1. Add a command object under the contact region to kill containing the following commands:
   cont=cid
   targ=tid

2. Set up Analysis settings for 2 loadsteps.

3. Add two command objects to the Static Structural Environment branch. One for EKILL and one for EALIVE and use the command object details window to assign each of these to be executed right before LS 1 and LS 2 respectively.

   EKILL command object should have the following:
   esel,s,type,,cont
   esel,a,type,,targ
   ekill,all
   allsel

   EALIVE command object should have the following
   esel,s,type,,cont
   esel,a,type,,targ
   ealive,all
   allsel

These commands will write to the output file when they are implemented, so if a model fails, the time of failure can be checked by examining the output files under the "./dp0/SYS/MECH" folder of the test being run (Figure 59). These output files also report solution times and processor usage, and can be useful in comparing computational requirements between models.
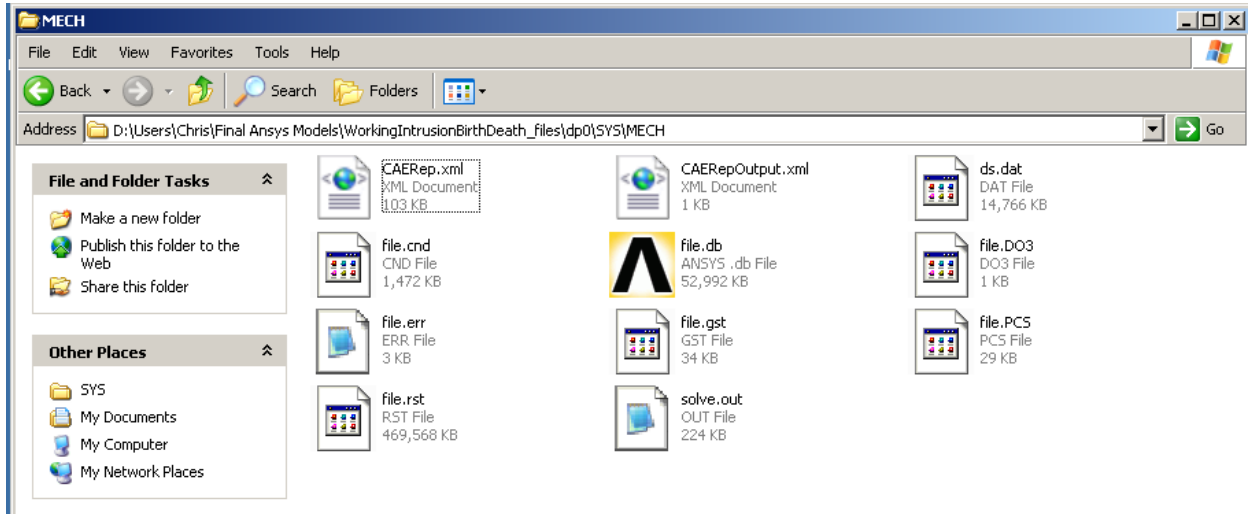
Figure 59: Output folder for Mechanical, showing the "solve.out" file and "file.err" file that can be examined when models fail to converge for errors or warnings.

vi. Meshing

As shown in this thesis and previous studies (Schmidt et al., 2009, Bright & Rayfield 2011), mesh sizing in very important in the accuracy of FE solutions. When non-ideal geometry is used, obtaining a mesh of any size can become difficult. For the labio-lingual model, before the surfaces were optimized, the mesh sizing previously shown in Table 6 was one of only options that obtained a proper mesh (0.2 mm for brackets and wire, 0.8 mm for teeth and PDL, and 2 mm for bone). The same sizing was used for the full half maxilla model. These options were added by the "body sizing" under the "mesh" menu (Figure 60). For the fine mesh size in the substructural model, the "contact sizing" option was used so that nodes were matched at the interface. This meshes the bodies simultaneously, so the computational requirements are increased. Additionally, ANSYS has added some tools to vary mesh size during the solution to achieve mesh convergence, but these tools were not used in this study.
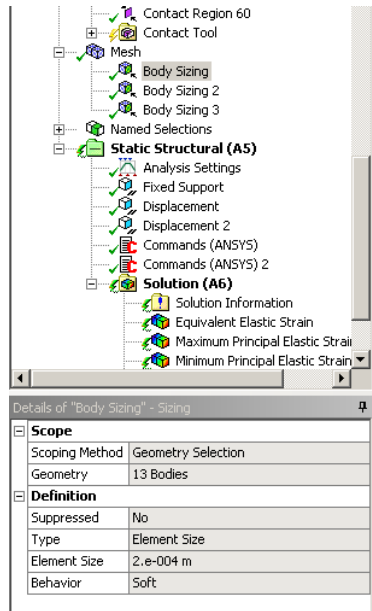
Figure 60: Mesh menu in Mechanical, showing the body sizing options typically used for the half maxilla and labio-lingual model. The element size can be manipulated from this menu.

vii. Static Structural

The static structural menu (Figure 61) is where the analysis settings, loading conditions, and boundary conditions were set. Under analysis setting, most options work very well under the "Program Controlled" selection. If the birth-death technique is being utilized, note that "Number of Steps" must be set to 2, as shown in Figure 61. This allows one step with the contact deactivated for the wire to be placed into the slot and one step with the contact activated for the wire to engage the bracket.

Loading conditions, such as forces or moments, can also be added under this section. They can be applied to surfaces, lines, or points. For this study, canine retraction forces were equally applied over the bracket hook surface.

Boundary conditions are set using "fixed support" or "displacement" commands. A fixed support will fully constrain the surface, line, or point in the x, y, and z dimensions. Meanwhile, using the displacement option allows constraint of the model in only one or two dimensions. It is preferred not to over-constrain a model, so attempt to place only the

boundary conditions that accurately represent the model (e.g. if a model is sectioned at the

midline, only limit displacement across that boundary).
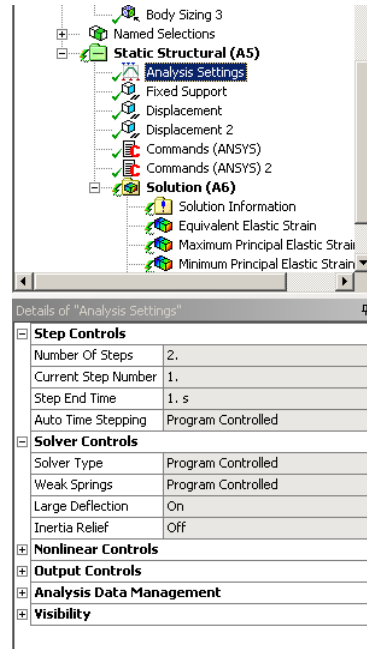
Figure 61: Static Structural menu in Mechanical, showing two steps and two command objects for the birth and death technique. All loading conditions and boundary conditions are set under this menu.

viii. Miscellaneous ANSYS Items
1. Updating academic licensing with ANSYS 13.0

   License - Start -> Program -> Ansys, Inc. License Manager -> ANSLIC_ADMIN

   Utility

   Go to "Set license preferences for use *****" and select "use academic license"

2. Changing background color. This option if found in the WorkBench program, not in

   Mechanical or DesignModeler, although it will affect all programs (Figure 62).
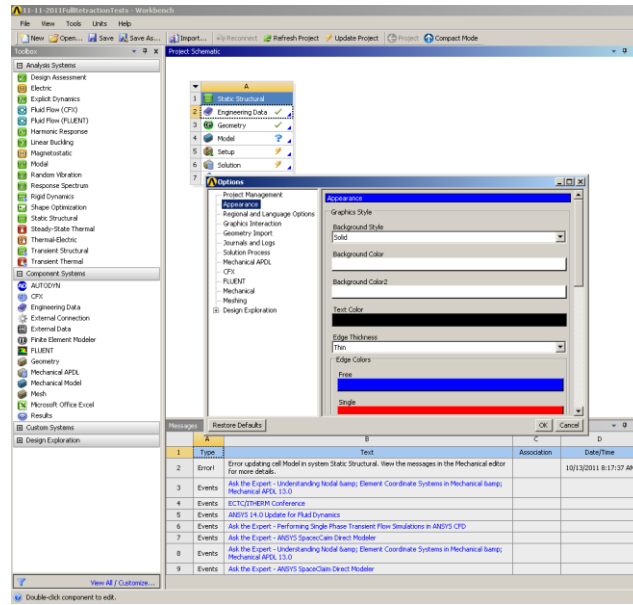
Figure 62: Menu for changing background color in ANSYS.

REFERENCES

Ammar, H. H., Ngan, P., Crout, R. J., Mucino, V. H., & Mukdadi, O. M. (2011). Three-dimensional modeling and finite element analysis in treatment planning for orthodontic tooth movement. *American Journal of Orthodontics and Dentofacial Orthopedics : Official Publication of the American Association of Orthodontists, its Constituent Societies, and the American Board of Orthodontics, 139*(1), e59-71. doi:10.1016/j.ajodo.2010.09.020

Andreasen, G. F., & Zwanziger, D. (1980). A clinical evaluation of the differential force concept as applied to the edgewise bracket. *American Journal of Orthodontics, 78*(1), 25-40.

Badawi, H. M., Toogood, R. W., Carey, J. P., Heo, G., & Major, P. W. (2009). Three-dimensional orthodontic force measurements. *American Journal of Orthodontics and Dentofacial Orthopedics : Official Publication of the American Association of Orthodontists, its Constituent Societies, and the American Board of Orthodontics, 136*(4), 518-528. doi:10.1016/j.ajodo.2009.02.025

Baumrind, S. (1969). A reconsideration of the propriety of the "pressure-tension" hypothesis. *American Journal of Orthodontics, 55*(1), 12-22.

Boester, C. H., & Johnston, L. E. (1974). A clinical investigation of the concepts of differential and optimal force in canine retraction. *The Angle Orthodontist, 44*(2), 113-119.

Bourauel, C., Freudenreich, D., Vollmer, D., Kobe, D., Drescher, D., & Jager, A. (1999). Simulation of orthodontic tooth movements. A comparison of numerical models. *Journal of Orofacial Orthopedics = Fortschritte Der Kieferorthopadie : Organ/official Journal Deutsche Gesellschaft Fur Kieferorthopadie, 60*(2), 136-151.

Bright, J. A., & Rayfield, E. J. (2011). The response of cranial biomechanical finite element models to variations in mesh density. *Anatomical Record (Hoboken, N.J.: 2007), 294*(4), 610-620. doi:10.1002/ar.21358; 10.1002/ar.21358

Burr, D. B., Schaffler, M. B., Yang, K. H., Lukoschek, M., Sivaneri, N., Blaha, J. D., et al. (1989). Skeletal change in response to altered strain environments: Is woven bone a response to elevated strain? *Bone, 10*(3), 223-233.

Canales, C., Larson, M., Grauer, D., Sheats, R., Stevens, C., & Ko, C. (In preparation). A novel biomechanical model assessing orthodontic, continuous archwire activation. *Am.J.Orthod.Dentofacial Orthop.,*

Cattaneo, P. M., Dalstra, M., & Melsen, B. (2005). The finite element method: A tool to study orthodontic tooth movement. *Journal of Dental Research, 84*(5), 428-433.

Cattaneo, P. M., Dalstra, M., & Melsen, B. (2008). Moment-to-force ratio, center of rotation, and force level: A finite element study predicting their interdependency for simulated orthodontic loading regimens. *American Journal of Orthodontics and Dentofacial Orthopedics : Official Publication of the American Association of Orthodontists, its Constituent Societies, and the American Board of Orthodontics, 133*(5), 681-689. doi:10.1016/j.ajodo.2006.05.038

Cattaneo, P. M., Dalstra, M., & Melsen, B. (2009a). Strains in periodontal ligament and alveolar bone associated with orthodontic tooth movement analyzed by finite element. *Orthodontics & Craniofacial Research, 12*(2), 120-128. doi:10.1111/j.1601-6343.2009.01445.x

Cattaneo, P. M., Dalstra, M., & Melsen, B. (2009b). Strains in periodontal ligament and alveolar bone associated with orthodontic tooth movement analyzed by finite element. *Orthodontics & Craniofacial Research, 12*(2), 120-128. doi:10.1111/j.1601-6343.2009.01445.x

Charras, G. T., Lehenkari, P. P., & Horton, M. A. (2001). Atomic force microscopy can be used to mechanically stimulate osteoblasts and evaluate cellular strain distributions. *Ultramicroscopy, 86*(1-2), 85-95.

Chen, W. P., Lee, B. S., Chiang, Y. C., Lan, W. H., & Lin, C. P. (2005). Effects of various periodontal ligament elastic moduli on the stress distribution of a central incisor and surrounding alveolar bone. *Journal of the Formosan Medical Association = Taiwan Yi Zhi, 104*(11), 830-838.

Corruccini, R. S., & Pacciani, E. (1989). "Orthodontistry" and dental occlusion in etruscans. *The Angle Orthodontist, 59*(1), 61-64. doi:2

Farah, J. W., Craig, R. G., & Sikarskie, D. L. (1973). Photoelastic and finite element stress analysis of a restored axisymmetric first molar. *Journal of Biomechanics, 6*(5), 511-520.

Fauchard, P. (1728). *The surgeon dentist* (L. Lindsay Trans.). (Reprinted 1946 ed.). London: Butterworth & Co.

Field, C., Ichim, I., Swain, M. V., Chan, E., Darendeliler, M. A., Li, W., et al. (2009). Mechanical responses to orthodontic loading: A 3-dimensional finite element multi-tooth model. *American Journal of Orthodontics and Dentofacial Orthopedics : Official Publication of the American Association of Orthodontists, its Constituent Societies, and the American Board of Orthodontics, 135*(2), 174-181. doi:10.1016/j.ajodo.2007.03.032

Frost, H. M. (2004). A 2003 update of bone physiology and wolff's law for clinicians. *The Angle Orthodontist, 74*(1), 3-15.

Hayashi, K., DeLong, R., & Mizoguchi, I. (2006). Comparison of the finite helical axis and the rectangular coordinate system in representing orthodontic tooth movement. *Journal of Biomechanics, 39*(16), 2925-2933. doi:10.1016/j.jbiomech.2005.10.030

Hayashi, K., Uechi, J., Lee, S. P., & Mizoguchi, I. (2007). Three-dimensional analysis of orthodontic tooth movement based on XYZ and finite helical axis systems. *European Journal of Orthodontics, 29*(6), 589-595. doi:10.1093/ejo/cjm061

Hixon, E. H., Aasen, T. O., Clark, R. A., Klosterman, R., Miller, S. S., & Odom, W. M. (1970). On force and tooth movement. *American Journal of Orthodontics, 57*(5), 476-478.

Hohmann, A., Wolfram, U., Geiger, M., Boryor, A., Kober, C., Sander, C., et al. (2009). Correspondences of hydrostatic pressure in periodontal ligament with regions of root resorption: A clinical and a finite element study of the same human teeth. *Computer Methods and Programs in Biomedicine, 93*(2), 155-161. doi:10.1016/j.cmpb.2008.09.004

Hohmann, A., Wolfram, U., Geiger, M., Boryor, A., Sander, C., Faltin, R., et al. (2007). Periodontal ligament hydrostatic pressure with areas of root resorption after application of a continuous torque moment. *The Angle Orthodontist, 77*(4), 653-659. doi:10.2319/060806-234

Ilizarov, G. A. (1989a). The tension-stress effect on the genesis and growth of tissues. part I. the influence of stability of fixation and soft-tissue preservation. *Clinical Orthopaedics and Related Research, (238)*(238), 249-281.

Ilizarov, G. A. (1989b). The tension-stress effect on the genesis and growth of tissues: Part II. the influence of the rate and frequency of distraction. *Clinical Orthopaedics and Related Research, (239)*(239), 263-285.

Jasmine, M. I., Yezdani, A. A., Tajir, F., & Venu, R. M. (2012). Analysis of stress in bone and microimplants during en-masse retraction of maxillary and mandibular anterior teeth with different insertion angulations: A 3-dimensional finite element analysis study. *American Journal of Orthodontics and Dentofacial Orthopedics : Official Publication of the American Association of Orthodontists, its Constituent Societies, and the American Board of Orthodontics, 141*(1), 71-80. doi:10.1016/j.ajodo.2011.06.031

Jones, M. L., Hickman, J., Middleton, J., Knox, J., & Volp, C. (2001). A validated finite element method study of orthodontic tooth movement in the human subject. *Journal of Orthodontics, 28*(1), 29-38.

Lanczos, C. (1962). *The variational principles of mechanics.* (2nd ed.) University of Toronto Press.

Liang, W., Rong, Q., Lin, J., & Xu, B. (2009). Torque control of the maxillary incisors in lingual and labial orthodontics: A 3-dimensional finite element analysis. *American Journal of Orthodontics and Dentofacial Orthopedics : Official Publication of the American Association of Orthodontists, its Constituent Societies, and the American Board of Orthodontics, 135*(3), 316-322. doi:10.1016/j.ajodo.2007.03.039

Melsen, B. (1999). Biological reaction of alveolar bone to orthodontic tooth movement. *The Angle Orthodontist, 69*(2), 151-158.

Natali, A. N., Pavan, P. G., & Scarpa, C. (2004). Numerical analysis of tooth mobility: Formulation of a non-linear constitutive law for the periodontal ligament. *Dental Materials : Official Publication of the Academy of Dental Materials, 20*(7), 623-629. doi:10.1016/j.dental.2003.08.003

Nekouzadeh, A., Pryse, K. M., Elson, E. L., & Genin, G. M. (2007). A simplified approach to quasi-linear viscoelastic modeling. *Journal of Biomechanics, 40*(14), 3070-3078. doi:10.1016/j.jbiomech.2007.03.019

Nikolai, R. J. (1975). On optimum orthodontic force theory as applied to canine retraction. *American Journal of Orthodontics, 68*(3), 290-302.

Oppenheim, A. (1911). Tissue changes, particularly of the bone, incident to tooth movement. *Am Orthod, 3*, 57-69.

Poppe, M., Bourauel, C., & Jager, A. (2002). Determination of the elasticity parameters of the human periodontal ligament and the location of the center of resistance of single-rooted teeth a study of autopsy specimens and their conversion into finite element models. *Journal of Orofacial Orthopedics = Fortschritte Der Kieferorthopadie :*

Organ/official Journal Deutsche Gesellschaft Fur Kieferorthopadie, 63(5), 358-370. doi:10.1007/s00056-002-0067-8

Proffit, W. R., Fields, H. W., & Sarver, D. M. (2007). *Contemporary orthodontics* (4th ed.). St. Louis, Missouri: Mosby.

Qian, L., Todo, M., Morita, Y., Matsushita, Y., & Koyano, K. (2009). Deformation analysis of the periodontium considering the viscoelasticity of the periodontal ligament. *Dental Materials : Official Publication of the Academy of Dental Materials, 25*(10), 1285-1292. doi:10.1016/j.dental.2009.03.014

Quinn, R. S., & Yoshikawa, D. K. (1985). A reassessment of force magnitude in orthodontics. *American Journal of Orthodontics, 88*(3), 252-260.

Reimann, S., Keilig, L., Jager, A., & Bourauel, C. (2007). Biomechanical finite-element investigation of the position of the centre of resistance of the upper incisors. *European Journal of Orthodontics, 29*(3), 219-224. doi:10.1093/ejo/cjl086

Reitan, K. (1967). Clinical and histologic observations on tooth movement during and after orthodontic treatment. *American Journal of Orthodontics, 53*(10), 721-745.

Ren, Y., Maltha, J. C., & Kuijpers-Jagtman, A. M. (2003). Optimum force magnitude for orthodontic tooth movement: A systematic literature review. *The Angle Orthodontist, 73*(1), 86-92.

Ren, Y., Maltha, J. C., Van 't Hof, M. A., & Kuijpers-Jagtman, A. M. (2004). Optimum force magnitude for orthodontic tooth movement: A mathematic model. *American Journal of Orthodontics and Dentofacial Orthopedics : Official Publication of the American Association of Orthodontists, its Constituent Societies, and the American Board of Orthodontics, 125*(1), 71-77. doi:10.1016/S0889540603007753

Sandstedt, C. (1904). Einige beiträge zur theorie der zahnregulierung. *Nord Tandlaeg Tidskr, 5*, 236-56.

Schmidt, H., Alber, T., Wehner, T., Blakytny, R., & Wilke, H. J. (2009). Discretization error when using finite element models: Analysis and evaluation of an underestimated problem. *Journal of Biomechanics, 42*(12), 1926-1934. doi:10.1016/j.jbiomech.2009.05.005

Schwarz, A. (1932). Tissue changes incident to orthodontic tooth movement. *Int J Orthod, 18*, 331-52.

Slomka, N., Vardimon, A. D., Gefen, A., Pilo, R., Bourauel, C., & Brosh, T. (2008). Time-related PDL: Viscoelastic response during initial orthodontic tooth movement of a tooth with functioning interproximal contact-a mathematical model. *Journal of Biomechanics, 41*(9), 1871-1877. doi:10.1016/j.jbiomech.2008.04.003

Timoshenko, S., & Goodier, J. (1951). *Theory of elasticity*. New York:

Toms, S. R., Dakin, G. J., Lemons, J. E., & Eberhardt, A. W. (2002). Quasi-linear viscoelastic behavior of the human periodontal ligament. *Journal of Biomechanics, 35*(10), 1411-1415.

Toms, S. R., & Eberhardt, A. W. (2003). A nonlinear finite element analysis of the periodontal ligament under orthodontic tooth loading. *American Journal of Orthodontics and Dentofacial Orthopedics : Official Publication of the American Association of Orthodontists, its Constituent Societies, and the American Board of Orthodontics, 123*(6), 657-665. doi:10.1016/S0889540603001641

Toms, S. R., Lemons, J. E., Bartolucci, A. A., & Eberhardt, A. W. (2002). Nonlinear stress-strain behavior of periodontal ligament under orthodontic loading. *American Journal of Orthodontics and Dentofacial Orthopedics : Official Publication of the American Association of Orthodontists, its Constituent Societies, and the American Board of Orthodontics, 122*(2), 174-179.

Williams, M. O., & Murphy, N. C. (2008). Beyond the ligament: A "whole bone" periodontal view of dentofacial orthopedics and falsification of universal alveolar immutability. *Seminars in Orthodontics, 14*(4), 246-259.

Wolff, J. (1892). *Die lehre von der functionellen pathogenese der deformitaten*. Band LIII, Heft 4: Archiv fUr klinische Chirurgie.

Zhao, Z., Fan, Y., Bai, D., Wang, J., & Li, Y. (2008). The adaptive response of periodontal ligament to orthodontic force loading - a combined biomechanical and biological study. *Clinical Biomechanics (Bristol, Avon), 23 Suppl 1*, S59-66. doi:10.1016/j.clinbiomech.2007.10.016

Ziegler, A., Keilig, L., Kawarizadeh, A., Jager, A., & Bourauel, C. (2005). Numerical simulation of the biomechanical behaviour of multi-rooted teeth. *European Journal of Orthodontics, 27*(4), 333-339. doi:10.1093/ejo/cji020